Electrochemistry and Electrokinetics in Microchannels

by

EthelMae Victoria Dydek

B.S., California Institute of Technology (2005)

Submitted to the Department of Chemical Engineering
in partial fulfillment of the requirements for the degree of

Doctor of Philosophy in Chemical Engineering

at the

MASSACHUSETTS INSTITUTE OF TECHNOLOGY

February 2012

Author .....

EthelMae Victoria Dydek
Department of Chemical Engineering
December 16, 2011

Certified by .....

Klavs F. Jensen
Department Head, Chemical Engineering
Warren K. Lewis Professor of Chemical Engineering
Professor of Materials Science and Engineering
Thesis Supervisor

Accepted by .....

William M. Deen
Carbon P. Dubbs Professor of Chemical Engineering
Chairman, Committee for Graduate Students

Electrochemistry and Electrokinetics in Microchannels

by

EthelMae Victoria Dydek

Submitted to the Department of Chemical Engineering
on December 16, 2011, in partial fulfillment of the
requirements for the degree of
Doctor of Philosophy in Chemical Engineering

Abstract

The main body of this work considers the design and development of a microfluidic, continuous electrochemical sensor capable of measuring accurate potential differences. The key challenge in creating such a device is the implementation of a miniaturized reference electrode and salt bridge. The purpose of a salt bridge is to allow ionic conduction between the reference and working electrodes while maintaining a physical separation between the two systems. Macro reference electrode and salt bridge techniques are difficult to implement on a micro scale. Instead of attempting to conform one of these techniques to function in a micro system, new methods were developed that take advantage of the conditions in a continuous microfluidic device. In particular, laminar flow and slow relative diffusion times allow for a reference electrode that does not require a physical salt bridge. Ionic conduction is maintained between neighboring reference and analyte streams while slow mixing effectively separates the two systems.

Several different device designs were investigated focusing on the prevention of reference electrode contamination. If the reference electrode is chemically contaminated it will no longer behave as expected and can not be used as a reference point. Contamination at the reference electrode was evaluated while varying flow rates and the geometry of the microfluidic device. Mathematical models were simulated in order to understand the mass transport in each device design. Based on these simulations, dimensionless groups were found that defined the dominant physics in each system. These dimensionless numbers were then validated experimentally and numerically over a range of device parameters. Subsequently, operation criteria were developed to ensure that the reference electrode remains stable and uncontaminated. By creating a stable reference electrode on chip, any homogeneous electrochemical system that was previously studied on the macro scale can now be studied continuously in a microfluidic device.

A secondary portion of this work investigates the role of surface charge with respect to electrodynamics in a microchannel. As the surface area to volume ratio increases, the concentration of charge at a channel wall may begin to approach the electrolyte concentration in the bulk solution. This phenomenon is studied numerically, with and

without convection, in particular as it relates to a possible mechanism for overlimiting current. Additionally, a potential de-ionization device is theorized based on this mechanism along with scaling arguments that can be used to aid device design.

Thesis Supervisor: Klavs F. Jensen
Title: Department Head, Chemical Engineering
Warren K. Lewis Professor of Chemical Engineering
Professor of Materials Science and Engineering

Acknowledgments

My advisor, Professor Klavs Jensen, has always been on my side. No matter what state my work was at, he had faith (no matter how misguided) that I would somehow succeed in the end. He once had to remind me that the primary purpose of graduate school was to get an education. As a result of his efforts, I have gotten a great education and have grown as a scientist. Thank you, Klavs.

I was fortunate to work with Professor Martin Bazant and have him on my thesis committee. While it was rewarding to work with him for academic reasons, I am particularly grateful to have been mentored by someone who loves science so openly. His love of the game is infectious.

I would also like to thank Professors William Deen and Patrick Doyle. Not only have they been supportive committee members, but they have inspired in me a love of teaching (and of transport phenomenon). TAing their class was the most rewarding time during my graduate career.

My sincere appreciation goes to Montana Petersen, my chemistry collaborator. Up until the end, most of the time our project didn't work. But we faced those challenges together. Much of the fabrication in this work was done in the Microsystems Technology Laboratories (MTL) at MIT. I'm so thankful for the patience and understanding displayed by the people at the MTL, in particular, Dave Terry and Dennis Ward.

This work was supported by Eni S.p.A. under the Eni-MIT Solar Frontiers Center in addition to a Graduate Fellowship from the National Science Foundation. I'd like to express my gratitude to these institutions for allowing me to pursue new challenges and still pay my rent.

I have been blessed with an abundance of supportive friends (12 year old me would be stunned). Graduate school was hard and there were several times where I was close to quitting. The only way I made it through was by leaning on their support. I'd like to thank my friends from MIT for their insightful discussions and for making me laugh: Jon, Chris, Nick, Kelly, Jerry, Andrea, Tanya, Jason, Jen, Patrick, Kevin, and

Mahmooda. Additionally, somehow I managed to make friends in Cambridge outside of MIT. I am so fortunate to have found the Vineyard and the wonderful people in it. I'm so grateful for the support and love from Ellie, Whitney, Kim, Liz, Sue and the rest of my Small Group. So much of who I am has been shaped by my girls from Caltech. Karin, Courtney, Hesper and Bernadette, over the last 10 years, have seen me through sorrow and joy and have held my hand all the way.

I'd like to thank all of my parents (in-laws too) and grandparents for their support and encouragement while I worked on this thesis. My family is many things, but never boring. I like them and I'm glad they are mine. My parents raised me in a non-competitive household. It didn't matter if I succeeded or failed, as long as I did my best. This is the only reason I'm not a megalomaniac. At the same time, they greatly valued education and learning for learning's sake. In particular, I'd like to thank my mom for reading to me the fictional works of Tolkien and Lewis and for taking me to the library when I was a child. Thank you for encouraging me to have an imagination and become independent. I would also like to begrudgingly thank my brother, Greg, for being unashamedly different and teaching me to control my anger. I'd also like to thank my much younger brother, Tommy, for not being as annoying as Greg.

Zac is the best thing that has ever happened to me. He liked me when I wore ripped jeans, baggy t-shirts and used an extension cord for a belt. He also read this thesis. Often when I was stuck in my research, I would find a breakthrough after talking about my problems with Zac. When work became overwhelming he brought me burritos. What more could a woman want? Thank you Zac for being better than everyone else.

Contents

List of Figures

List of Tables

Chapter 1

Introduction

As microfabrication techniques have advanced, the need for a better understanding of the chemistry and physics in a microchannel has become more apparent. The increased surface area to volume ratio inherent in a microchannel, as compared with a macro-sized channel, can alter the dominant physics of a system, placing a larger emphasis on surface effects. This work considers two problems involving surface behavior in a microchannel.

The first problem pertains to the development of a microfluidic electrochemical sensor. The physics of this system is controlled by diffusion in the microchannel, forced convection down the channel, and electrochemical reactions at an electrode embedded in the channel surface. An additional component is the miniaturization of macro-electrochemical techniques. While there are many advantages to using microstructure devices, it is not immediately apparent how to shrink down well-understood macro-sized methods. This topic is analyzed theoretically via simulations and empirically via experiments, including the design and use of novel microfluidic devices.

The second problem considered in this thesis looks more closely at the surface charge in a microchannel. Under classic conditions, surface charge on a vessel can be ignored since the chemistry of the bulk solution dominates. However, under certain micro-conditions, this is no longer a valid assumption. The presence of charge on the surface of a microchannel allows for an additional ion conduction pathway. This phenomenon is evaluated theoretically via analytical and numerical analysis.

1.1 Continuous Electrochemistry

1.1.1 Motivation

Continuous chemistry is a growing field, particularly under microfluidic conditions [1]. Due to the increase in surface area to volume ratio, reactions in microchannels exhibit an increase in heat and mass transfer [2]. This leads to enhanced mixing, more repeatable results, and more accurate analysis. The continuous nature increases the feasibility of kinetic studies as the reaction time is easily varied by altering the residence time [3]. In this manner, changing the fluid flow rate allows for kinetic investigation along the reaction coordinate. Additionally, automation can be simplified in a continuous device [4, 5]. Reactants can be injected into the system via a syringe pump, and this instrument can then be controlled by a computer. Experiments may then be varied and repeated by using automation software, such as LabVIEW, removing much of the manual effort. If a suitable detector can be found, in-line detection can be realized in a continuous setup [6]. Newly formed products are continuously detected, making optimization possible in real time [7]. Reaction conditions are altered in order to maximize the desired cost function, eventually leading to the optimum result. In addition to these advantages, microfluidic devices require much smaller volumes, leading to a decrease in cost and an increase in laboratory safety.

Given the advantages of microfluidic continuous chemistry, it is desirable to extend this field to electrochemistry. In fact, microfluidic electrochemical detectors are already in use, able to detect a wide variety of species (*e.g.* cocaine [8], lead [9], DNA sequences [10]). These types of detectors are either sensitive to the desired species itself or an electrochemically active product from a reaction with the desired species. In each of these cases the sensor was designed and calibrated to detect one particular species. Typically, the applied potentials are calibrated with the desired reaction in mind. As these methods are only able to detect a chemical species that has been decided *a priori*, many of the advantages of continuous chemistry are lost. Part of the power of continuous chemistry is the ability to run many different experiments under different conditions. In the current detection methods, any alteration of the original

conditions (*e.g.* changes in pH, concentration, temperature) could alter the potential of the system and require a re-calibration. This is not a problem in macro-scale electrochemical experiments because a true reference electrode is used to calibrate the system. However, miniaturizing a true reference electrode has been found to be challenging. In these instances of microfluidic detectors, a pseudo reference has been used. Unlike a true reference, a pseudo reference will be affected by changes in the experimental conditions, leading to calibration problems. A pseudo reference is not very precise and therefore is not sensitive to potential changes, limiting the experimental scope. In order to develop a continuous electrochemical detector capable of detecting more than one component with a higher degree of potential sensitivity, a more general device design is needed. To eliminate the need for individual calibration for each potential species a proper reference electrode is required.

1.1.2 Objective

The goal of the first portion of this work is to develop a continuous electrochemical detector. The main hurdle to achieving this goal is the miniaturization of a reference electrode. Several device designs were implemented and evaluated. Numerical simulation aided device design and helped to explain the experimental results. Background information on electrochemistry can be found in Chapter 2. An overview of the main type of experiment, cyclic voltammetry, and early experimental findings can be found in Chapter 3. Several device designs are analyzed and experimental results are discussed in Chapters 4 and 5.

1.2 Surface Conduction

1.2.1 Motivation

In classical electrochemical systems, the maximum sustainable current to a membrane or electrode is limited by diffusion and convection. However, overlimiting currents are often experimentally observed. There are two main mechanisms for this phenomenon.

Either there is an enhanced chemical effect which creates more ions [11], or there is a physical instability at the membrane/electrode surface which increases convection [12, 13]. These mechanisms focus on the bulk solution and can occur in macro sized systems. However, as the size of system decreases, the surface area becomes more relevant. If the concentration of surface charge is no longer negligible compared to the concentration of ions in the bulk solution, additional forces may become important. These additional terms may lead to another mechanism for overlimiting current.

1.2.2 Objective

The goal of the second portion of this work is to investigate the role of surface charge with respect to electrodynamics in a microchannel, in particular as it relates to a potential mechanism for overlimiting current. Specifically, the current-voltage response is studied in one and two dimensional systems, with and without convection. The development of an overlimiting current leads to ion depletion regions, which suggests that this phenomenon could be used to create a de-ionization device. Simple scaling arguments are made and can be used to aid device design in the future. Analytical and numerical results, including background material, can be found in Chapter 6.

Chapter 2

Background

Electrochemistry is the study of chemical reactions involving electron transfer to or from an electrode surface. One advantage in studying electrochemical reactions is that the rate of reaction can be determined *in situ* by measuring the current produced at the reacting electrode. Additionally, by imposing a voltage at the reacting electrode the energy of the system is altered, thereby driving the reaction rate. In this manner, electrochemical reactions have been studied and implemented into devices used in everyday life. Electrochemistry has made much of modern life possible from the development of portable electrochemical cells such as batteries to the blood glucose meters used by diabetics.

2.1 Macro Electrochemical Cell

An electrochemical reaction occurs when an electron is either produced or consumed in a chemical reaction. Electrons cannot easily be transported in solution, therefore this reaction must occur at a conducting surface, typically a metal electrode. The current produced in this reaction is the rate of electron production/consumption. As an electron is a product or reactant in this reaction, the resulting current is linearly proportional to the rate of reaction. In order for a current-generating reaction to occur, a second set of reactions must generate an opposite current of the same magnitude. In this way a complete circuit is created, with two half cells. The reaction

of interest is conducted at working electrode. The secondary reaction that completes the circuit, is conducted at a counter electrode. In order for the circuit to remain intact, the half cells must be in ionic contact with one another. If the two sets of reactions do not affect each other then they may be run in the same vessel and solution. If, however, contamination is an issue, the reactions can be conducted in separate vessels connected by a salt bridge. A salt bridge will allow charge to pass through (via conduction) but, typically, not bulk solution. A salt bridge can be as simple as filter paper soaked in an electrolyte solution. Ions conduct through the electrolyte soaked paper, completing the circuit.

An electrochemical cell can thus be implemented with two electrodes, each electrode in contact with one half cell reaction. A current may be imposed between the electrodes, forcing a reaction at each electrode. The difference in potential between the electrodes will depend on the ionic resistance of the solution (and salt bridge if included) and the thermodynamics of the reactions at the electrodes. In order to isolate the thermodynamics of the chemistry involved, the ionic resistance is minimized and often neglected. This is achieved by including a background electrolyte in the solution, which increases the conductivity of the solution and thereby reduces the resistance. Care must be taken to ensure that the background electrolyte remains inert and does not affect the reactions at the electrodes. If a salt bridge is used, it must be carefully designed and implemented to minimize added resistance.

The electrode reactions are governed by potential differences. However, it is not simply the potential difference between the two half cells that governs the thermodynamics. The reaction at an electrode surface is governed by the potential difference between the electrode surface and the adjacent solution. Consider a simple two electrode system with two half cell reactions. Originally the potential at the electrodes (V_1 and V_2) and the adjacent solution (V_{1s} and V_{2s}) are unknown. The chemistries at these electrodes will be governed by the quantities $\Delta V_1 = V_1 - V_{1s}$ and $\Delta V_2 = V_2 - V_{2s}$. Before any experiment takes place, the electrodes are allowed to reach equilibrium with the adjacent solution and the voltage difference is measured. This voltage difference is measured while no current is being applied and is referred to as the open

circuit potential (V_{OC}). The V_{OC} indicates the difference between V_{1s} and V_{2s}. When an experiment takes place, $V_{exp} = V_1 - V_2$ is either applied or measured (in the case of applied current). If no other information about this system is known it will be impossible to determine ΔV_1 and ΔV_2. A third equation is needed. If the half cell at the counter electrode is able to pass current while maintaining a constant potential difference, then $V_2 - V_{2s}$ can be determined by studying that half cell reaction. However, for most reactions, current does indeed change the electrochemical potential. If this is the case, there is no way to resolve the potential differences across the electrodes.

In order to ensure accurate potential monitoring a third electrode is often implemented. In the two electrode case, the counter electrode was responsible for passing current and maintaining a constant potential. As this can be difficult, the duties of the counter electrode are split. In a three electrode system the counter electrode is responsible solely for passing current. The third electrode is the reference electrode, which, ideally, maintains a constant potential. A reference electrode typically consists of a well understood electrochemical reaction at equilibrium. In order to maintain a constant potential the reference electrode must be protected from contamination. This is typically done by implementing a salt bridge between the reference and working electrodes. All of the concerns about potential differences in the two electrode system now apply to the three electrode system, particularly, the relationship between working and reference electrodes. The distance between working and reference electrodes is often minimized in order to reduce ionic resistance. Similarly, the type of salt bridge implemented is often chosen with ionic resistance in mind.

2.2 Hydrodynamic Electrochemical Cell

In batch electrochemistry the main method of mass transport is diffusion to the electrode surface. In order to study the kinetics of a particular reaction it must be clear that changes in reaction rate are not the result of a mass transport limitation. For faster kinetics, diffusion alone may not be sufficient to bring new material to

the electrode surface. In this case, the system is diffusion limited. One method to increase the rate of mass transport is to incorporate hydrodynamic methods. In these cases forced convection brings fresh solution to the electrode surface, increasing mass transport. If the transport rate is high enough, changes in kinetic behavior can be monitored. Additionally, by increasing mass transport, the resulting current often increases. A larger current can lead to a higher signal to noise ratio, allowing for more sensitive measurements. For these reasons, hydrodynamic techniques have been developed to study electrochemical systems.

2.2.1 Rotating Disk Electrode

Perhaps the most common hydrodynamic technique is the rotating disk electrode (RDE) [14]. It is a three electrode cell, where all three electrodes are submerged in a flask, often with salt bridge systems included. The working electrode is placed at the tip of a rotating cylinder attached to a motor. As the working electrode turns, the liquid electrolyte solution is pulled toward the electrode and then flung outward due to centrifugal force. A simple diagram of this method can be seen in Figure 2-1. The flux of material to the electrode surface depends on the rotation rate of the working electrode. Therefore the current depends on the rotation rate. One of the advantages of using an RDE is that the current can be treated as uniform across the electrode. This simplifies future calculations and makes kinetic analysis more straightforward. The steady state limiting current for the RDE is [15]

$$i_l = 0.62nFC_0D^{2/3}A\omega^{1/2}\nu^{-1/6}, \tag{2.1}$$

where i_l is the limiting current, n is the number of electrons involved per reaction, F is the Faraday constant (96485 C/mol), C_0 is the bulk analyte concentration, D is the diffusivity, A is the electrode area, ω is the angular velocity of the electrode, and ν is the kinematic viscosity. In this case the limiting current is a function of physical and chemical parameters, and relates linearly to the size of the electrode. Due to convection, a diffusion layer, of thickness δ, develops at the electrode. The

mass transfer coefficient, m, is equal to D/δ, and is indicative of how fast material is brought to the reactive surface. For the RDE m is defined as

$$m = 0.62 D^{2/3} \omega^{1/2} \nu^{-1/6}. \tag{2.2}$$

Commercial RDE equipment can reach a maximum rotation rate of 10,000 rpm giving a maximum ω of about 1000 Hz. Using Equation 2.2 this will yield a maximum mass transfer coefficient of about 0.2 mm/s for typical solutes in aqueous solutions.

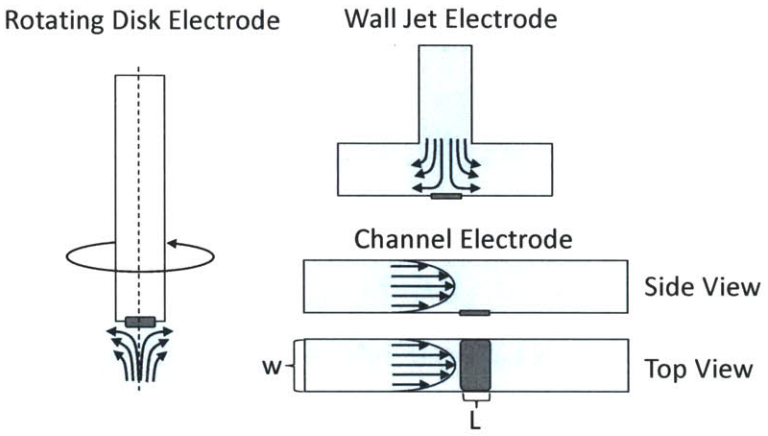

Figure 2-1: Diagrams of several hydrodynamic techniques

2.2.2 Wall Jet Electrode

A similar system to the RDE is a wall jet electrode (WJE) [16]. In this method, instead of moving the working electrode, fluid is pumped onto the electrode surface. The jet of electrolyte solution perpendicularly hits the working electrode as is shown in Figure 2-1. Depending on the type of opening or nozzle used, very high fluid velocities can be achieved. As a result shorter time scales can be investigated with a WJE than with an RDE [17]. If the jet is several times larger than the electrode, convection to the electrode surface can be considered one dimensional, simplifying further calculations. Alignment of the jet stream and the working electrode is critical to operation. This precise alignment makes miniaturization of this technique challenging.

2.2.3 Channel Electrode

In the cases of the RDE and WJE, the main direction of convection is normal to the electrode surface. In a channel electrode (CE), convection is parallel to the electrode surface (Figure 2-1). The CE consists of a rectangular working electrode embedded in one wall of a rectangular channel [18, 19]. Electrolyte solution flows down this channel, over the working electrode. Typically, the flow is laminar with a parabolic profile, with a mean velocity of U. When convection is the dominant form of mass transfer a diffusion boundary layer forms of thickness δ. For a channel of half-height, H, with an electrode width, L, δ can be described by

$$\frac{\delta}{H} = \mathrm{Pe}^{-1/3} \left(\frac{x}{H}\right)^{1/3}, \tag{2.3}$$

where Pe is the Péclet number, defined as Pe= UH/D, and x is the position on the electrode such that x varies from 0 to L. The slowest mass transfer will occur at the end of the electrode ($x = L$), where the diffusion layer is thickest. This will yield a minimum mass transfer coefficient of

$$m = D^{2/3} U^{1/3} H^{-1/3} L^{-1/3}. \tag{2.4}$$

Based on Equation 2.3 it is clear that the diffusion layer is not constant over the width of the electrode. As a result, the flux or current at the electrode will not be uniform. The resulting current is given by the Levich equation [20]

$$i_L = 1.165 n F C_0 D^{2/3} U^{1/3} w L^{2/3} H^{-1/3}, \tag{2.5}$$

where w is the channel width. In this case the electrode spans the entire channel and edge effects at the channel walls have been neglected.

Unlike the RDE and WJE, the current density is not uniform over a CE. While this does make calculations with the CE more complicated, the CE has advantages the other designs do not. Given modern microfabrication technology, microchannel CEs can be easily fabricated. Micro-RDE and -WJE are significantly more difficult to

manufacture due to alignment problems. For the RDE, the electrode must be centered on the rotating shaft. This becomes difficult as the electrode goes to sub-millimeter lengths [21]. Similarly, the WJE relies on precise alignment between the jet and the working electrode [17]. Additionally, it is possible to achieve higher mass transfer rates in a CE versus an RDE [22]. For these reasons, the overwhelming majority of hydrodynamic microelectrode electrochemistry occur in CEs.

2.3 Reference Electrodes

The purpose of a reference electrode is to give a reference point for potential measurements in an electrochemical system. A good reference system needs to be reversible and stable while under use. Any reversible electrochemical system can be used as a reference electrode. However, no perfectly reversible system exists. All systems will shift slightly when actively in use. Fortunately, there are a few systems that have small enough deviations to be implemented practically. The choice to use one particular type of reference electrode depends on how simple it is to incorporate the reference into the main system, the degree of possible contamination, and the stability of the reference at operating conditions.

2.3.1 True Reference Electrodes

Hydrogen Electrode

The hydrogen electrode is governed by the following half cell reaction: $H_2 \rightleftharpoons 2e^- + 2H^+$ [23]. This reaction typically occurs on a catalytic surface submerged in an acidic solution saturated in $H_2(g)$. Platinum is commonly used as the catalytic surface and saturation is achieved by constantly bubbling $H_2(g)$ in an acidic electrolyte. The hydrogen electrode is universally accepted as the primary standard for reference electrodes and potentials are frequently listed with respect to this electrode. This reference is simple to prepare and reproduce. One disadvantage is that aging or contamination of the catalytic surface will alter the potential of this electrode. There-

fore, if this reference is intended for long term use, care must be taken to protect the metal surface.

Calomel Electrode

Calomel is another term for mercurous chloride (Hg_2Cl_2). The calomel electrode is based on the equilibrium between this salt and liquid mercury metal: $Hg_2Cl_2 + 2e^- \rightleftharpoons 2Hg + 2Cl^-$ [23]. Typically this electrode is formed by placing a calomel/mercury paste in a saturated chloride solution. One advantage of using a calomel electrode over a hydrogen electrode is that there are only two phases present, liquid and metal. In order to use a hydrogen electrode, $H_2(g)$ must be safely added to the system. The main safety concern in using a calomel electrode is handling the mercury and mercury salt.

Silver-Silver Chloride Electrode

This reference is similar to the calomel electrode in that it involves the equilibrium between a metal and its salt: $AgCl + e^- \rightleftharpoons Ag + Cl^-$ [23]. The Ag/AgCl electrode is perhaps the simplest reference electrode to fabricate. A silver wire is coated with silver chloride, either thermally or chemically, and then dipped into a chloride solution. Unlike the calomel electrode, the components are relatively inexpensive and safe to handle. Additionally, out of the three main types listed here, the Ag/AgCl electrode is the only electrode that is easily miniaturized. The hydrogen electrode requires a gas phase and the calomel electrode requires containment of a mercury paste. For these reasons an Ag/AgCl reference electrode is commonly used in lab equipment, such as pH meters.

2.3.2 Pseudo Reference Electrodes

A pseudo reference is a general term for an electrode that is used as a reference that does not truly maintain a constant potential. For instance, any conducting material can be used as a reference in order to complete the circuit and run a three electrode experiment. If knowing the potential is not critical, than any pseudo reference can be used. It may be possible to compare a pseudo reference with a true reference

immediately before an experiment. If the pseudo reference undergoes no potential changes during the experiment, then the true potential can be determined. However, there is no way to ensure that the potential of the pseudo reference is not altered once the true reference is removed. Without a second reference, there is no method to determine if the pseudo reference potential is shifting. While this highlights the need for a true reference, there may be situations when a true reference is not available. For instance, if a salt bridge is not feasible, a pseudo reference may be used. In this case the pseudo reference electrode sits directly in the analyte solution. This greatly reduces ionic resistance and may allow the reference to be placed closer to the working electrode. Due to the lack of a proper micro-reference solution, pseudo reference electrodes are often used in micro-hydrodynamic techniques. Unfortunately, the use of a pseudo reference prevents a device from analyzing more than one analyte. Two experiments can not be compared because the affect of each analyte on the pseudo reference is unknown.

2.4 Microfluidic Reference Electrodes

In order to create a continuous electrochemical cell, a suitable reference electrode must be found. Currently, there are several methods to incorporate a reference electrode into a microfluidic system. The simplest solution is to use a pseudo reference. In the case of CE devices, a platinum or silver wire or band electrode can be placed upstream or downstream from the working electrode [24–29]. A more accurate pseudo reference electrode is an Ag/AgCl electrode that lies in the same channel as the working electrode [30]. Because the reference is in direct contact with the analyte solution, it is not a true reference. However, due to the known Ag/AgCl reaction it will be more stable than an Ag wire alone.

While pseudo references are simple to implement, they limit the scope of potential experiments. The difficultly in incorporating a true reference is the need for a salt bridge. In order for a reference to remain uncontaminated, it needs to be segregated from the analyte solution while maintaining ionic contact. Several methods have

been attempted to create a microfluidic electrochemical system with a true reference. Due to the ease of miniaturization, Ag/AgCl reference electrodes are predominantly used. Originally, attempts were made to miniaturize the porous plug typically used in macro references. Several materials such as porous silicon [31], porous glass [32], cellulose acetate [33], and a photocurable polymer [34] were successfully implemented as salt bridges for a Ag/AgCl reference electrode. However, these methods often required complicated fabrication steps and/or specialized equipment. Perhaps the simplest solution is to place a reference electrode in a macro reservoir connected to the microchannel [19, 35]. However, this places the reference far away from the working electrode, leading to a higher cell resistance. One method, used by Willey and West (2006) [36], is to have shallow channels that are wide enough to physically connect with a macro Ag/AgCl reference. In this manner, a macro salt bridge (a glass frit) is connected to a channel of sub-millimeter height. For this setup to work the tip of the reference must be submerged in the channel but not block the channel. This can become manually difficult to assemble as the reference electrode is several millimeters wide and the channel is on the order of 100 microns high. Kim *et al.* [37] created a sub-millimeter salt bridge using a polyelectrolyte gel. The UV-activated gel separates a true Ag/AgCl reference electrode from the working electrode. In order to create a geometry that makes this process feasible, the reference and working electrodes are forced to be almost a centimeter apart. This separation leads to a high ionic resistance which makes the system susceptible to increased noise. Zhou *et al.* (2010) [38] created a Ag/AgCl reference on a microfluidic chip taking advantage of the properties of polydimethylsiloxane (PDMS). In this device, small gaps in the PDMS create a porous structure between the reference and working electrodes. While this creates a stable reference in close proximity to the working electrode, the device was designed for static experiments. Under flow conditions, the analyte may contaminate the reference electrode and therefore would not be a good candidate for continuous experiments. Additionally, the fabrication technique used only applies to PDMS, it could not be easily replicated in a hard substrate, such as glass. While these methods offer some solutions, none of them can place a true reference electrode close to a

working electrode in a manner suitable for continuous work.

Chapter 3

Cyclic Voltammetry

There are many different techniques to investigate electrochemical behavior. In a three electrode cell either the potential is controlled (potentiostatic) and the current is measured, or the current is controlled (galvanostatic) and the voltage is measured. The applied property (voltage or current) can be held constant, undergo step increases, be ramped linearly, or undergo any number of analytical functions with time. In order to investigate the behavior of a system over a range of values, parameter scanning is often employed. The relevant range of voltages for a system are determined by thermodynamics while the equivalent range of currents is affected by reactant concentrations, material properties, and the physical constraints of the system. Therefore, it is commonly more feasible to predict the important voltage limits, typically between 0 and 1 volt, rather than the current limits, which can vary over several orders of magnitude. For all these reasons, cyclic voltammetry has become an important and frequently used electrochemical technique. In cyclic voltammetry the applied voltage, E_{appl}, is ramped linearly in one direction, with scan rate ν, while the resulting current is measured. After a set voltage point has been reached (E_2) the voltage is then ramped linearly in the opposite direction until the original potential (E_1) has been achieved. The applied voltage can therefore be written as

$$E_{appl} = \begin{cases} E_1 - \nu t & \text{if } 0 \leq t \leq \frac{E_1 - E_2}{\nu}, \\ E_2 + \nu \left(t - \frac{E_1 - E_2}{\nu} \right) & \text{if } \frac{E_1 - E_2}{\nu} \leq t \leq \frac{2(E_1 - E_2)}{\nu}. \end{cases} \tag{3.1}$$

This cycle can then be repeated any number of times. The resulting data, a cyclic voltammogram (CV), is a plot of measured current versus applied potential. The morphology of this plot is a function of the scan rate, ν, (in units of volts per time) in addition to chemical and physical parameters. The following sections address the structure of CVs in bulk and hydrodynamic techniques including some early CV experiments with a channel electrode.

3.1 Bulk Techniques

In classic bulk experiments there is no convection. In this case there are typically only two forces that dominate: chemical kinetics at the electrode and diffusion to the electrode surface. Consider the simple electrode reaction of an oxidant, O, electrochemically converted to a reductant, R, involving n electrons

$$\mathrm{O} + ne \rightleftharpoons \mathrm{R}. \tag{3.2}$$

For every molecule of O that reaches the electrode, n electrons are given up, generating a current. If the flux of O to a planar electrode surface is governed by Fickian diffusion and no other electrode reaction occurs, the resulting current can be described as

$$i = nFAD_O \left[\frac{\partial C_O}{\partial x}\right]_{x=0}, \tag{3.3}$$

where F is the Faraday constant, A is the electrode area, D_O is the diffusivity of species O, and x is the distance normal to the electrode where $x = 0$ corresponds to the electrode surface.

In order to calculate the resulting current, the flux of oxidant O must be determined. The governing equations, in one dimension, will be according to Fick's second law

$$\frac{\partial C_O(x,t)}{\partial t} = D_O \frac{\partial^2 C_O(x,t)}{\partial x^2}, \quad \frac{\partial C_R(x,t)}{\partial t} = D_R \frac{\partial^2 C_R(x,t)}{\partial x^2}. \tag{3.4}$$

If initially only species O is present then the boundary and initial conditions will be

as follows

$$\begin{aligned} C_O(x,0) &= C_{bulk},\ C_R(x,0) = 0, \\ C_O(\infty,t) &= C_{bulk},\ C_R(\infty,t) = 0. \end{aligned} \tag{3.5}$$

In order for this system to be solved, two more equations are needed. The first comes from balancing the oxidant and reductant fluxes. For every molecule of O that is consumed at the electrode, a molecule of R is produced, and vice versa. Therefore,

$$D_O \left[\frac{\partial C_O(x,t)}{\partial x}\right]_{x=0} + D_R \left[\frac{\partial C_R(x,t)}{\partial x}\right]_{x=0} = 0. \tag{3.6}$$

The last piece of information comes from the thermodynamics and potentially the kinetics of the electrode reaction. At equilibrium, the Gibbs free energy, ΔG is proportional the system's potential, E, as $\Delta G = -nFE$ [23]. At standard conditions $\Delta G^\circ = -nFE^\circ$. ΔG and ΔG° are related by the reaction quotient, Q, as $\Delta G = \Delta G^\circ + RT \ln Q$, where R is the universal gas constant and T is the temperature. Rearranging, we get the Nernst equation, an expression for the system potential at equilibrium

$$E = E^\circ - \frac{RT}{nF} \ln Q. \tag{3.7}$$

For the electrode reaction given in Equation 3.2 this becomes

$$E(t) = E^\circ - \frac{RT}{nF} \ln \frac{C_R(x=0)}{C_O(x=0)}, \tag{3.8}$$

if we assume the activity coefficients are equal to 1. Notice that the concentration of electrons does not appear in the equation because there are no free electrons in solution. If E° is known, the ratio of oxidant to reductant at equilibrium can be determined as a function of the system potential. The applied potential is the difference between the system potential and the reference potential: $E_{appl} = E - E_{ref}$. E° is a property of the electrochemical reaction and is often referred to as the reaction's redox potential. If the electrode reaction rapidly reaches equilibrium, then Equation 3.8 can be used as the final boundary condition. If the system can not be considered at thermodynamic equilibrium, the reaction kinetics must also be considered. In this

case, the flux at the electrode surface is governed by the rates of consumption and production of the oxidant [15]

$$D_O \left[\frac{\partial C_O(x,t)}{\partial x} \right]_{x=0} = k_f C_O(0,t) + k_b C_R(0,t), \tag{3.9}$$

where k_f and k_b are the potential-dependent forward and backward rate constants, respectively. With a full set of equations for equilibrium and non-equilibrium reactions, including Equation 3.1, the morphology of the CV can be predicted.

A simulated CV for a 1-electron, Nernstian reaction with matching diffusivities is shown in Figure 3-1. At the beginning of the cycle the applied potential is at its highest value. The potential is then ramped down, approaching the redox potential. As the applied potential gets closer to this value, reduction occurs which produces an anodic current. However, after the redox potential is reached the current hits its maximum value, i_{max}, and begins to decrease. At this point the rate of reaction is mass transfer limited. The oxidant is depleted at the electrode surface and diffusion is not fast enough to replenish it. As the potential continues to decrease the availability of oxidant decreases, further decreasing the produced current. As the potential reaches its minimum value the anodic current reaches its limit, $i_{a,lim}$. At this point the potential sweep changes direction and begins to linearly increase. The reverse curve is similar to the forward curve except that the produced current is cathodic in nature. The cathodic current reaches a minimum, i_{min}, and, at the maximum potential, reaches its limit, $i_{c,lim}$.

By examining the critical points of a CV, several properties of the reaction can be determined [15]. For instance, the potentials at i_{max} and i_{min} (E_{pa} and E_{pc}, respectively) should not vary with scan rate if the reaction is reversible. Additionally, for a reversible reaction, the width of the peaks is a function of n, the number of electrons in the reaction. The half-peak potentials, $E_{pa,1/2}$ and $E_{pc,1/2}$, are the potentials corresponding to the current halfway between i_{max} and $i_{c,lim}$, and the current halfway between i_{min} and $i_{a,lim}$, respectively. The difference between the peak potential and the half-peak potential is $56.5/n$ mV at 25° for Nernstian reactions [15]. The key

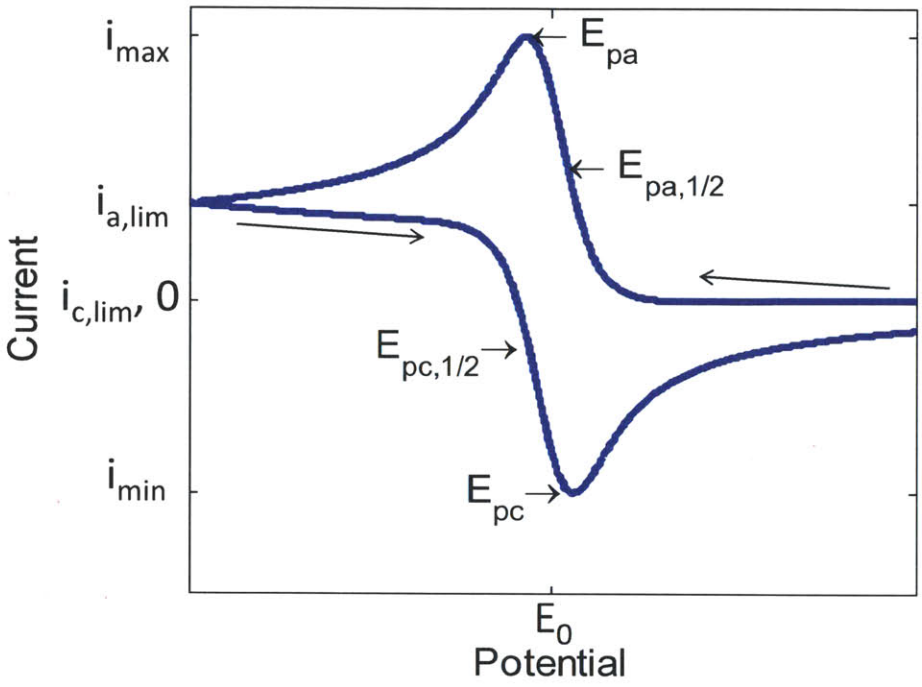

Figure 3-1: Bulk Cyclic Voltammogram. The key to the morphology of a bulk CV is the diffusion-limited mass transfer which leads to peaks in the measured current.

to the morphology of a bulk CV is the diffusion-limited mass transfer. Adding an additional method of mass transfer (*e.g.* convection) can drastically change the form of these curves.

3.2 Channel Electrode Techniques

The added mass transport in a channel electrode system (Figure 3-2) plays an important role in the current-voltage response. Many of the equations from the previous section are relevant here. Equations 3.4 and 3.5 need to be altered to include convection and the boundaries of the channel. If the channel aspect ratio (width:height) is high, the problem can be approximated in two dimensions [39], neglecting the effects of the lateral channel wall. As the aspect ratio decreases, axial and lateral diffusion begin to play a larger role, and a full three dimensional solution should be considered [40]. For simplicity, only the two dimensional problem is considered here. The resulting partial differential equations for the oxidant and reductant are as follows

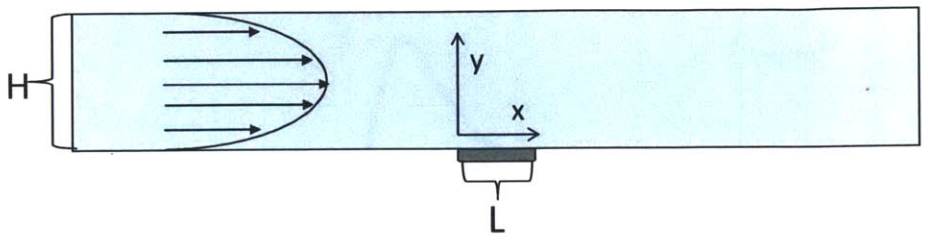

Figure 3-2: Channel Electrode Schematic. The electrode with width, L, sits at the bottom of the channel of height, H.

$$\begin{aligned}\frac{\partial C_O}{\partial t} &= D\left(\frac{\partial^2 C_O}{\partial x^2}+\frac{\partial^2 C_O}{\partial y^2}\right)-u_x(y)\frac{\partial C_O}{\partial x},\\ \frac{\partial C_R}{\partial t} &= D\left(\frac{\partial^2 C_R}{\partial x^2}+\frac{\partial^2 C_R}{\partial y^2}\right)-u_x(y)\frac{\partial C_R}{\partial x},\end{aligned} \tag{3.10}$$

where the diffusivities are set to be equal for simplicity ($D_O = D_R = D$). Due to the laminar flow in the channel, the flow profile can be considered uni-directional and parabolic, that is

$$u_x(y) = 6U\frac{y}{H}\left(1-\frac{y}{H}\right). \tag{3.11}$$

The necessary 8 boundary conditions (for a Nernstian reaction) and 2 initial conditions are as follows:

$$\begin{aligned}
&C_O(x,y,0) = C_{bulk}, \quad C_R(x,y,0) = 0,\\
&C_O(-\infty,y,t) = C_{bulk}, \quad C_R(-\infty,y,t) = 0,\\
&\left.\frac{\partial C_O(x,y,t)}{\partial x}\right|_{x\to\infty} = 0, \quad \left.\frac{\partial C_R(x,y,t)}{\partial x}\right|_{x\to\infty} = 0,\\
&\left.\frac{\partial C_O(x,y,t)}{\partial y}\right|_{y=H} = 0, \quad \left.\frac{\partial C_R(x,y,t)}{\partial y}\right|_{y=H} = 0,\\
&\left.\frac{\partial C_O(x,y,t)}{\partial y}\right|_{y=0} = 0, \quad \left.\frac{\partial C_R(x,y,t)}{\partial y}\right|_{y=0} = 0 \quad (0>x, \quad x>L),\\
&D\left.\frac{\partial C_O(x,y,t)}{\partial y}\right|_{y=0} + D\left.\frac{\partial C_R(x,y,t)}{\partial y}\right|_{y=0} = 0 \quad (0\le x\le L),\\
&\frac{C_O(y=0)}{C_R(y=0)} = \exp\left[(E(t)-E^\circ)\frac{nF}{RT}\right] \quad (0\le x\le L).
\end{aligned} \tag{3.12}$$

Far upstream, only the oxidant is present, and at the walls and outlet there is

no diffusive flux. At the electrode, the oxidant and reductant fluxes balance and Nernstian kinetics control the ratio of the species. In this hydrodynamic problem there are several important physical parameters: the diffusivity (D), the average velocity (U), the length of the electrode (L), the height of the channel (H), and the scan rate (ν). Depending on the ratio of these parameters, the problem may fall into one of three regimes. The following sections discuss the differences in these regimes as well as the different outcomes in channel electrode CVs versus bulk CVs.

3.2.1 Levich vs Thin Layer

In bulk experiments the only mode of mass transfer is diffusion. However, in hydrodynamic techniques, convection often plays a critical role. For a channel electrode the steady state has two potential regions. If diffusion remains the dominant mode of mass transfer then the cell has a 'thin-layer' limitation. However, if convection dominates, a convection-diffusion boundary layer develops over the electrode (Figure 3-3). This concept has been well defined by V. G. Levich [20]. In a thin layer case the channel height is small enough that it prevents a boundary layer from forming, and hence applied to 'thin' channels. A theoretical and numerical comparison of thin-layer and Levich cells was done by Amatore *et al.* (2007) [28].

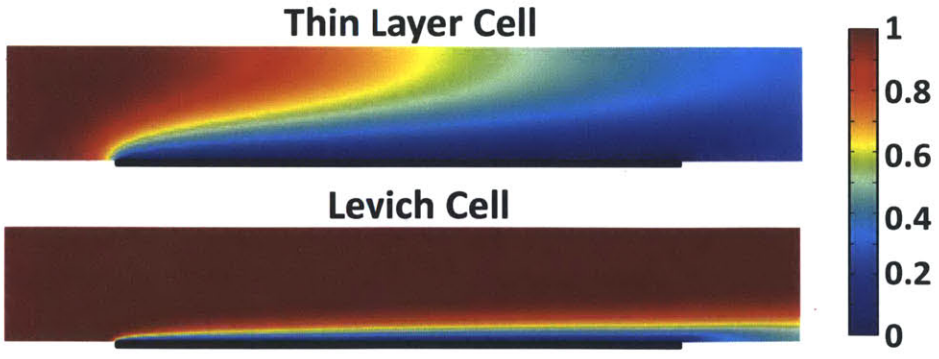

Figure 3-3: Thin Layer Cell vs. Levich Cell. In a Levich cell the convection-diffusion boundary layer is fully developed. In a thin layer cell the convection-diffusion layer spans the height of the channel. In this side view, the electrode (black bar) is at the bottom of the channel, convection is from left to right.

The thickness of the convection-diffusion boundary layer, δ, can be estimated

using an order of magnitude analysis on the mass transfer equation, Equation 3.10. In the presence of a boundary layer, the majority of the mass transfer occurs near the electrode where y is small. Therefore, we can approximate the velocity in this region as

$$u_x(y) \approx 6U\frac{y}{H}. \tag{3.13}$$

Non-dimensionalizing the steady state mass transfer equations yields

$$\begin{gathered}\frac{D}{\delta^2}\frac{\partial^2 C_O}{\partial \tilde{y}^2} \approx 6U\frac{\delta}{H}\frac{1}{L}\frac{\partial C}{\partial \tilde{x}}, \\ \tilde{x} = \frac{x}{L} \quad \tilde{y} = \frac{y}{\delta}.\end{gathered} \tag{3.14}$$

In this case it is assumed that the characteristic height of the system is δ and the characteristic length is L. Assuming that the characteristic lengths were chosen correctly, the derivatives in this equation should be of order 1. Therefore, balancing the diffusion and convection terms gives the following estimate for δ:

$$\delta \approx \left(\frac{DHL}{6U}\right)^{1/3}. \tag{3.15}$$

When $\delta \ll H$ the system behaves like a Levich cell. When $\delta \gg H$ the system behaves as a thin-layer cell. Amatore *et al.* [28] found that the transition between the two regimes occurs when $\delta/H = 0.454$.

3.2.2 Scan Rate

The previous section only considered the steady state case. However, cyclic voltammetry is inherently transient. In the case of bulk CVs a characteristic peak occurs in the scan due to diffusion limitations. However, as shown in the previous section, convection plays an important role, altering the concentration gradient. In the case of a Levich cell, the concentration gradient is limited to a convection-diffusion layer of thickness δ. If the characteristic scanning time is longer than the diffusion time across the boundary layer, the flux at the electrode will no longer be diffusion limited. In this case, convection is strong enough to replace the consumed material at the electrode,

eliminating the peak in the current-voltage profile. This can be seen in Figure 3-4. In this figure several simulated CVs are shown for increasing flow rates. As the velocity increases, the peak in current decreases, eventually disappearing completely.

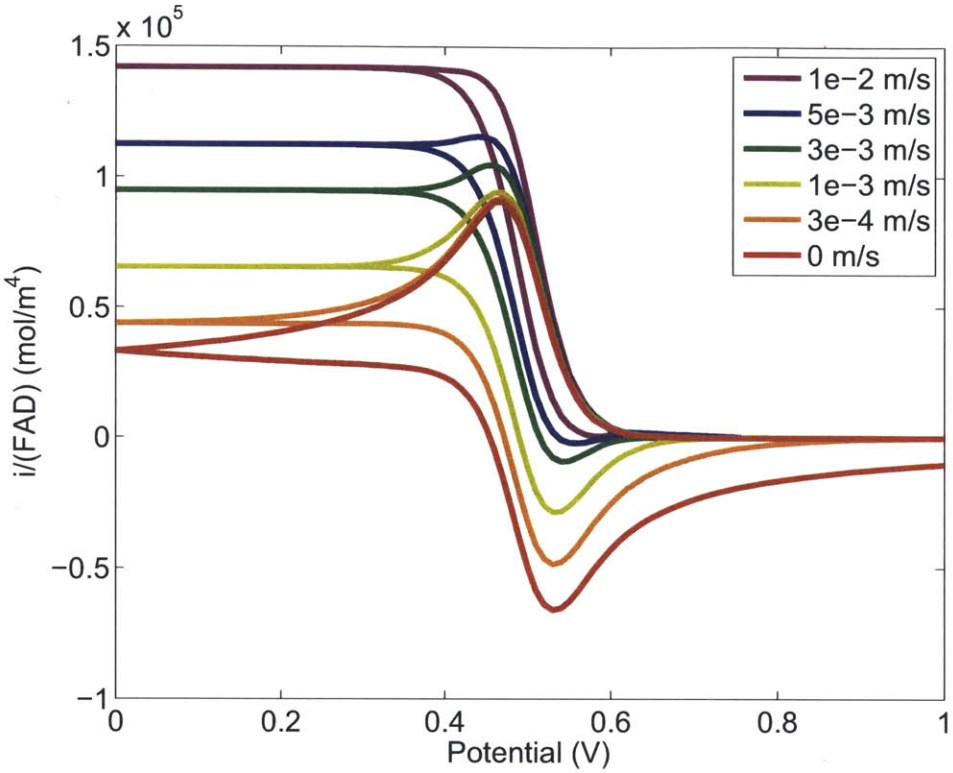

Figure 3-4: Simulated Hydrodynamic Cyclic Voltammograms. Channel height: 100 μm, electrode length: 100 μm, scan rate: 1 V/s, flow rate: variable. Note that in the case of 0 flow rate, this reduces to the same curve as shown in Figure 3-1

For a CV the characteristic time is inversely proportional to the scan rate ν. The characteristic voltage of the system will be the thermal voltage, RT/F, which is equal to 25.7 mV at 20°C. Therefore, the characteristic time in a CV will be $RT/F\nu$. The system will no longer be diffusion limited when

$$\frac{RT}{F\nu} \gg \frac{\delta^2}{D} \quad \text{or} \quad \alpha = 0.085\frac{D^{1/3}U^{2/3}}{\nu H^{2/3}L^{2/3}} \gg 1 \quad (20°C). \tag{3.16}$$

To demonstrate this relationship, CVs were simulated using COMSOL Multiphysics, a finite element solver. A two dimensional channel of height, H, with electrode length, L, was created. The channel spans $3L$ upstream of the electrode and $5L$

downstream for a total length of $9L$. The finite element mesh was set to the COMSOL mesh level of 'Extremely Fine', with 100 points distributed over the electrode. Equations 3.10-3.12 were implemented to define the mass transfer of the system. Noticing that when the diffusivities for the oxidant and reactant are equal, the total species concentration ($C_O + C_R$) is constant everywhere at all times, so that the final boundary condition can be simplified from a Neumann type to a Dirichlet type. Therefore,

$$C_0 = \frac{C_{bulk} \exp\left[(E(t) - E^\circ)\frac{nF}{RT}\right]}{1 + \exp\left[(E(t) - E^\circ)\frac{nF}{RT}\right]} \quad (0 \leq x \leq L). \tag{3.17}$$

This decouples the equations for each species, requiring only one set of equations be solved. The applied potential at the electrode is governed by Equation 3.1, where E_1 was set to 1 V, E_2 was set to 0 V and E° was set to 0.5 V. Three orders of scan rates (ν) were chosen: 1, 0.1, 0.01 V/s. Two channel heights (H), 500 μm and 100 μm, as well as two electrode lengths, 100 μm and 50 μm, were investigated. The average velocity, U, was varied in order to achieve different values of α. The diffusivity, D, was kept constant at 10^{-9} m^2/s. A total of 8 simulation series were conducted, with 5 simulations (at different values of U) in each series. Table 3.1 gives the details for each series.

Series	ν (V/s)	H (μm)	L (μm)
1	1	100	100
2	0.1	100	100
3	0.01	500	100
4	1	100	50
5	0.1	100	50
6	0.1	500	100
7	0.01	500	50
8	1	500	50

Table 3.1: Simulation Parameters

While the parameter space was not exhaustively searched, the range of parameters investigated accurately spans the range that can be studied with common materials and equipment. In order to quantify the degree of diffusion limitation, the size of the current peak was measured. This was done by examining the ratio of $i_{a,lim}$, the

limiting current, to i_{max}, the maximum current. When there is diffusion limitation, the current peaks, giving a ratio less than 1. This ratio is plotted against α in Figure 3-5 for each simulation series. For each series, the peak in current disappears for $\alpha > 1$. This indicates that the simple order of magnitude analysis used to obtain Equation 3.16 correctly estimates the mass transfer conditions for a CV in a channel electrode. In order to ensure that convection always dominates, a channel electrode device should be designed with Equation 3.16 in mind.

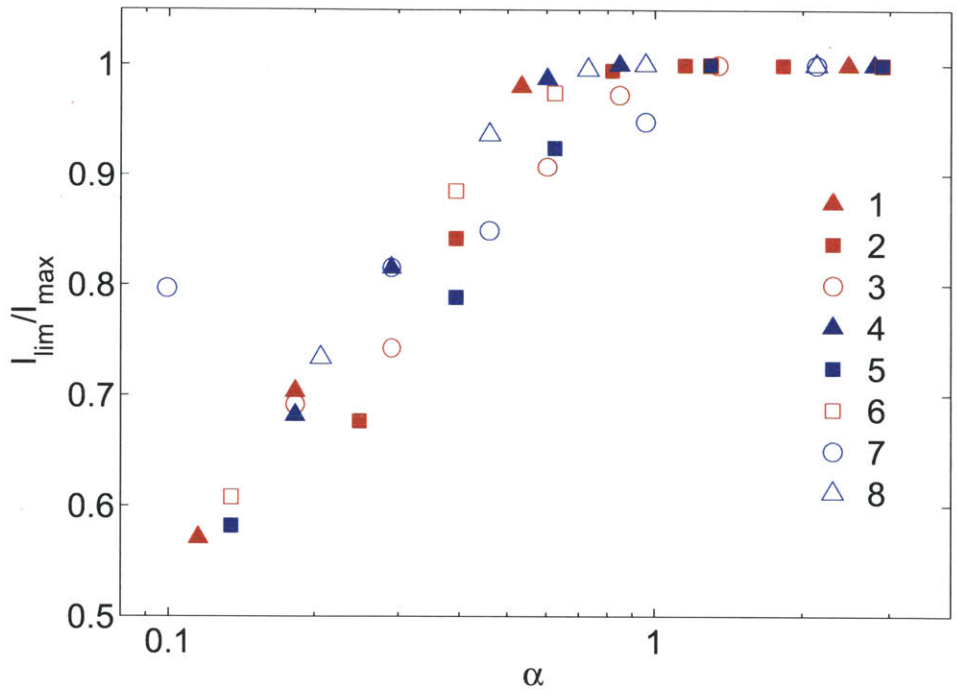

Figure 3-5: Current Peak vs α. The ratio of limiting to maximum current is plotted versus α. The data series correspond to Table 1. Scan rates: 1 V/s, (△), 0.1 V/s, (□), 0.01 V/s, (◯). Channel height (H): 100 μm (filled) and 500 μm (unfilled). Electrode length (L): 100 μm (red) and 50 μm (blue).

3.2.3 Oxidizing and Reducing Currents

In the case of bulk cyclic voltammograms, the products produced during one half of a cycle will affect the results from the second half of the cycle. Consider the n electron, reversible process in Equation 3.2. During the anodic half of the cycle, reductant R is produced. On the return scan (cathodic), this reductant is then oxidized back to

O. This process makes it difficult to determine if R was present originally, or formed by the scan itself. However, under hydrodynamic conditions, the products formed during the scan are convected away. When convection is dominant, the products are completely cleared from the system and do not affect subsequent scans.

This difference can be seen in Figure 3-6. On the left are two CVs from a bulk system. The blue curve is for an initial C_O concentration of 3 mol/m^3 with initially no R present ($C_R = 0$). In the second case (red curve), the total initial concentration is 3 mol/m^3 but with a 1:2 initial ratio of C_O and C_R. The initial presence of R does change the CV by shifting the current more negative. But it is not immediately apparent how this shift quantitatively relates to the change in initial conditions. On the right side of Figure 3-6 are comparable CVs in a channel electrode cell. In this case the presence of initial R results in a dramatic shift in current. The ratio of initial species will be equal to the ratio of the maximum and minimum currents. For instance, when $C_O(t = 0) = 1$ mol/m^3 and $C_R(t = 0) = 2$ mol/m^3, the ratio of maximum and minimum currents, $|i_{max}/i_{min}|$ is 0.5. In this manner, CVs in hydrodynamic techniques avoid contamination from the scan itself, isolating the original components.

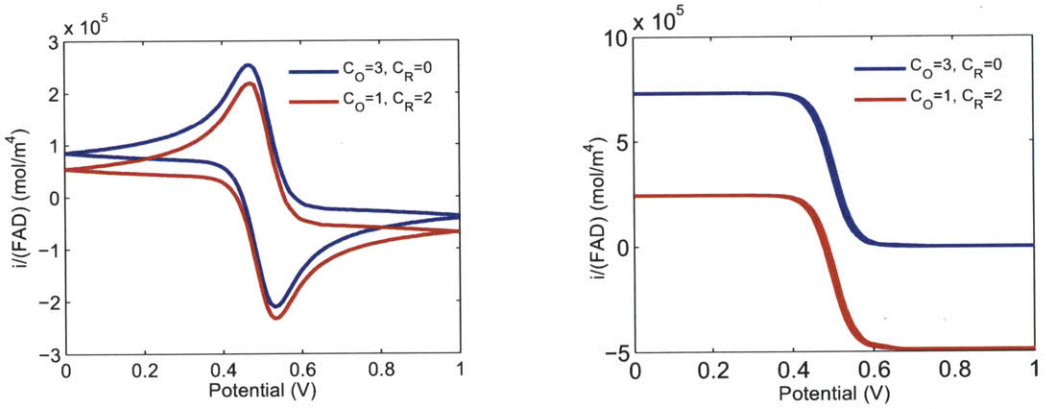

Figure 3-6: Cyclic Voltammograms with Initial Oxidant and Reductant. (a) Bulk CVs (b) Hydrodynamic CVs. The presence of initial reductant (red) shifts the current more negative compared to the case where only oxidant is initially present (blue). However, this shift is significantly larger in the hydrodynamic case, giving a clearer indication that the initial species for each scan are different.

3.3 Noise Reduction

While reducing channel size has many advantages (*e.g.* less consumed material, increased mass transfer, greater uniformity), the main drawback in the case of electrochemistry is ionic resistance. Resistance is inversely proportional to cross-sectional area, therefore smaller channels will have a higher ionic resistance across a fixed distance. One way this increased resistance can lead to problems is by increasing the system's susceptibility to noise.

Perhaps the simplest way to reduce noise is to increase the conductivity of the background electrolyte solution. Resistance is inversely proportional to conductivity, so as the conductivity goes up the resistance goes down. This can be done by increasing the concentration of background electrolyte. However, the more concentrated the background electrolyte, the more likely it will begin to affect the current response of the system.

If the electrochemical system can not be altered, the experimental setup can be manipulated to reduce noise. For instance, capacitors can be used to filter out high frequency noise. By placing a capacitor between the reference electrode and the counter electrode, a high frequency shunt is created, preventing high frequencies from entering the electrochemical cell. Alternatively, a high resistance reference electrode can be capacitively coupled with a low resistance electrode. For example, a platinum wire placed close to the working electrode will have low resistance. When a capacitor is placed between this wire and the reference electrode, high frequencies (AC current) will pass only through the platinum wire while DC current passes through the reference.

Not all noise is generated internally. External electromagnetic fields can generate noise in an electrochemical system, particularly in a system with small currents. To prevent noise from external sources, a Faraday cage can be used. A Faraday cage consists of a conductive mesh that is placed around the electrochemical cell. The external fields force the electrons in the conductive mesh to rearrange in such a way as to cancel the external fields, preventing them from reaching inside the mesh. This

prevents external electromagnetic fields from producing noise in the internal system.

It is not alway clear if experimental noise is from external or internal sources. Figure 3-7 demonstrates how noise can be progressively reduced. In Fig. 3-7a a low resistance in-channel, pseudo reference is used in a channel electrode device. While this type of reference is not an acceptable reference solution for our problem, the resulting low-resistance scan can be used as a reference point from which to compare an off-channel reference. The CV is relatively noise free and the scan's morphology is clear. In Fig. 3-7b an off-channel reference is used (for details see Chapter 4) with an electrolyte concentration of 0.25M. The signal of the curve's morphology is completely lost in the noise. In Fig. 3-7c-d the electrolyte concentration is increased to 0.5M and 3M, respectively. At the higher concentration the morphology of the curve begins to appear; however, oscillations are still present. A Faraday cage removes these oscillations (Fig. 3-7e), however the scans appear to shift with each cycle. Finally, a 5nF shunt capacitor is added to the system and the majority of the noise has been eliminated (Fig. 3-7f). By using one or more of these techniques, noise in a high resistance system can be reduced or even eliminated.

3.4 iR Drop

Even when noise has been significantly reduced, large resistances can still affect an electrochemical system. If the resistance is large enough it will begin to alter the current-voltage relationship of the system. For a single-electron, Nernstian reaction, the steady state current-voltage relationship is as follows [15]

$$i = \frac{i_{lim}}{1 + exp\left[-(E^\circ - E)\frac{F}{RT}\right]} \tag{3.18}$$

where i is the measured current, E is the voltage difference between the solution adjacent to the working electrode and the working electrode itself, i_{lim} is the limiting current determined by mass transport at the electrode surface, and E° is the redox potential relative to the reference. A slight voltage gradient develops in solution

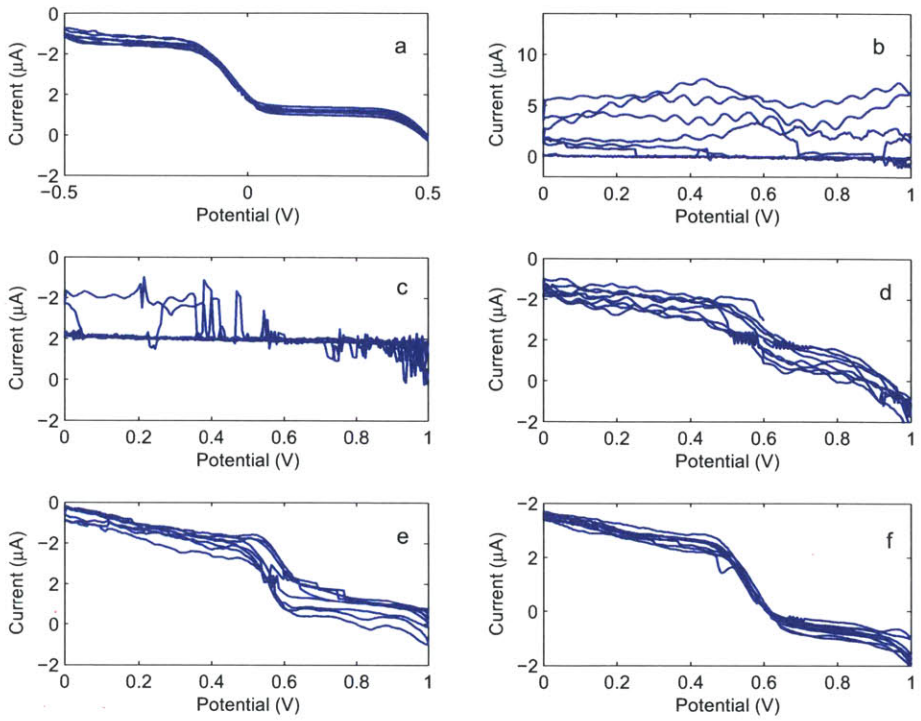

Figure 3-7: CV Noise Reduction Techniques. a) In-channel platinum pseudo reference, b) Off-channel reference in 0.25M PO^{-4}, c) Off-channel reference in 0.5M PO^{-4}, d) Off-channel reference in 3M PO^{-4}, e) Off-channel reference in 3M PO^{-4} in a Faraday cage, f) Off-channel reference in 3M PO^{-4} in a Faraday cage with a shunt capacitor (5 nF)

due to the current passing between the working and counter electrodes. Often this potential gradient extends to the reference electrode. This voltage gradient may lead to a current dependent offset between the applied voltage difference between the working and reference electrodes and the *in situ* voltage difference between the solution and the working electrode. This offset is referred to as iR drop as it is equal to the current multiplied by the resistance, R, between the working and reference electrodes. To correct for this offset, the steady state relationship becomes:

$$i = \frac{i_{lim}}{1 + exp\left[-(E^{\circ} - (V_{app} + iR))\frac{F}{RT}\right]} \tag{3.19}$$

where V_{app} is the applied voltage difference between the reference and working electrodes.

The effect of iR drop on a single-electrode, Nernstian reaction can be seen in

Figure 3-8. The effects of this phenomenon depend equally on the limiting current as well as the resistance. If resistance can not be reduced, it may be possible to decrease i_{lim} by altering the experimental conditions, thereby reducing the overall iR drop. However, reducing i_{lim} may decrease the signal to noise ratio, leading to other problems.

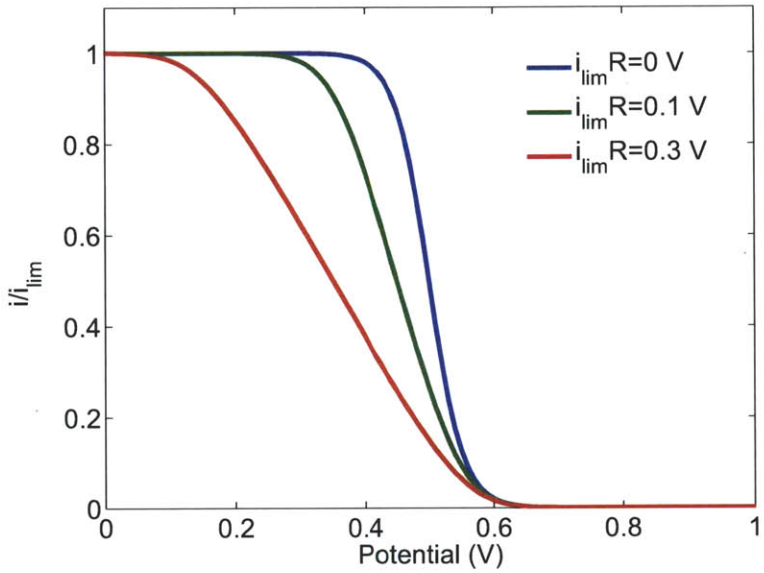

Figure 3-8: Effect of iR Drop on Current-Voltage Relationship. Steady state current-voltage curves are shown for different levels of iR drop ($E^\circ = 0.5\ V$).

In certain situations, iR drop can not be eliminated. In those cases it may be possible to account for the iR drop and transform the experimental data, even when R is unknown. For instance, even in cases where R is unknown, it is still possible to determine E° experimentally. It can be seen in Equation 3.19 that at $i = i_{lim}/2$, the quantity $(E^\circ - (V_{app} + iR))\frac{F}{RT}$ approaches zero. Noticing that the expansion of $\frac{1}{1+exp(-x)} \rightarrow \frac{1}{2} + \frac{x}{4}$ as $x \rightarrow 0$, the current-voltage relationship near $i = i_{lim}$ can be approximated as:

$$i = \left(\frac{-i_{lim}}{\frac{4F}{RT} + i_{lim}R}\right) V_{app} + \left(\frac{E^\circ i_{lim} + \frac{2F}{RT} i_{lim}}{\frac{4F}{RT} + i_{lim}R}\right) = mV_{app} + b \qquad (3.20)$$

where m and b are the slope and intercept, respectively. Solving for E° in terms of

m and b results in

$$E^{\circ} = -\frac{b}{m} - \frac{2F}{RT}. \tag{3.21}$$

E° can then be determined experimentally by linearizing the current around $i = i_{lim}/2$. In this manner, electrochemical information can be obtained despite the presence of significant iR drop.

3.5 Preliminary Experiments

The goal of this work was to develop a microfluidic electrochemical detector capable of functioning continuously. While miniaturizing the working and counter electrodes is fairly simple, miniaturizing a reference electrode is not straight-forward. In the beginning, this issue was avoided by incorporating a macro sized reference electrode with a microchannel. This was done by fabricating a polydimethylsiloxane (PDMS) channel of sub-millimeter height (approximately 100 μm) with a macro sized port for the reference channel. The channel width was 3 mm with an 8 mm square port capable of fitting a 4 mm diameter reference electrode (Figure 3-9). An Ag/AgCl reference electrode was then inserted into the port and then glued in place.

In addition to the implanted reference electrode, the device contained three platinum electrodes of equal length: a working electrode, a counter electrode, and a spare electrode that could be used as a pseudo reference. The platinum electrodes were deposited onto a glass substrate (see Appendix) and this glass substrate became the bottom wall of the channel. The electrodes span the entire channel and therefore are active over the 3 mm channel width. Several different working/counter electrode lengths (L) were investigated: 50, 100, and 150 μm (metal dots were placed on each chip to indicate the electrode thickness). The thicker electrodes were more robust, while the thinner electrodes often did not survive the fabrication process. Additionally, thicker electrodes result in a higher current, as shown in Equation 2.5, which increases the signal to noise ratio.

In order to assess the device, $IrCl_6^2$ (Ir^{+IV}) is used as a test case. The redox couple $Ir^{+IV} + e^- \rightleftharpoons Ir^{+III}$ has a reversible Nernstian reaction with well-known characteristics.

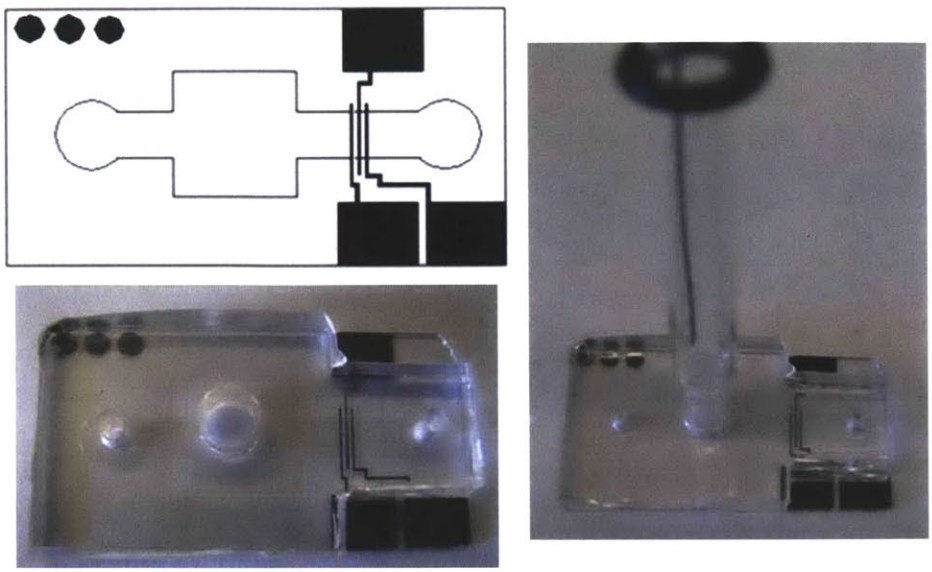

Figure 3-9: Macro Reference/Microchannel. On the top left is a schematic of the device showing the outline of the channel and the position of the electrodes (in black). The bottom left is a picture of the device prior to the insertion of the reference electrode. The picture on the right shows the device with the reference electrode inserted.

Solutions of K_2IrCl_6 were injected into the device and CVs were taken at various scan rates (Figure 3-10). Looking at the schematic and pictures in Figure 3-9, the solution flowed from left to right, passing under the reference electrode and then over the working and counter electrodes.

While this device did allow for a true reference electrode on chip, there were some drawbacks. It was critical that the reference electrode tip remained fully in the channel while avoiding contact with the base of the channel. Otherwise, the reference electrode could not be guaranteed to be in contact with fresh solution. This was manually difficult due to the shallow height of the channel ($\sim 100\mu$m). Additionally, the presence of the reference electrode in the channel will alter the fluid flow profile. This particular problem was avoided in Willey and West (2006) [36]. In this paper a macro reference is inserted into a microchannel in a similar fashion. In order to prevent the reference from altering the flow of the analyte, two channels are used, connected by a fluidic bridge. In this H-shaped design, fluid flows down both arms, analyte on one side and background electrolyte in the other. The reference electrode

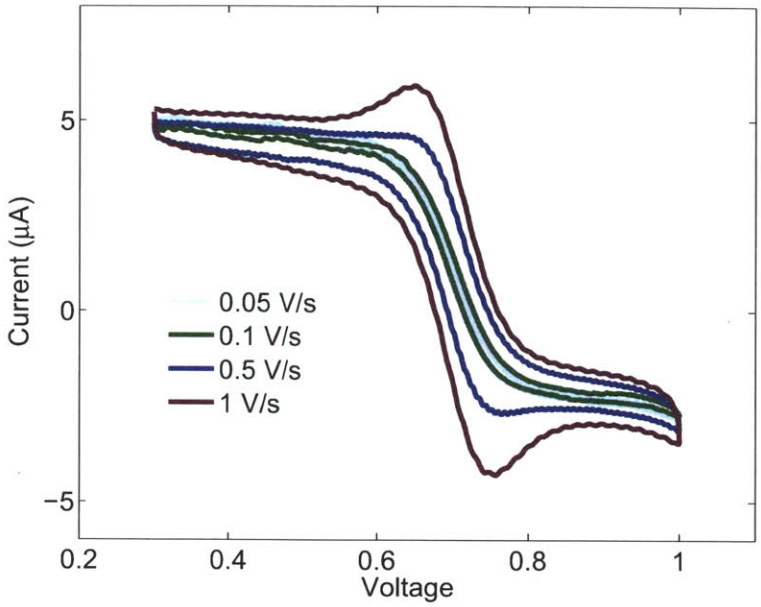

Figure 3-10: Cyclic Voltammograms with the Macro Reference/Microchannel Device. CVs taken at four scan rates, the volumetric flow rate in the channel was 20 μL/min

is implanted on the background electrolyte side. Ionic contact is made through the bridge in the middle of the 'H'. While this solves the problem of a reference interfering with the analyte flow profile, it can lead to a new problem. By further separating the reference electrode from the working electrode, the resistance is increased. This is particularly undesirable in a micro-device because high resistance is already an issue due to the smaller cross-sectional area. Additionally the electrodes in a micro-device often yield small currents on the order of 10 μA (or smaller). Smaller currents are more susceptible to noise and high resistance exacerbates this problems. Based on this analysis, it would appear that the only way to incorporate a macro reference into a continuous micro-device is to either position the reference in the analyte flow stream close to the working electrode, potentially disturbing the flow field, or placing the reference far from the working electrode. As a result, it became a goal of this work to develop a micro-reference system that would allow for a true reference on-chip while maintaining close proximity to the working electrode.

Chapter 4

T-cell

In order to establish a true reference electrode, a secondary electrochemical reaction must occur undisturbed by the primary reaction while maintaining ionic contact with the working electrode. In macro scale experiments, this is achieved by using a salt bridge. The bridge allows charge to pass through via ion conduction but prevents bulk mass transfer, thereby keeping the reference reaction and the main reaction separate, but in ionic communication with each other. As discussed in Section 2.4, creating a physical barrier in a micro device can be difficult. However, the type of devices considered here are not only small, but continuous as well. Herein lies an advantage. Convection itself can be used to separate two chemistries. With this in mind, microfluidic electrochemical cells were created in a T-geometry (Figure 4-1).

In this device, reference and analyte streams flow towards each other at 90° in a T-junction. The analyte flows from left to right in the main channel, passing over a working electrode, and the reference solution flows down a side channel, passing over the reference electrode. By placing the reference electrode in a side channel, it is removed from the analyte solution and can remain unaffected. However, since both solutions carry background electrolyte, there is sufficient conductivity to allow ionic communication between the reference and working electrodes. In this manner the reference electrode is protected from contamination but is not cut off from the main system.

There are four reasonable configurations for such a T-cell geometry, all of which

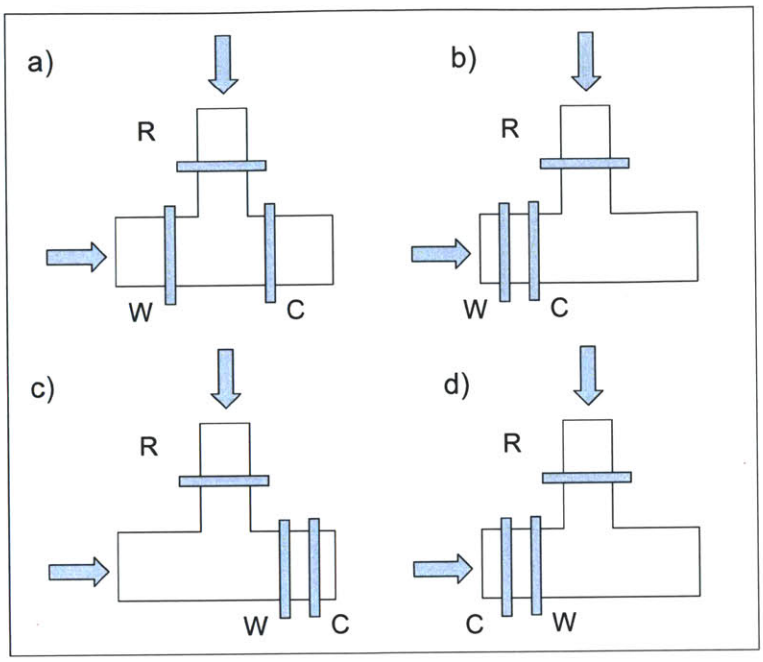

Figure 4-1: T-cell Configurations. R-Reference, W-Working, C-Counter

are shown in Figure 4-1. The configurations vary on the order and position of the three electrodes: reference, working, and counter. There are three factors to consider when choosing a T-cell configuration: contamination, resistance, and iR drop (resistance and iR drop are covered in Chapter 3). In Figure 4-1a the reference is positioned between the working and counter electrodes and will therefore experience some iR drop but it is as close to the working electrode as possible thereby minimizing resistance. However depending on the flow rates chosen, the reference solution may contaminate the working electrode. To reduce this problem configuration b) can be used, however this will increase the resistance and iR drop. Configuration c) almost eliminates iR drop and maintains relatively low resistance, however contamination of the working electrode is inevitable. If slight contamination is acceptable then this configuration may be best. Configuration d) at first glance appears to take the best from the previous models. The reference is close to the working electrode and iR drop is greatly reduced. However, in order for a current to pass through the counter electrode a reaction must occur at its surface. These reactions are generally ignored and remain unknown. Placing the counter electrode upstream creates the possibility

for an additional source of contamination at the working electrode from the products of these unknown reactions. This is highly unfavorable and makes choice d) the least useful of the configurations.

Both configurations 'a' and 'c' were explored and the advantages and disadvantages of each were investigated. Due to ease of fabrication (simple alignment), type 'c' was fabricated first and the degree of main channel contamination was analyzed. Additionally a proof of concept kinetic experiment was done with type 'c' as an electrochemical detector. The results of the these analyses are in Section 4.1. After improving alignment techniques, devices with configuration type 'a' were implemented and investigated as well. Unlike with type 'c' devices, it is possible to completely avoid contamination in type 'a' devices. The criteria for eliminating contamination in this configuration are described in Section 4.2. The analyses of the devices included investigating the effect of geometry and flow rate on device performance. The parameters investigated were the side channel width (L_x), the main channel width (L_y), the side channel velocity (V) and the main channel velocity (U) as shown in Figure 4-2.

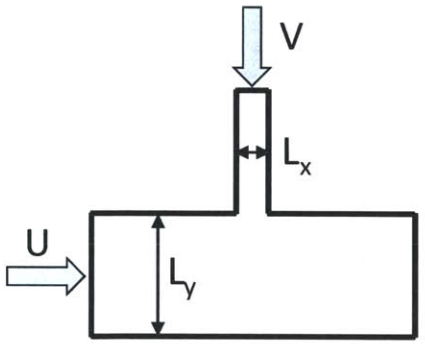

Figure 4-2: T-cell Geometry. The parameters investigated were the side channel width (L_x), the main channel width (L_y), the side channel velocity (V) and the main channel velocity (U).

4.1 Type 'c' Devices

Configuration type 'c' T-cells were fabricated with polydimethylsiloxane (PDMS) channels and metal electrodes deposited onto a glass substrate (Figure 4-3). Devices discussed in this section have a silver reference electrode (150 μm wide) and platinum working (150 μm wide) and counter electrodes (1.5 mm wide). The fabrication process is detailed in the Appendix. As can be seen in Figure 4-3, there are several platinum electrodes. Three working electrodes were deposited for redundancy and the possibility of multi-electrode experiments. Additionally, one of these platinum electrodes can be used as a pseudo reference electrode and the performance compared with the side channel reference. Alternatively, a spare platinum electrode can serve as a low resistance electrode and be capacitively coupled with the reference electrode in an effort to reduce noise (Section 3.3). The counter electrode is 10 times as wide as the working electrodes to ensure that slow reactions at the counter electrode do not limit the measured current. Fluid is injected into the channels at given volumetric flow rates. The fluid flows into the channels and over the deposited electrodes.

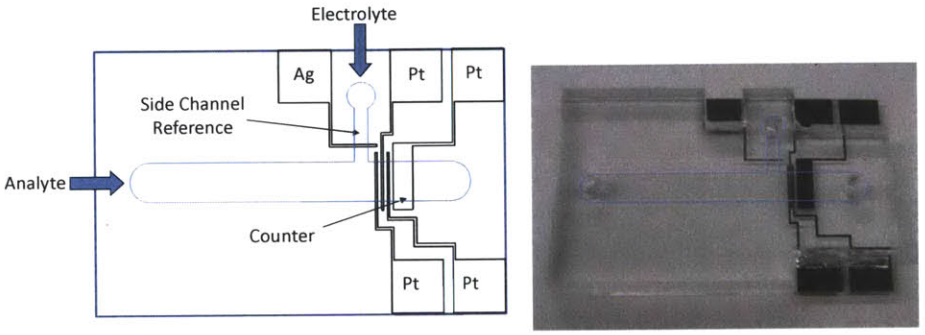

Figure 4-3: Type 'c' T-cell. Analyte flows from left to right over the working and counter electrodes (Pt). Reference electrolyte flows over the reference electrode (Ag) in a side channel and then enters the main channel, passing over the working and counter electrodes.

Due to the position of the electrodes, fluid from the side channel will pass over the working electrodes. This will dilute the analyte passing over that part of the electrode and will affect the measured current at that electrode. Simulations were conducted in COMSOL Multiphysics to determine how severe the contamination

would be. Based on these simulation results, experimental parameters were chosen to minimize contamination to an acceptable level. Experiments with configuration 'c' then revealed some advantages and disadvantages of this system.

4.1.1 Contamination Simulations

In configuration type 'c', the reference fluid flows into the side channel and then into the main channel, passing over the working and counter electrodes. This dilutes the analyte at the working electrode and will alter the observed current. In order to determine the degree of this type of contamination, 2D simulations were conducted based on the top view of the device (Figure 4-2). Several flow velocities were investigated (V = 0.001, 0.005, 0.01, 0.05 mm/s) with U:V ratios of 5:1, 20:1, and 50:1. The flow in the side channel (L_x = 1 mm) has an initial analyte concentration of 0 and the entrance to the main channel (L_y = 3 mm) has a dimensionless analyte concentration of 1. This simulates the experimental conditions of analyte flowing into the main channel and reference analyte flowing into the side channel.

The concentration 0.5 mm downstream of the side channel was monitored to determine the impact at a potential working electrode (Figure 4-4). The average concentration along this line, C_{avg}, was determined for each set of velocity conditions. However, this does not directly correspond to the effect on current measured along that line. Current is linearly proportional to analyte concentration, but it is also proportional to $U^{1/3}$ as discussed in Chapter 2, where U is the average velocity in a rectangular channel with parabolic flow. A more accurate indication of the effect on current is the weighted concentration average, $C_{avg,w}$, where the average is weighted by $V_x^{1/3}$, where V_x is the axial velocity. Due to the parabolic velocity profile in the main channel, concentration aberrations near the wall will have less effect than those closer to the center of the channel.

The resulting average concentration and weighted average concentration, C_{avg} and $C_{avg,w}$, are given in Table 4.1. As expected, increasing the ratio of U and V, reduces the dilution of the analyte steam. At the highest ratio, 50:1, the current 0.5 mm downstream of the side channel should experience only a 1-2% drop based on

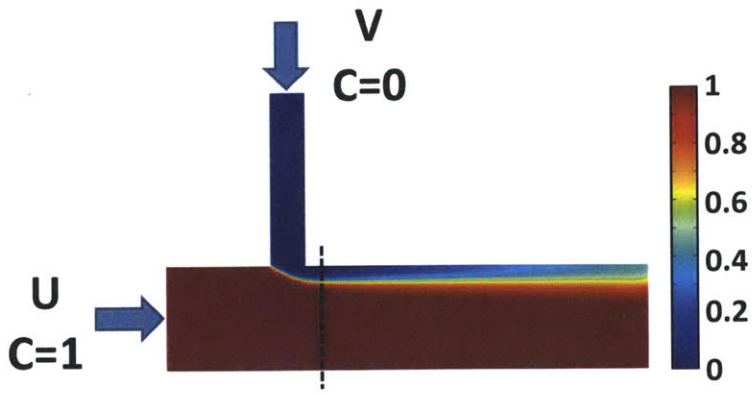

Figure 4-4: Type 'c' Simulated Concentration Profile. Analyte flows in from the left down the main channel and reference solution flows down the side channel. C_{avg} and $C_{avg,w}$ were measured along the dashed line, 0.5 mm downstream of the side channel.

$C_{avg,w}$. Additionally, for a given U:V ratio, the faster the flow velocity the greater the contamination. This is more clearly seen in Figure 4-5. At slower flow rates, diffusion allows for a more uniform concentration distribution. As the flow rate increases, convection becomes more dominant and axial diffusion is suppressed.

$C_{avg}/C_{avg,w}$			
	Flow Rate Ratio (U:V)		
V (mm/s)	5:1	20:1	50:1
0.001	0.927/0.932	0.972/0.977	0.985/0.989
0.005	0.894/0.913	0.956/0.969	0.976/0.985
0.01	0.877/0.904	0.947/0.965	0.971/0.983
0.05	0.855/0.893	0.931/0.958	0.960/0.979

Table 4.1: Average Concentration and Weighted Concentration in Main Channel. Simulated results for configuration type 'c' devices.

T-cell devices with configuration type 'c' will always have some degree of reference electrolyte contamination at the working electrode. However, if the U:V ratio is 20:1 or higher and $V < 0.05$ mm/s, the observed current should be less than 5% off of the true value. Depending on the application, this may be within the range of acceptable error.

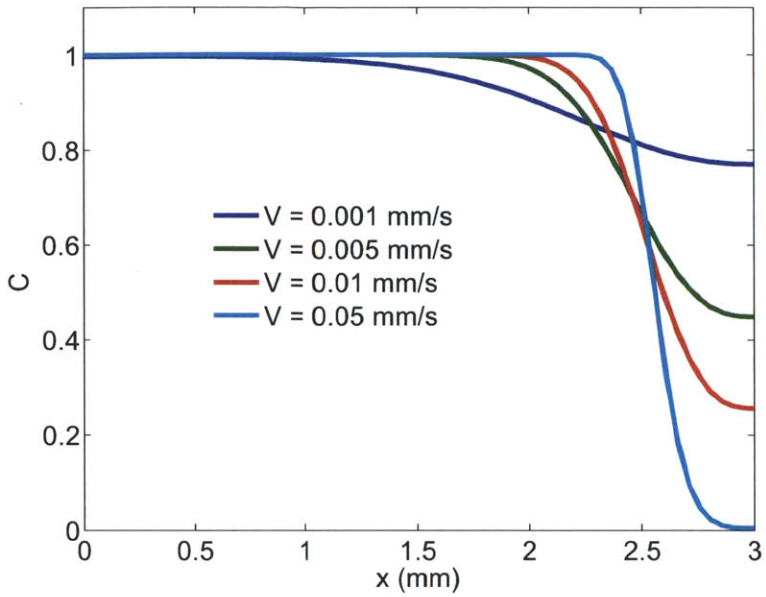

Figure 4-5: Main Channel Concentration Distribution. U:V = 5:1 at four different side flow rates. For a given U:V, the faster the flow velocity the greater the contamination, here represented by a low C value.

4.1.2 Kinetic Experiments

In order to test the applicability of this device, a kinetic experiment was designed with a T-cell (type 'c') as an electrochemical detector. For this experiment a T-cell was placed downstream of a continuous chemical reactor and was used to detect the presence of unreacted reactant at various residence times, thereby indicating the rate of reaction. Furthermore, this experiment was run at several reaction temperatures in an effort to determine the activation energy.

The reaction studied was the decomposition of $IrCl_6^{2-}$. This decomposition reaction is currently being investigated as a potential method for synthesizing electrocatalytic IrO_2 nanoparticles with the proposed reaction

$$IrCl_6^{-2} + 2H_2O \xrightarrow{Heat,\ Base} IrO_2 + 4H^+ + 6Cl^-$$

In this case 20mM Na_2IrCl_6 is added to a basic (pH=10) 0.1M trisodium citrate solution, where the citrate acts as a stabilizing surfactant for the produced nanoparticles. As mentioned in Chapter 3, $IrCl_6^{2-}$ is electrochemically active and produces a classic

Nernstian cyclic voltammogram (CV). The amount of Ir($^{+}$IV) present in solution can therefore be determined by hydrodynamic CVs, as the limiting current in such a scan is linearly proportional to the Ir($^{+}$IV) concentration.

This reaction was implemented in a simple microfluidic chemical reactor, a Teflon tube of 160 μL internal volume with 0.254 mm internal diameter. A micromixer [41] was used upstream of the reactor to ensure rapid mixing of the $IrCl_6^{2-}$ and the basic solution. The Teflon tube was submerged in a temperature regulated oil bath and data was taken at reaction temperatures of 30, 40, 60, and 80°C. Due to the small length scales of the Teflon tube, the reaction mixture cools down rapidly after exiting the oil bath. 1M K_3PO_4 is added in a 1:1 ratio to the reaction outflow as background electrolyte in order to conduct the electrochemical scans. In-line characterization then occurs as the electrolyte solution flows into the T-cell. The T-cell channel height is 31 μm with L_x = 1mm and L_y = 3mm. 3M K_3PO_4 is used as the reference solution and flows into the side channel at 0.1 μL/min. This experimental design can be seen in Figure 4-6.

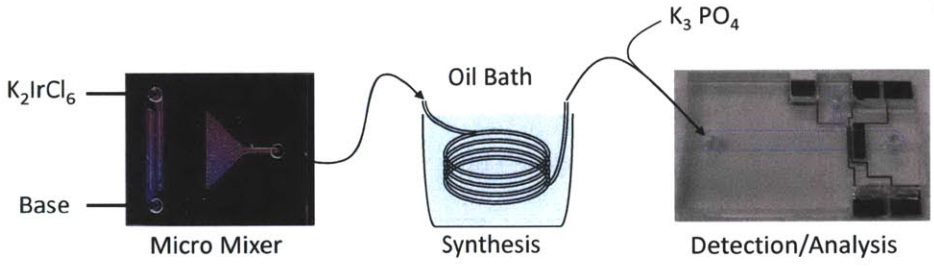

Figure 4-6: $IrCl_6^{2-}$ Kinetic Experimental Setup. $IrCl_6^{2-}$ and base rapidly mix in a micromixer and then flow through 160 μL of Teflon tubing. The solution then enters the electrochemical detector and the presence of unconsumed reactant is measured.

For this proof-of-concept experiment, the reaction was analyzed at 4, 8, 16, and 32 minute residence times. This was achieved by varying the flow rate of the $IrCl_6^{2-}$ and base solutions. At the slowest flow rate the observed current is expected to vary only 3% due to the reference flow, with a simulated $C_{avg,w}$ of 0.971. At 80°C, the highest resisdence time (32 min.) resulted in large amounts of gas bubbles evolving from the aqueous solution. Apparently, at this slower flow rate there is not sufficient backpressure to prevent degassing. As a result, the evolved gas bubbles increased the

residence time by a substaintial, unknown amount. Consequently, the data for 80°C and 32 min. residence time is not included in the results.

If the decomposition of $IrCl_6^{2-}$ is 1st order, then the concentration of $IrCl_6^{2-}$, C, should be equal to C_0e^{-kt} where k is the 1st order rate constant and C_0 is the original concentration. According to Equation 2.5, $C \propto i/U^{1/3}$. If the reaction is 1st order, plotting $\ln(i/U^{1/3})$ versus residence time will yield a linear expression with slope equal to $-k$. According to the Arrhenius equation, plotting $\ln(k)$ versus $1/T$ yields a line with a slope equal to $-E_a/R$, where E_a is the activation energy and R is the universal gas constant. Following this method, rate constants were found at each temperature and E_a was found to be 37.2 kJ/mol (Figure 4-7). While this result was obtained with only 15 data points, it demonstrates the ability of the T-cell to perform in-line characterization of an electrochemically active species.

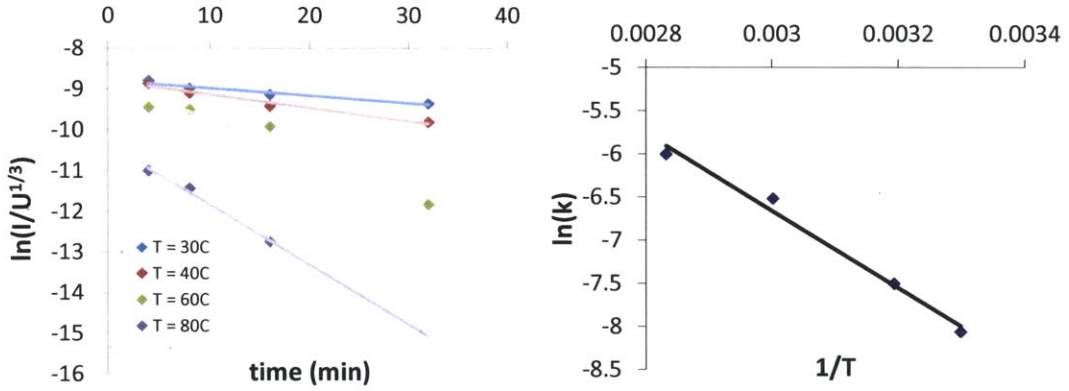

Figure 4-7: Kinetic Results for the Decomposition of $IrCl_6^{2-}$.

The kinetics of this reaction were studied by running CVs on the effluent. CVs after a 4 min. residence time are shown in Figure 4-8. Several notable characteristics appear in this figure. As the reaction temperature increases, the observed current decreases, particularly at 60 and 80°C. The decrease in anodic current corresponds to the consumption of Ir($^+$IV), however, the cathodic current also goes more negative. As discussed in Section 3.2.3, this corresponds to an increase in reductant, in this case a reaction intermediate. The ability to detect a reductant intermediate in this manner is restricted to hydrodynamic techniques. If this experiment was done in a bulk system, the cathodic current from the reductant intermediate would be hidden in

the rest of the bulk CV. At 80°C the cathodic current drops rapidly at higher voltages, no longer reaching a limiting value. This jump in negative current corresponds to a second electrochemical reaction, likely the result of electrolysis. The purpose of the original reaction was to synthesize IrO_2, a potential catalyst for electrolysis. It's possible that this large cathodic current indicates that IrO_2 was indeed formed and is acting as a catalyst for water-splitting.

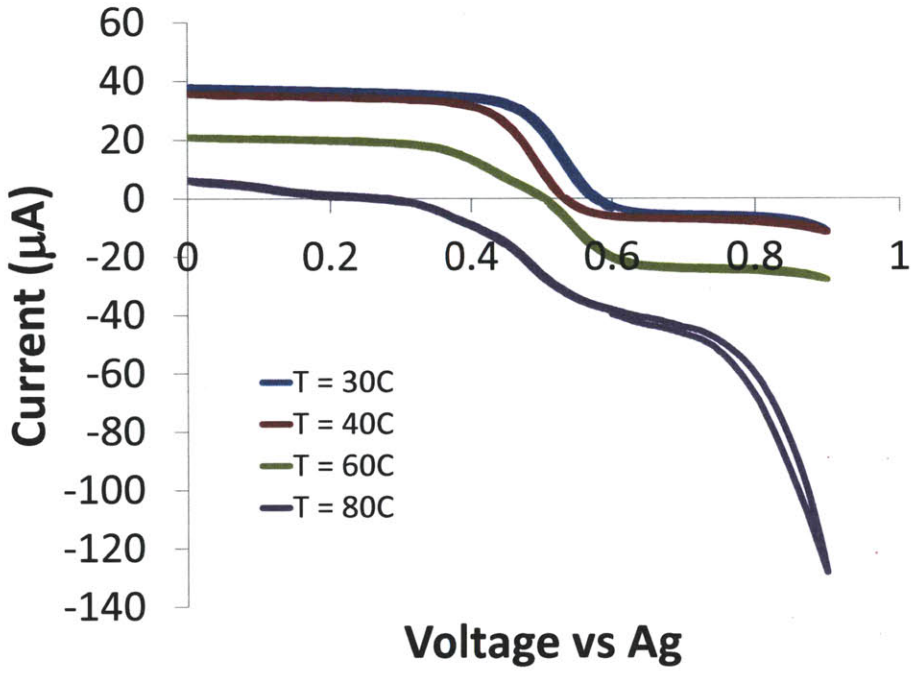

Figure 4-8: CVs after a 4 minute Residence Time. Experimental data shows the consumption of $Ir(^{+}IV)$ with increasing temperature as well as the production of a reductant intermediate.

This iridium reaction was chosen because $Ir(^{+}IV)$ produces a stable Nernstian CV with a fixed redox potential. However, in Figure 4-8 the CVs for $T = 30°C$ and $T = 40°C$ appear shifted about 50 mV from each other. This shift was observed periodically throughout the experiments. Theoretically the Ag reference electrode is protected from the analyte and should remain at a fixed potential. However, the shifting of the iridium redox potential indicates otherwise. The cause of this shifting is investigated in the Section 4.2.

4.2 Type 'a' Devices

As shown in the previous section, a T-cell can be used as an electrochemical detector, in particular it can be implemented as an in-line characterization tool. However, the reference electrode in the type 'c' devices exhibited occasional drifting and may be unstable. In this section, the fabrication of a stable on-chip Ag/AgCl reference electrode is discussed as well as design criteria to ensure that the reference remains stable and contamination is avoided at the working electrode. Fabrication techniques were improved, making configuration type 'a' possible. In particular, the method of aligning the T-channel and the electrode pad is discussed in the Appendix. The advantage of this configuration is that contamination at the working electrode can be completely avoided as the working electrode is upstream from the side channel. However, as noted in the previous section, it appears that the side channel reference is not stable and the potential was observed to shift about 50 mV during experiments. In order to understand the possible cause of this shifting, 2D simulations were conducted spanning a wide range of parameters (U, V, and L_x, L_y). These simulations revealed two possible modes of aberration (Figure 4-9). Under low side channel flow rates, analyte is able to diffuse up the side channel, thereby contaminating the reference electrode (Figure 4-9b). Additionally, if the side channel flow rate is too high, recirculation occurs upstream of the side channel (Figure 4-9c). For configuration type 'a', this recirculation will encroach on the working electrode and alter the measured current. In order to successfully implement a T-cell, criteria need to be developed to predict and avoid these two modes of contamination.

Experiments in this section were run in devices similar to those in the previous section. The PDMS channels were 86 μm high with $L_x = 0.6$ mm and $L_y = 1.8$ mm. During fabrication, the side channel is manually placed between the working and counter electrodes, roughly 0.3 mm from each side. The reference electrode in this case is a Ag/AgCl electrode (see Appendix) kept in 1M KCl, 0.75 mm wide and about 1 mm up the side channel.

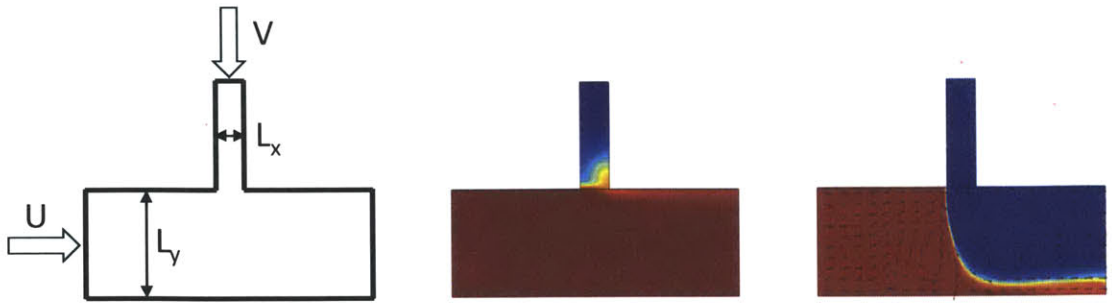

Figure 4-9: T-Cell Contamination. a) T-Cell geometry, b) Side channel contamination, c) Main channel contamination. The analyte concentration range (0 to 1) is indicated via a color surface plot ranging from blue to red. The arrows in c) signify the velocity profile.

4.2.1 Side Channel Contamination

The side channel is contaminated when analyte diffusion up the channel is no longer balanced by sufficient convection out of the channel. An order of magnitude analysis gives some insight as to how the physical parameters bring this about. Consider the dashed box in Figure 4-10. In this box diffusion is moving analyte in the $+y$ direction and convection is pushing analyte out in the $-y$ direction. According to continuity, $dV_x/dx = -dV_y/dy$, where V_x and V_y are the x and y components of flow velocity, respectively. In this region $V_x \sim U$, $V_y \sim V$, and $x \sim L_x$. But the characteristic length in the y direction, $L_{\text{char},y}$ is not obvious. However, using an order of magnitude estimate of continuity, it can be said that $L_{\text{char},y} \sim VL_x/U$.

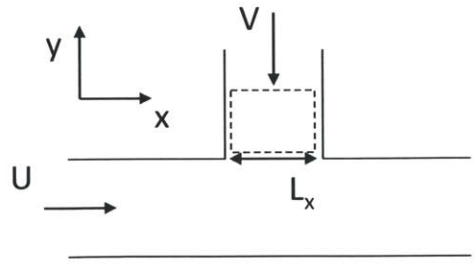

Figure 4-10: Order of Magnitude Diagram. The area inside the dashed box is considered in order to estimate the conditions which lead to analyte diffusing up the side channel.

In order to prevent analyte from diffusing up the side channel, the characteristic time for diffusion, t_{diff}, should be longer than the characteristic time for convection, t_{conv}, such that $\beta = t_{\text{diff}}/t_{\text{conv}} > 1$. In the area under consideration, $t_{\text{diff}} = L_{\text{char},y}^2/D$ and $t_{\text{conv}} = L_{\text{char},y}/V$. Applying continuity, an order of magnitude estimate on the ratio of convection to diffusion is achieved

$$\beta = \frac{V^2 L_x}{DU}. \tag{4.1}$$

When $\beta > 1$ convection will dominate and analyte diffusion in the side channel will be suppressed.

To demonstrate this criteria, 2D simulations were run in COMSOL. In these simulations U, V, L_x, L_y and D were varied. The initial analyte concentration was 1 at the main inlet and 0 at the reference inlet. The concentration was then averaged at a position L_x into the side channel. The results are shown in Figure 4-11. There are 7 data series where U, L_x, L_y, and D are held constant (Table 4.2). V was varied and the concentration profile was measured. The data was then rescaled to β. For each series, once β is no longer greater than 1, contamination begins and the analyte is detected in the reference channel. If this were to happen in a physical experiment the presence of the analyte would shift the potential of the reference electrode.

Series	U (mm/s)	L_x (mm)	L_y (mm)	$D(10^{-9}\text{m}^2/\text{s})$
1	1	1	1	1
2	10	0.1	0.1	1
3	10	0.01	0.1	1
4	0.1	0.1	0.5	1
5	0.1	0.1	0.3	1
6	0.1	0.1	0.3	0.1
7	1	0.1	1	1

Table 4.2: Simulation Parameters for Testing Side Channel Contamination

Experimental data shows similar results (Figure 4-12). In these experiments the redox potential of $IrCl_6^{2-}$ was measured against the in-channel Ag/AgCl reference electrode for three different values of U (40, 80, and 120 μL/min). The side channel flow rate, V, was varied in order to examine different values of β. At $\beta > 10$ the redox

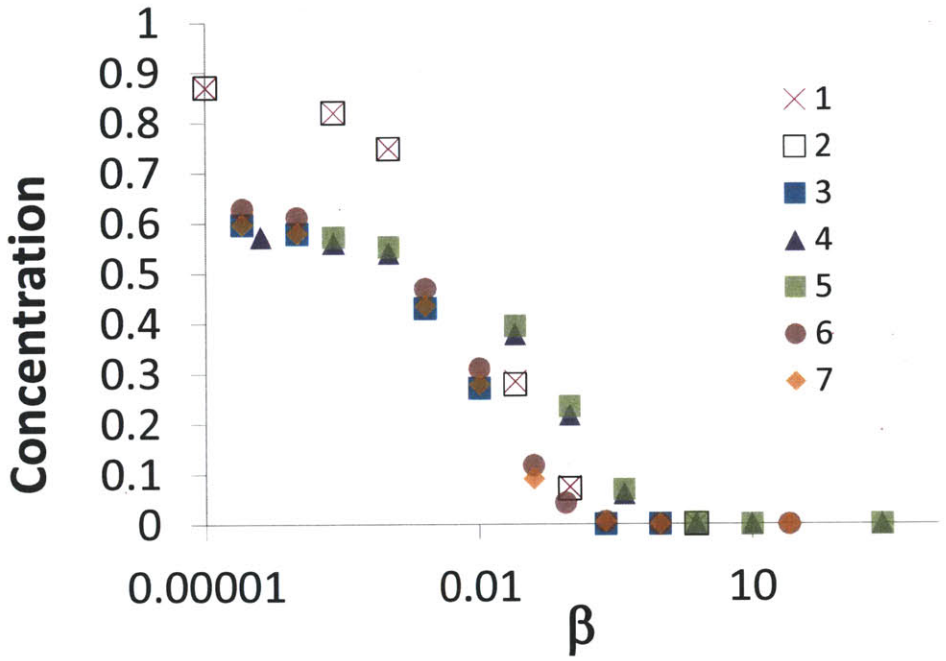

Figure 4-11: Contamination as a Function of β. Simulation parameters for each data series are listed in Table 4.2.

potential is measured to be 0.691 V $\pm$ 4 mV, which is in good agreement with the literature value of 0.696 V [42, 43]. However, as β decreases the measured potential shifts as much as 55 mV. This demonstrates the range in which a T-cell geometry can be used. If $\beta \gg 1$, reference contamination can be neglected and the in-channel reference can be trusted. In the previous section, the observed potential shifted during experiments. The β values in these experiments ranged from 0.01-0.1. These low values indicate that the system was susceptible to side channel contamination and it is likely this is what lead to the shifting potential.

4.2.2 Main Channel Contamination

Depending on the conditions mentioned in Section 4.2.1, the reference flow rate might be high enough to force recirculation in the main channel. This recirculation may lead to chemical contamination at the working electrode or an alteration of the flow rate over the working electrode. Both cases will lead to a decrease in limiting current. Recirculation in this case arises from the competition between inertial forces (the

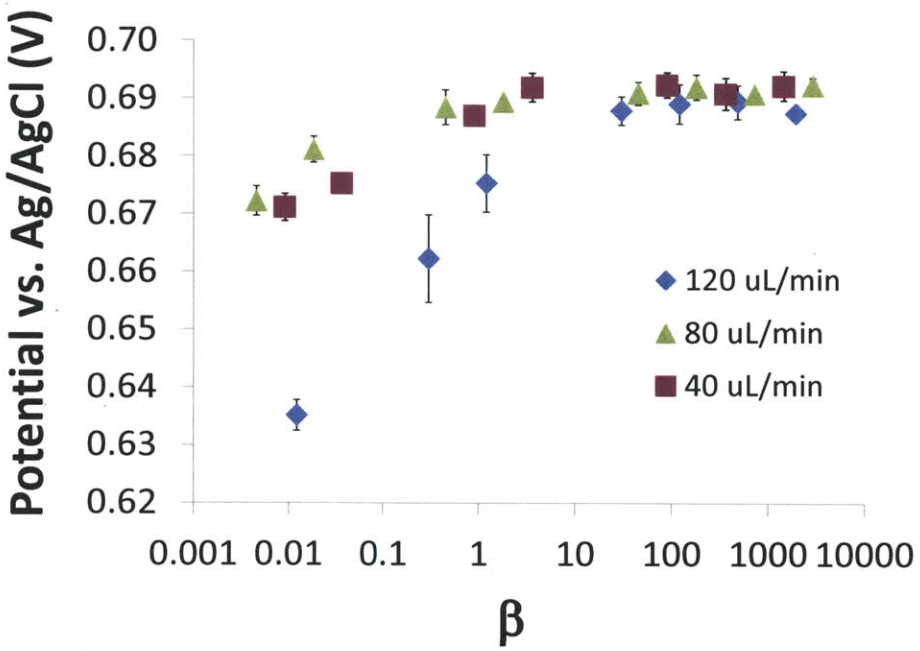

Figure 4-12: Ir(+IV) Redox Potential vs β. In these experimental results, the measured redox potential remains constant when $\beta \gg 1$. As β decreases, the measured redox potential begins to fall indicating contamination at the reference electrode.

reference flow) and viscous forces. It was found that the Reynolds number based on L_y and V determines whether or not recirculation occurs. This is defined as $Re_y = \rho L_y V/\mu$, where ρ is the fluid density and μ is the dynamic viscosity. When $Re_y \gg 1$ inertial forces will dominate. In order to ensure recirculation does not occur, Re_y should be less than 1. This can be shown in Figure 4-13. Similar $IrCl_6^{2-}$ experiments were conducted as before, this time focusing on the limiting current. The true limiting current was taken to be the limiting current measured at the slowest reference flow rate. Each subsequent limiting current was scaled to that value. U was held constant (20, 40, or 80 μL/min) while V was varied in order to examine the effect of Re_y. As Re_y increases, the limiting current appears be unaffected by flow rates until Re_y gets close to 1, then the limiting current begins to decrease. This decrease is less pronounced for larger values of U. This corresponds to the competing inertial effects from the main flow. The faster the flow in the main channel, the larger the necessary force is to displace it. Therefore at larger values of U ($Re_x = \rho L_y U/\mu > 1$) this recirculation effect can be neglected.

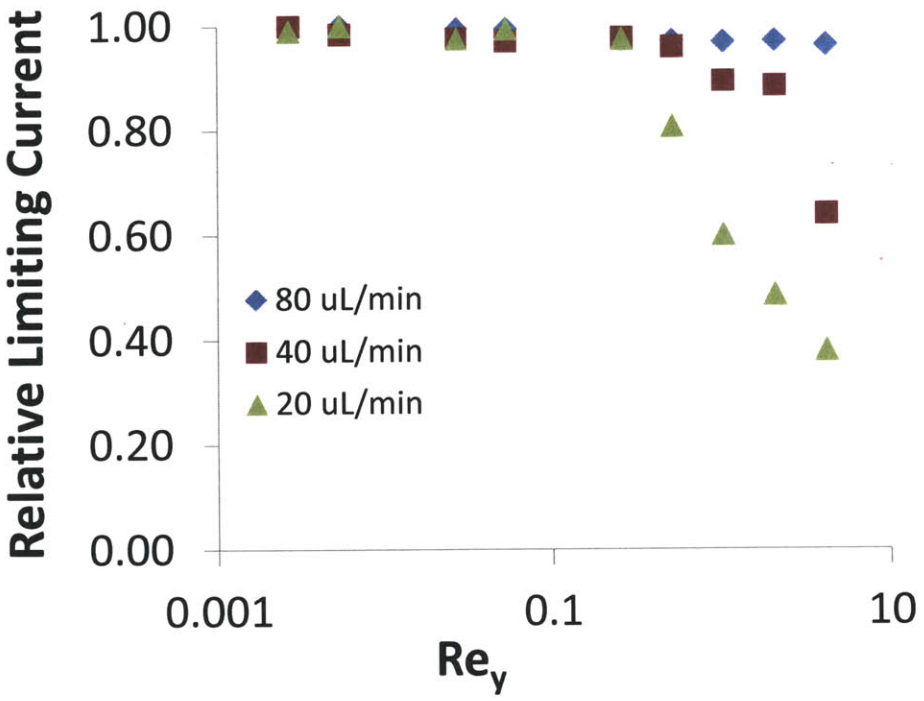

Figure 4-13: Limiting Current vs Re_y (Experimental). When $Re_y < 1$ the limiting current is unaffected by the flow rate in the side channel. However, as Re_y increases the limiting current decreases indicating contamination at the working electrode.

A microfluidic Ag/AgCl reference has been developed that can be used continuously and fabricated on-chip. The key to implementing this reference electrode is using convection to separate the reference system instead of physical barrier. Additionally, design criteria has been developed that will ensure reliable performance of the reference electrode and prevent contamination at the working and/or reference electrodes. For a set of given physical parameters and desired analyte flow rate, a reference flow rate should be chosen such that

$$\frac{\mu}{\rho L_y} > V > \sqrt{\frac{DU}{L_x}} \tag{4.2}$$

This relationship will ensure that contamination does not occur, avoiding unreliable potential and current measurements.

Chapter 5

Alternate Cell Designs

As demonstrated in previous sections, a key barrier to designing a continuous electrochemical cell is the fabrication of a proper reference electrode, preferably on-chip near the working electrode. This was addressed in Chapter 4, where a functioning micro Ag/AgCl reference electrode was fabricated using convection to separate the reference and analyte systems while maintaining conduction between them.

Several other designs were investigated as alternate reference electrode techniques. These methods were developed in order to probe the characteristics of the reference/working electrode connection. One method (Y-cell) uses diffusion as well as convection to protect the reference electrode and requires fewer constraints than the T-cell. Another method (D-cell) investigates the conduction required between the reference and working electrode. Previously the conduction between the two electrodes has been solely ionic (in solution), however the D-cell combines ionic and electronic conduction to connect the reference and working electrodes. Additionally, the electrodes are physically separated and contamination is completely prevented. The details and results of these two designs can be found in the following sections.

5.1 Y-cell

Implementing a physical barrier is the way macro electrochemistry has solved the problem of creating a reference electrode for over a hundred years. Therefore, it

is natural for a microfluidic system to mimic the same technique. In the T-cell, convection is used in place of a physical barrier, protecting the reference electrode from contamination. In this case, flow rates and cell geometry must be chosen to prevent analyte diffusion into the side channel and/or re-circulation over the working electrode (Chapter 4). These conditions become particularly important for smaller channels (Equation 4.1). In a macro device these conditions are much easier to satisfy, and a larger velocity range is possible. This is an example of how simply shrinking down a macro system does not always yield the desired results. However, instead of conforming a macro-technique to fit into a micro-system, it may be advantageous to create a new technique that is enhanced by microfluidic conditions rather than diminished by them.

By taking advantage of laminar flow and slow relative diffusion times in a micro-channel, an Ag/AgCl reference has been created on microfluidic chip without a salt bridge or physical barrier in a device called the Y-cell (Figure 5-1). In this device two solutions come together in a y-geometry and flow over three electrodes. The reference solution flows in with mean velocity, V, and flows immediately over the reference (R) electrode. The analyte solution has a mean velocity, U, and flows over the working (W) and counter (C) electrodes. Under laminar flow conditions, mixing between reference and analyte solutions will only occur by diffusion. The degree of diffusive mixing will depend on the distance from the y-junction to the electrodes, L_x, and the distance from the dividing line (dashed line in Figure 1) to the electrodes, L_y. Contamination at the reference electrode will be avoided if the time it takes to diffuse across L_y, t_{diff}, is much larger than convection time across L_x, t_{conv}. Let $\gamma = t_{\text{diff}}/t_{\text{conv}}$ so that contamination is avoided when $\gamma \gg 1$. The characteristic time for diffusion is $t_{\text{diff}} = L_y^2/D$, where D is the analyte diffusivity. If U and V are equal, the characteristic convection time will be $t_{\text{conv}} = L_x/U$. Therefore, contamination will be avoided when

$$\gamma = \frac{U{L_y}^2}{DL_x} \gg 1 \tag{5.1}$$

This simple device was fabricated in polydimethylsiloxane (PDMS), which is then

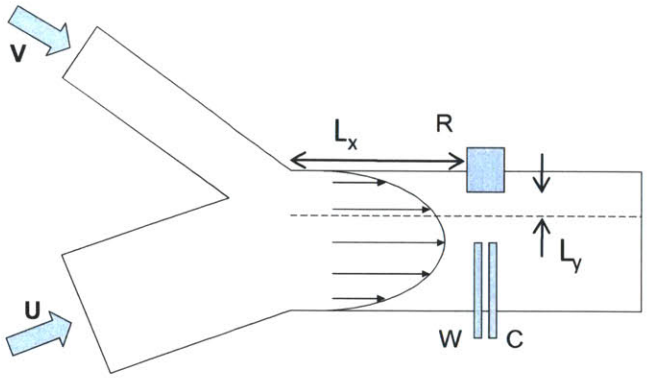

Figure 5-1: Y-geometry schematic. Analyte and reference solutions flow into a main channel with average velocities U and V, respectively. The solutions pass over three electrodes: reference (R), working (W), and counter (C).

bonded to a glass substrate that has been imprinted with gold electrodes that are approximately 200 nm thick. The working and counter electrodes are 150 μm wide and the reference electrode is 750 μm wide. A Ag/AgCl layer is grown on the gold reference electrode (see Appendix) before bonding, while maintaining the gold surface of the working and counter electrodes. In this manner, the electrodes lay at the bottom of the channel while various solutions flow over them. The channels are about 200 μm high with a main channel width of 3 mm. The analyte inlet is 2 mm wide and the reference inlet is 1 mm wide. If U and V are equal then the initial dividing line between the two solutions will be 2 mm from the analyte side. The working and counter electrodes are positioned such that they span 1.5 mm into the channel. In order to maintain a symmetric distance from the desired dividing line, the reference electrode is placed 0.5 mm into the channel. As a result, L_y is 0.5 mm. In order to properly align the channel and electrodes, gold alignment marks were placed on the glass substrate to guide the manual bonding process. When the pieces are properly aligned, the distance between the electrodes and the inlet (L_x) is 5 mm.

Channel electrodes, or electrodes that are placed on one wall of a rectangular channel, are well understood [19]. Equations that describe the current measured at such an electrode have been developed for a large variety of parameters and chemical mechanisms [28, 44, 45]. These studies typically consider an electrode that is cen-

tered across the channel. In this configuration (y-geometry) the working and counter electrodes are positioned such that they span only half of the channel width. Due to the symmetric parabolic flow profile, the current experienced in this new system should be half of what would be expected if the electrodes and analyte spanned the entire channel. Therefore, any previous work with channel electrodes can easily be applied to this system.

In order to access the degree of potential cross-contamination, $IrCl_6^{2-}$ is once again used as a test case. The redox couple $Ir^{+IV} + e^- \rightleftharpoons Ir^{+III}$ has a reversible Nernstian reaction with well-known characteristics. A solution of 10mM K_2IrCl_6 in 0.1M K_3PO_4 was used as the analyte source. The reference solution was 1M KCl. The two solutions, analyte and reference, were injected into the y-channel with a volumetric flow rate ratio of 2:1. This ensured that the dividing line between the solutions would be 2/3 of the channel width from the analyte side. Cyclic voltammograms (CVs) were taken at various flow rates to determine the degree of contamination (several are shown in Figure 5-2). The limiting current (maximum current) over a range of flow rates is plotted in Figure 5-3.

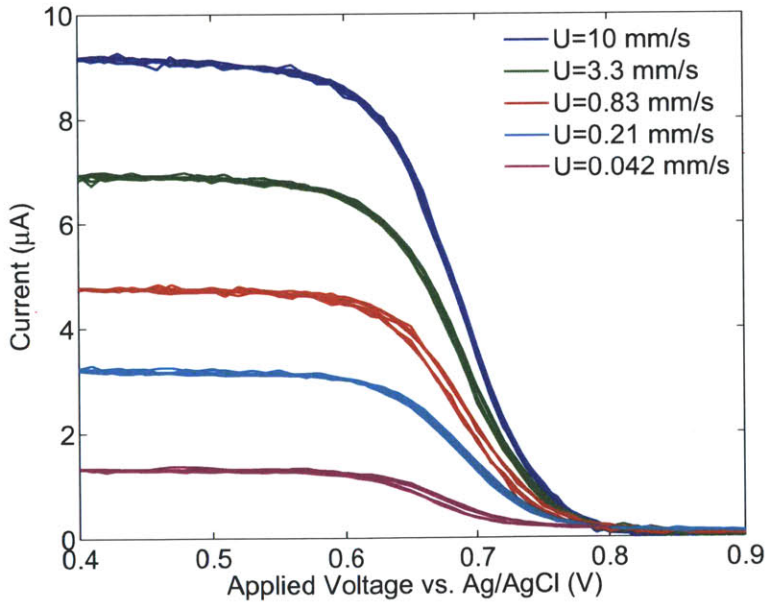

Figure 5-2: Cyclic Voltammograms in the Y-cell. CVs were taken for a variety of flow rates with scan rates between 0.01 and 0.05 V/s.

If there is no contamination present, the limiting current from the CV should vary

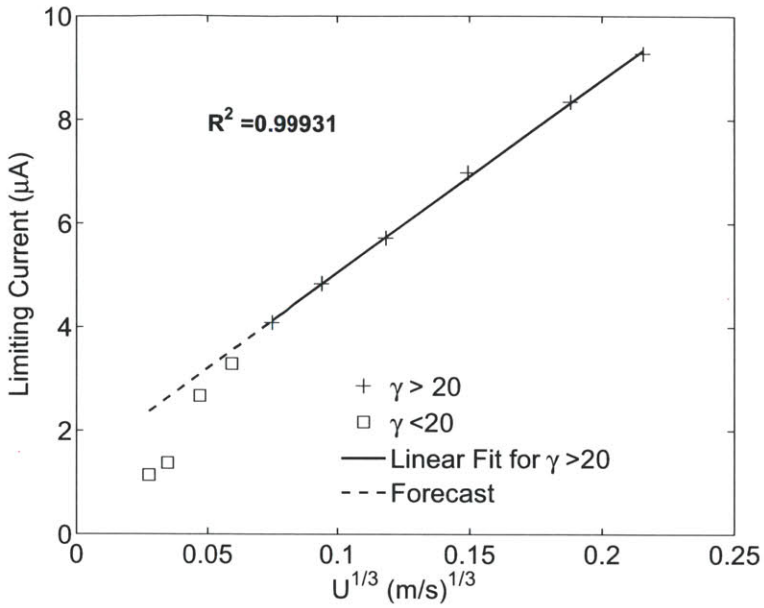

Figure 5-3: Limiting current vs. $U^{1/3}$. Plus signs designate values for $\gamma > 20$ and squares designate values for $\gamma < 20$. The solid line is the linear regression of the data for $\gamma > 20$ with R^2 of 0.99931. For $\gamma < 20$, analyte begins to diffuse away from the working electrode, reducing the limiting current.

with $U^{1/3}$, as seen in Equation 2.5. If the limiting current drops below its expected value, that indicates that the analyte concentration at the working electrode has begun to drop due to diffusion. In Figure 5-3, it is shown that when $\gamma > 20$ the limiting current indeed varies linearly with $U^{1/3}$. As γ decreases, the limiting current drops from the expected value, indicating that the analyte has begun to significantly diffuse away from the working electrode.

By measuring the redox potential of Ir^{+IV}/Ir^{+III}, the degree of reference electrode contamination can be observed. If the redox potential, $E°$, does not change with flow rate it indicates that the reference is stable and un-contaminated. This redox potential was determined by methods described in Chapter 3. The literature value for the Ir^{+IV}/Ir^{+III} couple is 0.696 V with respect to Ag/AgCl electrode in 1M KCl [42, 43]. Over the range of flow rates where $\gamma > 20$, the measured redox potential, as determined by the CVs, is on average 0.699 V with a standard deviation of only 3 mV. This small change in potential indicates that the reference electrode remains un-affected by the analyte at these higher flow rates. In this manner, contamination

is avoided at both electrodes while maintaining an ionic connection between them.

By taking advantage of the differences in going from a macro-system to a micro-system, a new reference technique has been developed. Engineering the design and operation around Equation 5.1 allows for the reference and working electrodes to be placed close together (minimizing resistance), maintaining ionic contact while avoiding contamination. In this manner, any channel electrode system can be altered to incorporate a true Ag/AgCl reference without the need for complex materials or complicated fabrication steps.

5.2 D-Cell

In a T-cell design of configuration type 'c', the reference solution flows over a part of the working electrode (Figure 4-4). The remainder of the working electrode is in contact with the flowing analyte solution. If the flow rates of these two streams were high enough, diffusion would prevent mixing similar to the Y-cell. In this manner the reference and analyte solutions would be separated and yet both would be in contact with the working electrode. This was the inspiration for a double channel device (D-cell). Instead of diffusion separating the two streams, channel walls are used to keep the streams apart (Figure 5-4).

Analyte flows into the bottom stream with mean velocity, U, and reference solution flows into the top stream with mean velocity, V. Several working electrodes (Au and/or Pt) and a counter electrode (Pt) are placed such that they cross both channels. Each channel has a reference electrode (Pt, Ag, or Ag/AgCl) that only spans that particular channel. If analyte flows in one channel, a reference electrode in the second channel would still be in ionic contact with the working electrode via the second channel. The reference electrode would be completely protected from contamination while still maintaining contact. It is necessary for reference and working electrodes to have ionic contact. Up until this point, the contact between the two electrodes was solely ionic, meaning passed by conduction of ions. However, in this design there is an additional electronic component (conduction passed by electrons) via the working

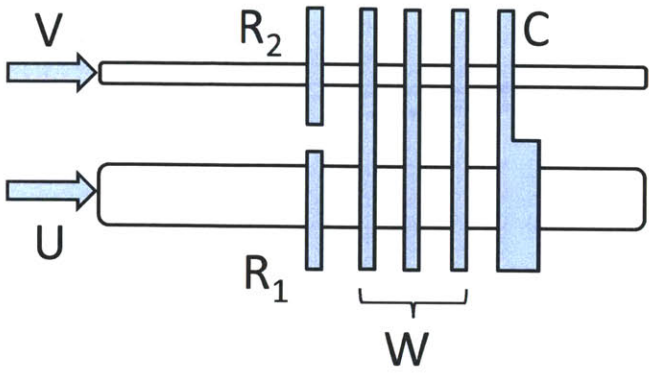

Figure 5-4: D-cell Schematic. Analyte flows in the bottom channel with mean velocity U and reference solution flows in the top channel with mean velocity V. Working (W) and counter (C) electrodes span both channels. Reference electrodes (R_1 and R_2) are placed in each channel.

electrode itself. Ionic conduction occurs in the reference channel between the reference electrode and one part of the working electrode. Electronic conduction occurs along the working electrode, between the two channels. The addition of electronic conduction in this manner appears to be a novel concept, previously unstudied.

Cyclic Voltammograms (CVs) can be successfully conducted with this device, using reference R_2, demonstrating that the addition of electronic conduction completes the necessary circuits. However, often the morphology of these CVs does not agree with classical expectations (*e.g.* Figure 5-2). In Figure 5-5 the CV has a gap ($\sim$ 100 mV) between the anodic and cathodic curves. This voltage gap disappears when reference R_1 (or a second working electrode) is used instead. The presence of this gap indicates that the potential being applied by the potentiostat is not equal to the potential actually experienced at the working electrode. Unless the cause of this gap can be accounted for, this method of protecting the reference electrode is not a viable solution.

The size of the gap in the CV is not consistent day-to-day and occasionally disappears all together. Eventually, however, the gap returns and can not be eliminated. The size of this gap appears to be unaffected by altering the flow rate. This indicates that the gap in the scan is unrelated to mass transfer limitations. Interestingly, the

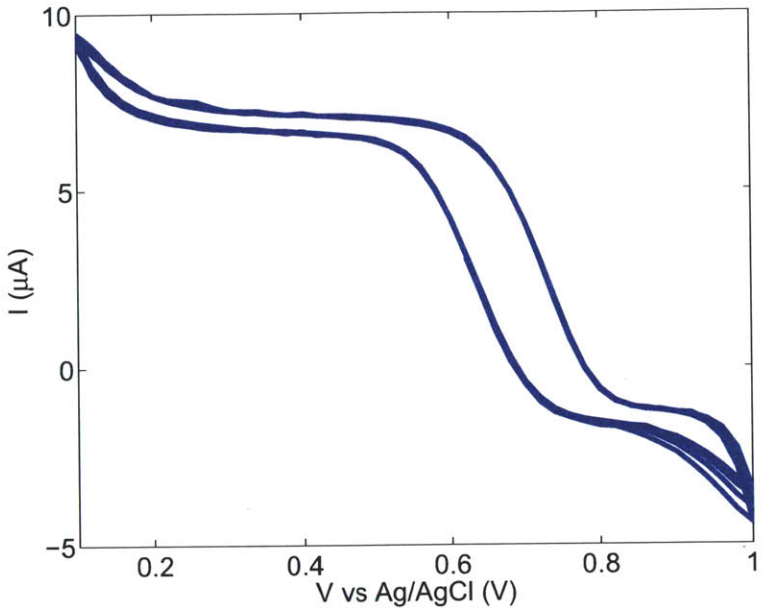

Figure 5-5: D-cell Cyclic Voltammogram. CV of $IrCl_6^{2-}$ with scan rate of 0.04 V/s using reference R_2. A voltage gap of about 100 mV is present between the anodic and cathodic scans.

size of the gap is affected by the voltage scan rate. The slower the scan rate in the CV, the smaller the gap between anodic and cathodic scans (Figure 5-6). In particular, the cathodic scan appears to shift to higher potentials at slower scan rates. The effect of scan rate suggests that a time delay is present in the system. At faster scan rates this time delay becomes more noticeable and the gap increases. It's clear that the addition of an electronic conduction pathway, in this manner, alters the electrochemical response of the cell in an as yet unknown way.

This method of separating the reference and working electrodes is not limited to microfluidic systems. A batch system analog was investigated in order to further probe this phenomenon. Two batch electrochemical cells were implemented in way similar to the two channels in a D-cell. $IrCl_6^{2-}$ was contained in one batch cell and 1M KCl in the other. Placing a macro Ag/AgCl reference electrode in the $IrCl_6^{2-}$ solution is analogous to using R_1 in the D-cell and placing it in the KCl solution is analogous to using R_2. Initially, working electrodes were placed in each system and connected via a copper wire. Counter electrodes were handled similarly. CVs in both arrangements

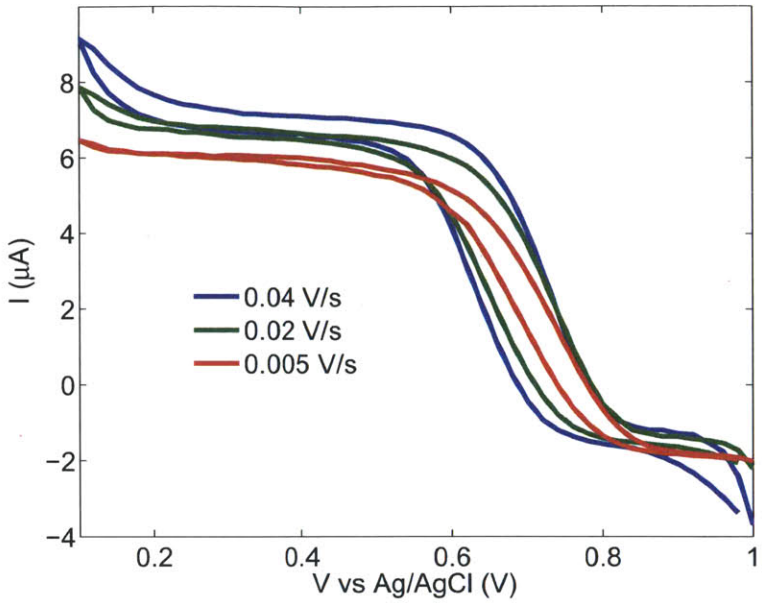

Figure 5-6: D-cell Cyclic Voltammogram with Varying Scan Rates. CVs of $IrCl_6^{2-}$ using reference R_2 under varying scan rates. The slower the scan rate, the smaller the gap between anodic and cathodic scans. This suggests that the gap is caused by a time delay in the system.

(reference electrode in analyte or reference solution) are shown in Figure 5-7. The top part of this figure shows the CV when the reference electrode is in the analyte solution. The resulting CV has the classic morphology. When the reference electrode is placed into a separate vial, connected via the working and counter electrodes, the CV has a different shape. Again, there is an increase in the gap between the anodic and cathodic scans.

One possible explanation for the change in CV morphology is that the two systems, while connected, have a slightly different potential. This difference in potential may lead to a capacitor-like effect, where the difference in solution potentials acts like separated charges. This capacitor-like effect may then couple with the potentiostat's circuitry, leading to a time delay. This would account for the slower voltage scan rates in the D-cell resulting in smaller gap sizes. One way to eliminate any charge separation is to connect the solutions with a conductive wire. During a CV, the background potentials of each solutions can be equilibrated with each other. The resulting CV with a connecting wire is shown in Figure 5-8. The morphology of this

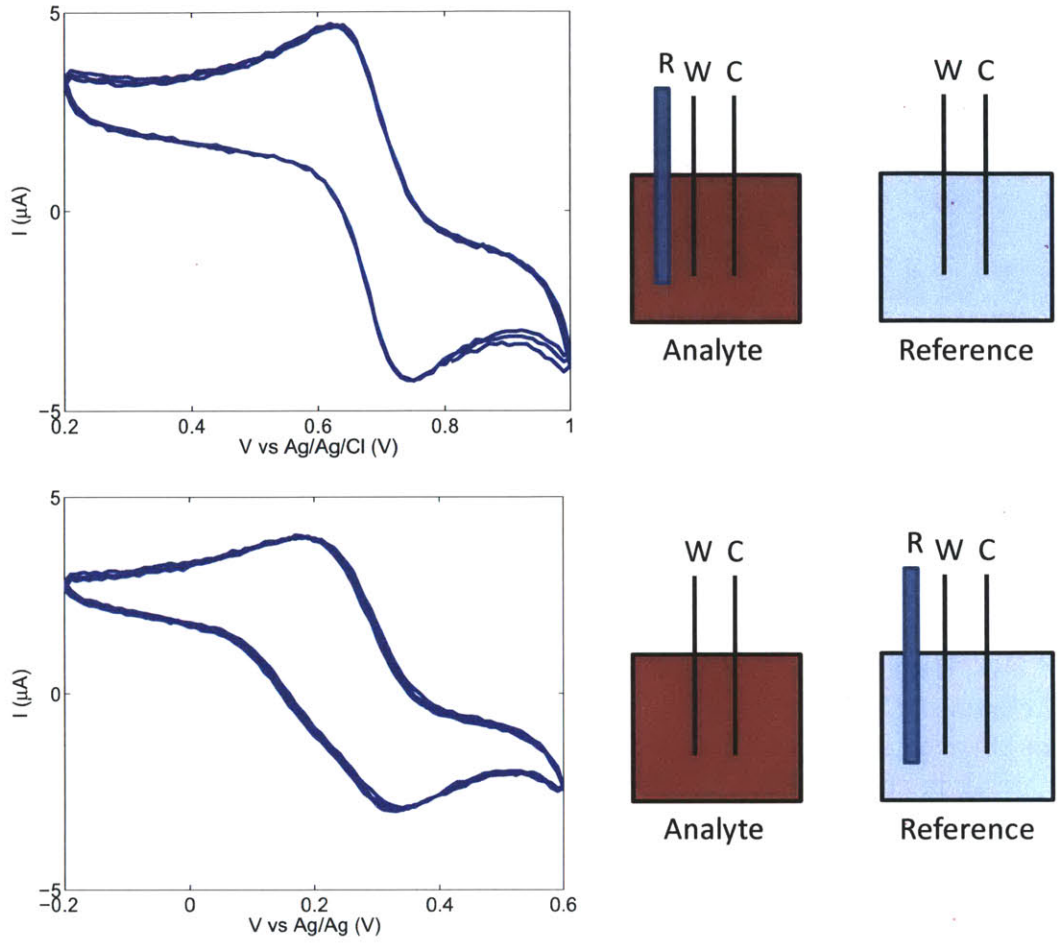

Figure 5-7: Batch Experiments. Top: CV with the reference electrode placed in the analyte solution. Bottom: CV with the reference electrode placed in a separate reference solution. To the right of the CVs are schematics of the experimental setup.

CV is quite similar to classic case and it appears that adding a connecting wire does prevent the time shift phenomena.

In the previous cases, the working and counter electrodes extended into both solutions. It was thought that the reference electrode would communicate with one part of the working electrode ionically through the reference solution. This part of the working electrode would then communicate electronically with the part of the working electrode in the analyte solution. However, the presence of the connecting wire makes the electrical connection through the working electrode unnecessary. The reference electrode can communicate ionically with the connecting wire. The connecting wire communicates electronically between each solution. Finally, the connecting wire

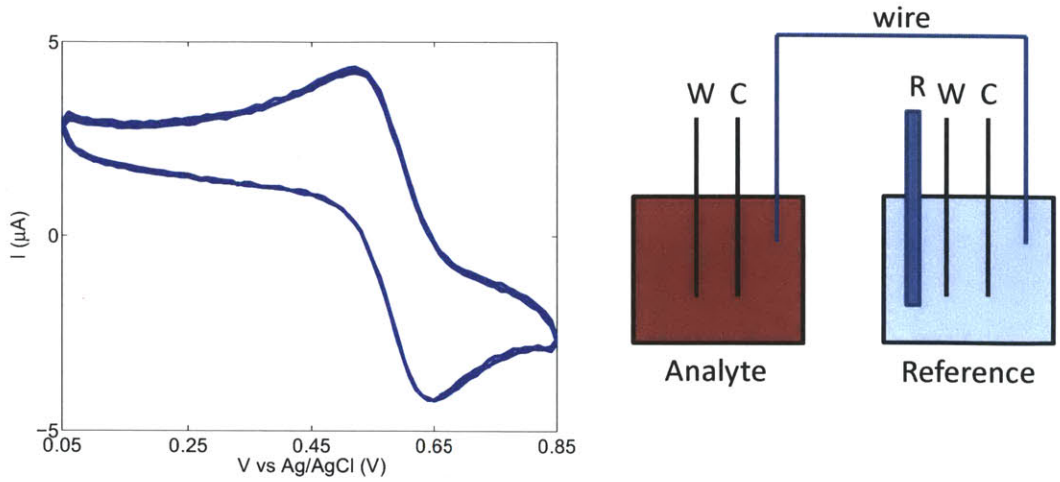

Figure 5-8: Batch Experiment with Connecting Wire. CV with the reference electrode placed in a separate reference solution with a connecting wire. To the right of the CV is a schematic of the experimental setup.

communicates ionically with the working electrode in the analyte solution. Therefore, the working and counter electrodes need only be in the analyte solution. The resulting CV is shown in Figure 5-9. In this case the CV maintains the classic morphology and the reference electrode is completely separated from the analyte solution. However, the potentials of the $IrCl_6^{2-}$ scans are shifted from the expected values when the reference is placed in the analyte solution directly. This shift in potential is problematic as it indicates an unknown voltage drop in the system. This voltage drop is most likely along the reference/working conduction pathway. In this case it is important to remember that the potential at an electrode surface is controlled by surface reactions as discussed in Chapters 2 and 3. For the connecting wire to conduct any charge, reactions must be occurring at the wire surface. Each end of the wire is in a different solution, meaning that different reactions may be occurring at either end. These reactions may then lead to a potential difference across the wire. The only way to determine the potential at either end of the wire is to compare the wire's potential to a known system, in other words, a reference electrode.

Unfortunately, this problem is now circular, with a reference electrode needed to test a potential reference electrode. While the addition of an electronic component allows the reference electrode to be completely separated from the analyte system, in

the end it does not allow for accurate potential readings. Unlike the T-cell and the Y-cell, the D-cell design does not successfully implement a micro reference electrode. However, the insights gained in studying the characteristics of the D-cell elucidated the physics of the reference/working electrode connection.

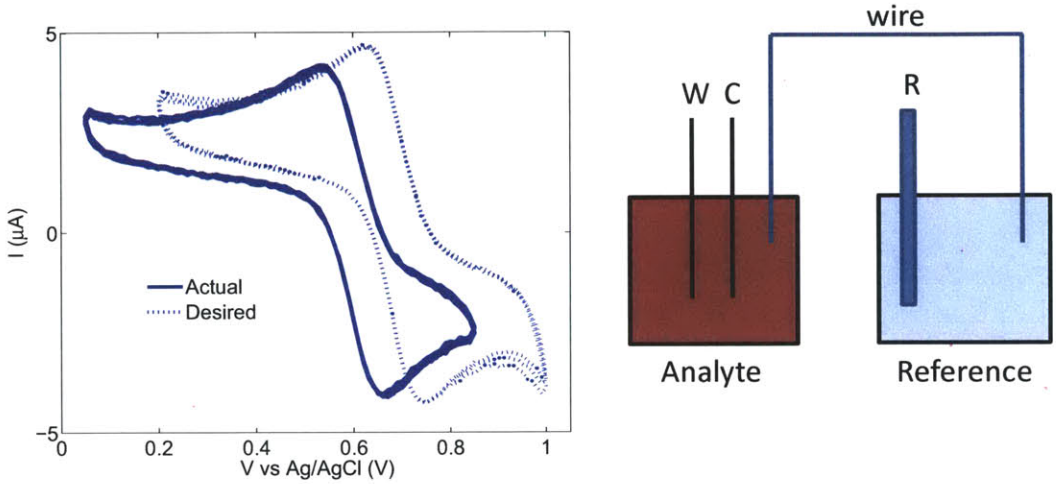

Figure 5-9: Batch Experiments Comparison. The solid blue line is a CV with the reference electrode placed in a separate reference solution with a connecting wire without connecting working and counter electrodes. The dashed blue line is the CV with the reference placed directly in the analyte solution. To the right of the CV is a schematic of the experimental setup.

Chapter 6

Surface Conduction

The role and application of surface conduction in microchannels is explored throughout this chapter. In classical electrokinetic systems, the term 'surface conduction' refers to the excess conduction that arises from increased ion concentrations in the electric double layer (EDL) [46]. Surface conduction in this case can be found by taking the total conduction and subtracting the conduction that would be found in the absence of an EDL. Bikerman first laid out a theory for surface conduction in the 1930's [47, 48]. For a particle or pore of characteristic length a, the ratio of surface conductivity, K_s, to bulk conductivity, K_b, is given by the Dukhin number: $Du = \frac{K_s}{aK_b}$.

While classic surface conduction is a function of the excess ion concentration, the type of surface conduction of interest in this work is related to the total surface charge density. The difference between these two values is shown in Figure 6-1. Let $\Gamma\pm$ be the total excess surface concentration (Figure 6-1a). This can be written as

$$\Gamma_+ = \int (c_+ - c_{bulk})dx, \ \Gamma_- = \int (c_- - c_{bulk})dx.$$

For a negatively charged surface, $\Gamma_+ > 0$ and $\Gamma_- < 0$. In classical electrokinetics, the excess surface conductivity will come from the excess neutral salt concentration, w [49, 50].

$$w = \int (c_+ + c_- - 2c_{bulk})dx = \Gamma_+ + \Gamma_-$$

However, in this work, the total surface ion concentration, or surface charge (q), plays an important role and is given by

$$q = \int (c_+ - c_-)dx = \Gamma_+ - \Gamma_-.$$

Here we consider an EDL at equilibrium and examine a new mechanism for conduction along a charged surface. This surface conduction is in *addition to*, rather than in *excess of*, the conduction through the bulk material. Throughout this chapter, only the surface conduction due to the total surface charge density will be discussed, and will be referred to as SC.

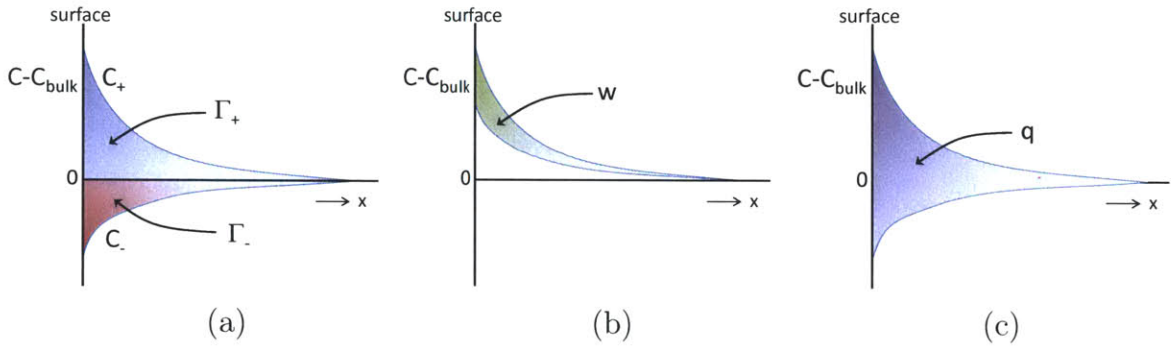

(a) (b) (c)

Figure 6-1: Ion Distribution Near a Charged Surface. a) Excess ion concentration, b) Excess neutral concentration, c) Surface charge density

Surface phenomena becomes particularly important at smaller length scales. For a surface with surface charge density, σ_s, the volume charge density, ρ_s will be equal to σ_s/a. As a decreases, the total amount of surface charge in a given volume may approach the amount of charge in the bulk material, ec_{bulk}. As will be demonstrated, the dimensionless volume surface charge density, $\tilde{\rho}_s = \frac{\sigma_s}{zeac_{bulk}}$, is an important quantity that will control the degree of SC. It is important to note that this term, while similar, is not the same as the Dukhin number. The Dukhin number depends on w, while $\tilde{\rho}_s$ depends on σ_s which is related to q. It is possible for w to be very small while maintaining a large q value, resulting in a large value for $\tilde{\rho}_s$ and a small Dukhin number.

Without SC, convection, or additional reactions, the amount of sustainable current in a system is limited by diffusion. At the limiting current, the reacting ion

concentration drops to zero at the reacting surface, and the reaction rate (current) can not go any faster. The addition of SC makes overlimiting current possible. While the bulk ion concentration may be zero at the reacting surface, ions remain near the charged surface and can still transmit current. This is achieved by ions moving from the bulk to the EDL, creating a depletion zone and concentration polarization (CP).

Steady depletion zones have been observed in microfluidic devices [51, 52] and have been shown to be affected by the channel geometry [53, 54]. Additionally, it has been shown that in very thin (1 μm) channels, these depletion interfaces can propagate with shock-like behavior [55, 56]. It was found that these shocks are due to geometry-dependent surface conduction [57].

In this chapter SC is shown to produce overlimiting current and CP. This was achieved by forming a simple 1D model that captures the nonlinear SC behavior (Sections 6.1-6.3). The 1D model was generated by taking an area average over the system's cross section and considering only the direction of the applied current or voltage. This method lends itself well to considering not only planar channels, but porous material as well. By averaging over the cross section, the pores in a porous structure need not be studied individually. This becomes particularly important as the dominance of SC increases with decreasing system length. While conventional microfabrication techniques allow for the creation of very thin microchannels, a porous structure can have a multitude of micro or nano pathways at once and can be readily fabricated. One possible application for this phenomenon is using the production of an ion depletion region to de-ionize water. In order to practically apply this technique, many fluidic pathways will be needed. Instead of fabricating an array of coupled microchannels, a large porous material can be used to scale up this technique while keeping a large surface area to volume ratio. Criteria for developing and using such a device are considered in Section 6.4.

6.1 1D Steady State Model without Convection

The simplest case to consider is a one-dimensional problem with no convection. This can done by averaging over the system's cross section and making several assumptions. One of the most significant assumptions is neglecting any electroosmotic flow. The presence of an electric field will force convection at a charged surface, and therefore could certainly play a role in this method of surface conduction. It should be noted that at smaller length scales, convection can be suppressed. Further more, this type of convection along the charged surface would only enhance the surface conduction predicted here. Therefore, neglecting convection in this study will yield the minimum possible surface conduction and isolate the effects of this phenomenon.

To begin, consider a single 2D channel of length L and width h. This channel is open at the left edge and sealed on the right edge by a perfectly cation-selective solid surface (e.g., metal electrode, perfect cation-selective membrane or a suitable nano-channel). The side walls of the channel are charged with a constant surface charge density σ_s, where $\sigma_s < 0$ to be relevant for most materials used in micro-structures, *eg.*, glass, silicones, silica, *etc.* The channel is filled by a symmetric, binary z:z electrolyte with concentration c_0 maintained at the open end of the channel. It will be shown that the non-linear effects of the wall's surface charge become increasingly important as dimensionless volume surface charge density, $\tilde{\rho}_s = \frac{\sigma_s}{zec_0h}$, increases. As a result, these effects may become noticeable even in a moderately charged pore if the pore size and/or initial electrolyte concentration are sufficiently low.

For long, narrow channels with thin double layers, the area-averaged Nernst-Plank equations are as follows:

$$D\left[\frac{d^2c_+}{dx^2} + \frac{d}{dx}\left(c_+\frac{d\tilde{\phi}}{dx}\right)\right] = 0,\ D\left[\frac{d^2c_-}{dx^2} - \frac{d}{dx}\left(c_-\frac{d\tilde{\phi}}{dx}\right)\right] = 0, \tag{6.1}$$

where $c_\pm$ is the area averaged concentration for the positively and negatively charged species, respectively, D is the diffusivity for the positive and negative ions (for simplicity is assumed to be the same), $\tilde{\phi}$ is dimensionless potential scaled to the thermal

voltage, kT/ze. The current density in the channel is defined by

$$i = i_+ + i_-,\ \frac{i_+}{ze} = -D\left(\frac{dc_+}{dx} + c_+\frac{d\tilde{\phi}}{dx}\right),\ \frac{i_-}{ze} = D\left(\frac{dc_-}{dx} - c_-\frac{d\tilde{\phi}}{dx}\right) = 0, \tag{6.2}$$

where i_+ is current density contribution from the cations and i_- is that from the anions. As the surface at the end of the channel is perfectly cation-selective, $i_- = 0$ there. Additionally, because the system is at steady state, the current in the channel is constant, that is, $\nabla \cdot i = 0$. Combining these two equations reduces the problem to first order:

$$\frac{dc_+}{dx} + c_+\frac{d\tilde{\phi}}{dx} = -\frac{i}{Dze},\ \frac{dc_-}{dx} - c_-\frac{d\tilde{\phi}}{dx} = 0. \tag{6.3}$$

In an electroneutral solution $c_+ = c_-$, however in this case the cations must balance not only the bulk anions but also the charge on the side walls. Therefore, c_+ and c_- are related by

$$c = c_- = c_+ + \frac{\rho_s}{ze}. \tag{6.4}$$

At the left edge of the channel, the boundary conditions are $\tilde{\phi}(0) = 0$ and $c = c_0$, where c_0 is the initial anion concentration. Integrating Equation 6.3 gives an implicit solution for the concentration profile (Equation 6.5). Setting the potential at the the right edge ($x = L$) equal to $-V$ provides an analytical relationship between the current and the voltage across the channel (Equation 6.6).

$$\tilde{\phi} = \ln(\tilde{c}),\ \tilde{c} - \tilde{\rho}_s \ln(\tilde{c}) = 1 - \tilde{i}\tilde{x}, \tag{6.5}$$

$$\tilde{i} = 1 - e^{-\tilde{V}} - \tilde{\rho}_s\tilde{V}. \tag{6.6}$$

These equations were nondimensionalized with $\tilde{\rho}_s = \frac{\rho_s}{2zec_0}$ as the dimensionless fixed charge density, $\tilde{c} = c/c_0$, and $\tilde{x} = x/L$, and $\tilde{i} = \frac{iL}{2zeDc_0}$ as the dimensionless current density scaled by the limiting current, corresponding to the case with neutral side walls.

In Figure 6-2 we illustrate the current-voltage dependence and the anion concentration profile for varying parameters. The current-voltage relationship has two linear

regions. At low voltages and high bulk conductivity $\tilde{i} \approx \tilde{V}(1-\tilde{\rho}_s)$, corresponding to a linear ohmic regime mediated by bulk conduction. At high voltages and low bulk conductivity $\tilde{i} \approx 1-\tilde{\rho}_s\tilde{V}$, corresponding to the dominance of SC.

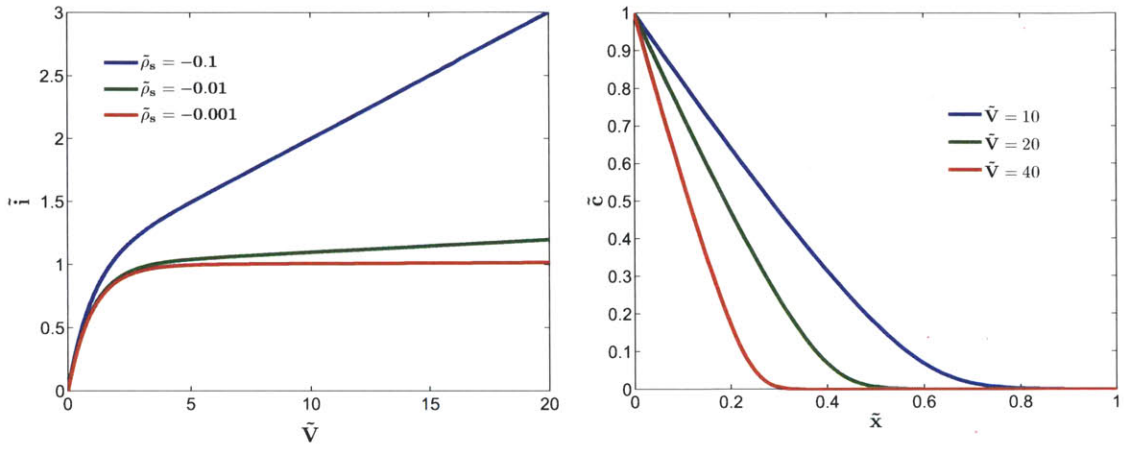

Figure 6-2: Numerical Results for 1D Model without Convection. (a) Current-voltage relationship; (b) Concentration profile for $\tilde{\rho}_s = -0.1$

The system inside the channel may be interpreted by considering two parallel resistances, a variable bulk resistance dependent on ion concentration and a constant surface resistance. In the case of relatively high ion concentration at the selective interface (underlimiting conditions), the bulk resistance is much lower than the surface resistance and the majority of the current passes through the bulk. When the system approaches the limiting current the co-ion concentration near the selective surface approaches zero. As the concentration drops, the resistivity of the bulk solution increases. Without SC this increase in resistance would limit the amount of current possible in the system. However, if SC is considered, current is diverted to the electric double layers along the side walls. The bulk current, $\tilde{i}_b$, and surface current, $\tilde{i}_s$, can be described as

$$\tilde{i}_b = -\tilde{c}\frac{d\tilde{\phi}}{d\tilde{x}}, \quad \tilde{i}_s = \tilde{\rho}_s\frac{d\tilde{\phi}}{d\tilde{x}}. \tag{6.7}$$

The bulk current [58] is determined by treating the electroneutral bulk as a uniform electrolyte and is proportional to the conductivity of the electrolyte and the applied electric field. The surface current is defined similarly, with the conductivity of the surface equal to $\tilde{\rho}_s$. The resulting current distributions are shown in Figure 6-3. In this

example the current is set to twice the limiting value. The bottom half of this figure displays the concentration profile in the channel, with the depletion region beginning around $\tilde{x} = 0.5$. Before the depletion region, nearly all the current is carried in the bulk, but at the beginning of the depletion region, the current rapidly switches to being carried almost entirely by surface current. It is the availability of this surface current that allows a depletion region to develop. In this manner, including the surface charge allows for a new mechanism for concentration polarization.

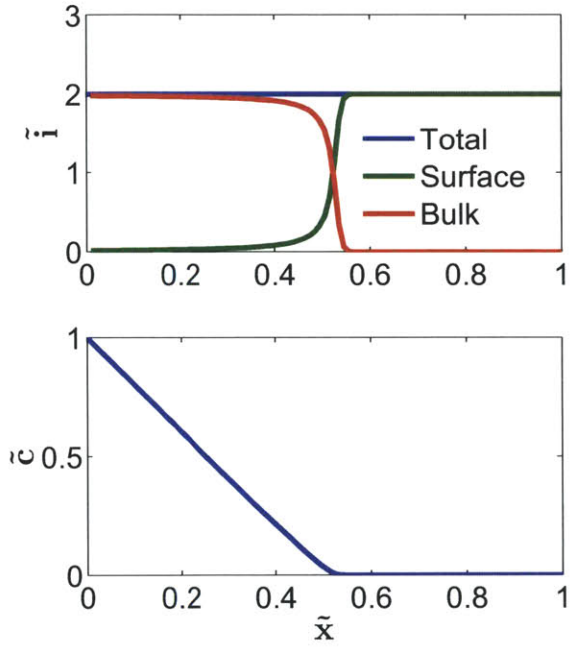

Figure 6-3: Overlimiting Current Distribution. The total current is set to twice the limiting value. Before the depletion region, current is carried mostly in the bulk. However, once the system is depleted, current is carried almost entirely by surface current.

6.1.1 Non-ideal Diffusivity

Throughout this chapter, diffusivity is treated as a constant physical parameter, independent of concentration. However, due to the depleted region with theoretically no bulk ions, concentration may vary significantly throughout the system. Re-writing

Equation 6.3 with a non-ideal diffusivity, gives

$$\tilde{D}\frac{d\tilde{c}}{d\tilde{x}} - \tilde{D}\tilde{\rho}_s\frac{d\ln(\tilde{c})}{d\tilde{x}} = -\tilde{i}, \tag{6.8}$$

with $\tilde{D} = \frac{D(c)}{D(c_0)}$ and $\tilde{i} = \frac{iL}{2zeD(c_0)c_0}$. Integrating by parts then yields

$$\tilde{D}\tilde{c} - \tilde{D}\tilde{\rho}_s \ln\tilde{c} - \int_1^{\tilde{c}} (\tilde{c}' - \tilde{\rho}_s \ln\tilde{c}')\frac{d\tilde{D}}{d\tilde{c}'}, d\tilde{c}' = 1 - \tilde{i}\tilde{x}. \tag{6.9}$$

Incorporating $\tilde{c}(1) = e^{-\tilde{V}}$ gives the revised current-voltage relationship

$$\tilde{i} = 1 - e^{-\tilde{V}}\tilde{D}(e^{-\tilde{V}}) - \tilde{\rho}_s\tilde{V}\tilde{D}(e^{-\tilde{V}}) + \int_1^{e^{-\tilde{V}}} (\tilde{c} - \tilde{\rho}_s \ln\tilde{c})\frac{d\tilde{D}}{d\tilde{c}}\, d\tilde{c}. \tag{6.10}$$

If D varies significantly along the channel, the current-voltage relationship will begin to deviate from the ideal case. In particular, overlimiting current will increase if the diffusivity strongly increases with decreasing concentration.

As an example, consider a diffusivity correction from the Debye-Huckel theory. The Debye-Huckel formula for the activity of an ionic species is given by

$$\ln\gamma = -\frac{(ze)^2}{8\pi\epsilon kT\lambda}, \ \lambda = \sqrt{\frac{\epsilon kT}{2(ze)^2 c}}, \tag{6.11}$$

where γ is the activity coefficient, ϵ is the permittivity of the solvent, and λ is the Debye length. λ is assumed to be larger than the effective ion size, and the electrolyte is binary and symmetric (z:z). The relationship between a non-ideal diffusivity and the activity coefficient [58] is given by

$$D(c) = D_i\left(1 + c\frac{d\ln\gamma}{dc}\right), \tag{6.12}$$

where D_i is the ideal diffusivity found by the Einstein relationship and is assumed to be constant.

Combining Equations 6.9-6.12, the effect of a non-ideal diffusivity can be found for varying initial ion concentration. In Figures 6-4 and 6-5 we see that for very dilute

solutions (1mM) there is very little change in the current-voltage relationship and concentration profile. However, at larger concentrations (1M) there is a significant deviation. The overlimiting current is larger than expected from the ideal case and the depletion region is wider. This arises as a result of the diffusivity increasing in the depleted region leading to an increase in mass transfer. While the Debye-Huckel theory specifically applies to dilute solutions, this result indicates that a non-ideal diffusivity may need to be incorporated when considering higher initial ion concentrations.

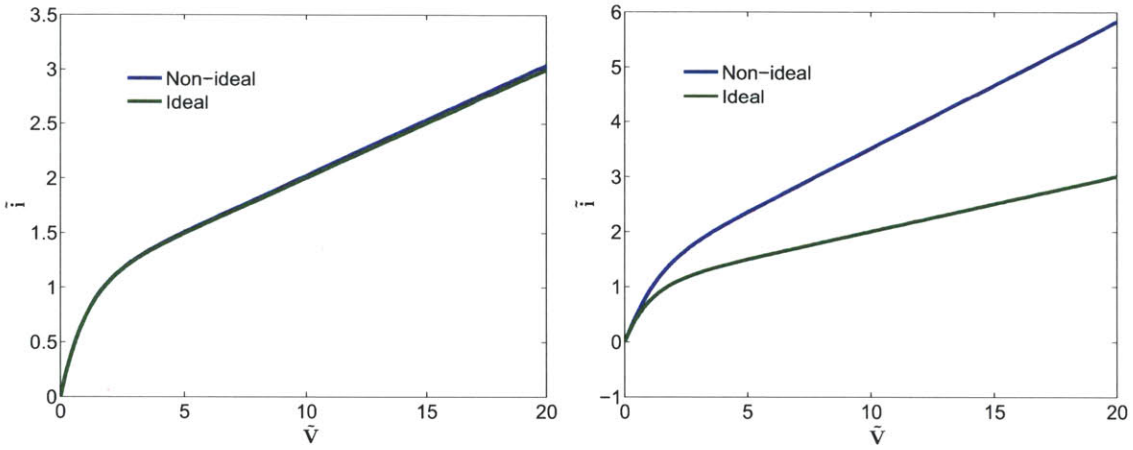

Figure 6-4: Current-Voltage Relationship with Non-ideal Diffusivity. (a) c_0=1mM; (b) c_0=1M. The current-voltage relationship due to a non-ideal diffusivity only deviates from the ideal case at larger initial ion concentrations.

6.2 1D Transient Model without Convection

In the previous section, it was shown that overlimiting current could be achieved in the steady state case. However, for short times, overlimiting current can be easily achieved in a classical system even without SC. In the classical case, this overlimiting current cannot be sustained and the voltage across the system goes to infinity. In this section the temporal voltage response is explored when SC is included.

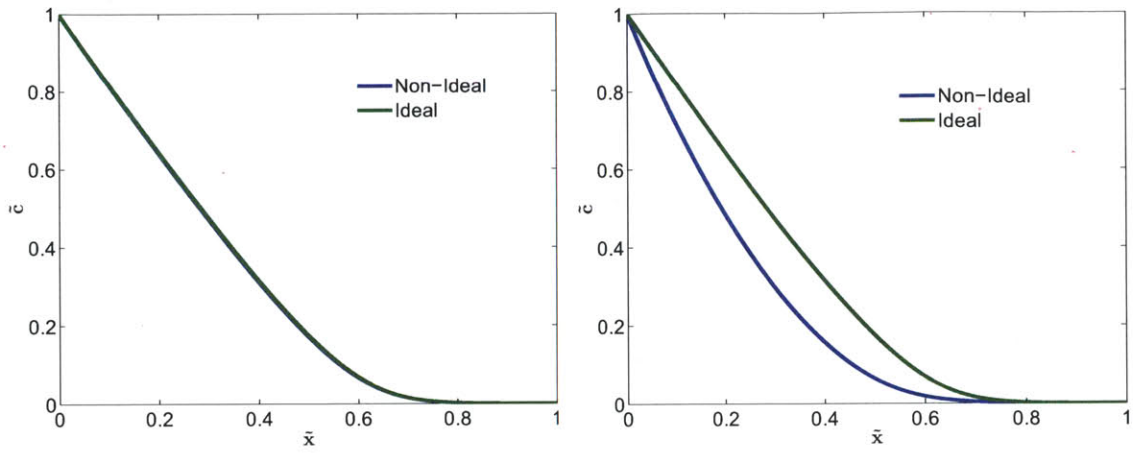

(a) (b)

Figure 6-5: Concentration Profile with Non-ideal Diffusivity. (a) c_0=1mM; (b) c_0=1M. In the case of a non-ideal diffusivity, the diffusivity increases in the depleted region, leading to an increase in mass transfer. This then results in a slightly larger depleted region for cases with a higher initial ion concentration.

The one dimensional, transient conservation and current equations are given by

$$\frac{dc_+}{dt} = D\left[\frac{d^2c_+}{dx^2} + \frac{d}{dx}\left(c_+\frac{d\tilde{\phi}}{dx}\right)\right],\ \frac{dc_-}{dt} = D\left[\frac{d^2c_-}{dx^2} - \frac{d}{dx}\left(c_-\frac{d\tilde{\phi}}{dx}\right)\right], \tag{6.13}$$

$$i = i_+ + i_-,\ \frac{i_+}{ze} = -D\left(\frac{dc_+}{dx} + c_+\frac{d\tilde{\phi}}{dx}\right),\ \frac{i_-}{ze} = D\left(\frac{dc_-}{dx} - c_-\frac{d\tilde{\phi}}{dx}\right). \tag{6.14}$$

Nondimensionalizing as in the previous section with $\tilde{t} = \frac{tD}{L^2}$, the conservation equations can be written as shown in Equation 6.15. The reaction boundary condition for concentration ($i_- = 0$) and the current-voltage equation are shown in Equation 6.16. If $\tilde{\rho}_s$ and $\tilde{V}$ are known, the concentration profile and current-voltage relationship can be found.

$$\frac{d\tilde{c}}{d\tilde{t}} = \frac{d^2\tilde{c}}{d\tilde{x}^2} - \tilde{\rho}_s\frac{d^2\tilde{\phi}}{d\tilde{x}^2},\ \frac{d}{d\tilde{x}}\left[\left(\tilde{c} - \tilde{\rho}_s\right)\frac{d\tilde{\phi}}{d\tilde{x}}\right] = 0 \tag{6.15}$$

$$\tilde{i} = -\left(\tilde{c} - \tilde{\rho}_s\right)\frac{d\tilde{\phi}}{d\tilde{x}},\ \left.\frac{d\ln\tilde{c}}{d\tilde{x}}\right|_{\tilde{x}=1} = \left.\frac{d\tilde{\phi}}{d\tilde{x}}\right|_{\tilde{x}=1} \tag{6.16}$$

In some cases the voltage across the system is not known *a priori*. In these cases it may be easier to rewrite the problem in a galvanostatic manner. In this way,

the concentration and potential equations can be decoupled and solved sequentially. When rewriting these equations, it may be simpler to consider the total ion concentration, $k = c_+ + c_-$, instead of the anion concentration, $c = c_-$. Setting $\tilde{k} = \frac{k}{2c_0}$ the galvanostatic equations are

$$\frac{d\tilde{k}}{d\tilde{t}} = \frac{d^2\tilde{k}}{d\tilde{x}^2} - \frac{\tilde{\rho}_s\tilde{i}}{\tilde{k}^2}\frac{d\tilde{k}}{d\tilde{x}}, \quad \frac{d}{d\tilde{x}}\left[\tilde{k}\frac{d\tilde{\phi}}{d\tilde{x}}\right] = 0, \tag{6.17}$$

$$\tilde{i} = -\tilde{k}\frac{d\tilde{\phi}}{d\tilde{x}}, \quad \left.\frac{d\tilde{k}}{d\tilde{x}}\right|_{\tilde{x}=1} + \frac{\tilde{\rho}_s\tilde{i}}{\tilde{k}(\tilde{x}=1)} = -\tilde{i}. \tag{6.18}$$

If $\tilde{i}$ is known, the concentration profile can be determined separately from the potential distribution. This method may aid computational problems and fitting experimental data.

The transient concentration profile for three different currents is shown in Figure 6-6 ($\tilde{\rho}_s = -0.01$). In the case of underlimiting current ($\tilde{i} = 0.9$) and slightly overlimiting current ($\tilde{i} = 1.1$), the system has reached equilibrium by the time the anion concentration reaches its lowest value. However, in the case of high overlimiting conditions ($\tilde{i} = 5$), a depletion region develops and grows with time. As predicted by Mani *et al.* [55], a concentration polarization shock appears and pushes the ions away from the selective surface.

As mentioned earlier, in a classical system with no SC, an overlimiting current will force the voltage drop to increase infinitely with time. The voltage drop goes to infinity because the concentration goes to zero at one wall, which results in an infinite resistance at that point. The time at which the concentration reaches zero is referred to as Sand time, t_{Sand}, for H.J.S. Sand [59]. In a finite system $t_{\text{Sand}} = \frac{\pi L^2}{4D\tilde{i}^2}$ [60]. The transient voltage response for varying applied currents is shown in Figure 6-7 ($\tilde{\rho}_s = -0.01$). At a certain point in each curve the voltage rapidly increases until it reaches the steady value. The point of rapid increase corresponds to the creation of a depletion region. In the second half of Figure 6-7 the time is rescaled with respect to Sand time. The curves overlap with the point of rapid increase corresponding to $t = t_{\text{Sand}}$. The time scales for the classical case still apply when SC is taken

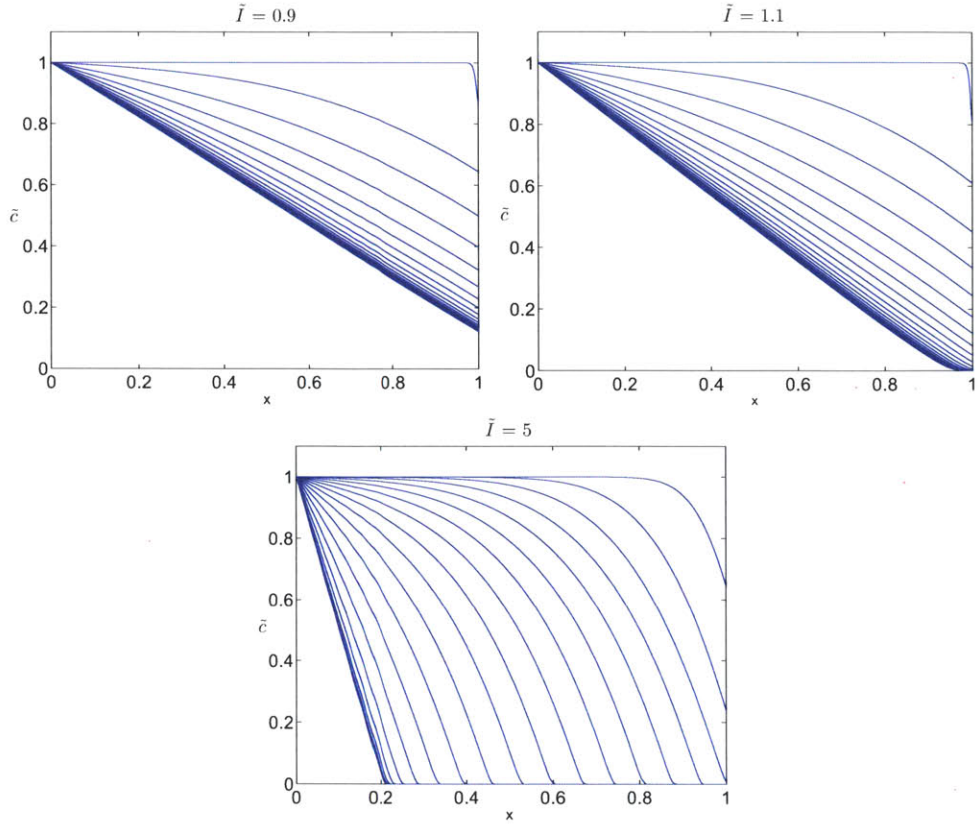

Figure 6-6: Transient Concentration Profiles. In each plot, concentration profiles are shown at increasing times. At early times the concentration profile is almost flat at a value of 1. As time increases the ion concentration at the right edge decreases and, depending on the applied current, a depletion region will form and grow.

into consideration. This can be further shown by demonstrating the impact of $\tilde{\rho}_s$ in Figure 6-8. In this figure the voltage response is shown for decreasing surface charge. As $\tilde{\rho}_s$ decreases an order of magnitude the voltage drop increases about an order of magnitude. As the dimensionless surface charge continues to decrease the system grows closer to the classical result, as expected.

6.3 1D Steady State Model with Convection

In the previous sections, it was shown that SC can allow for overlimiting currents that force ion depletion regions to develop. Theoretically, in the bulk of these depletion regions the ion concentration is zero. If properly harnessed, this method could be used as a de-ionization technique. However, for this to work, there needs to be a

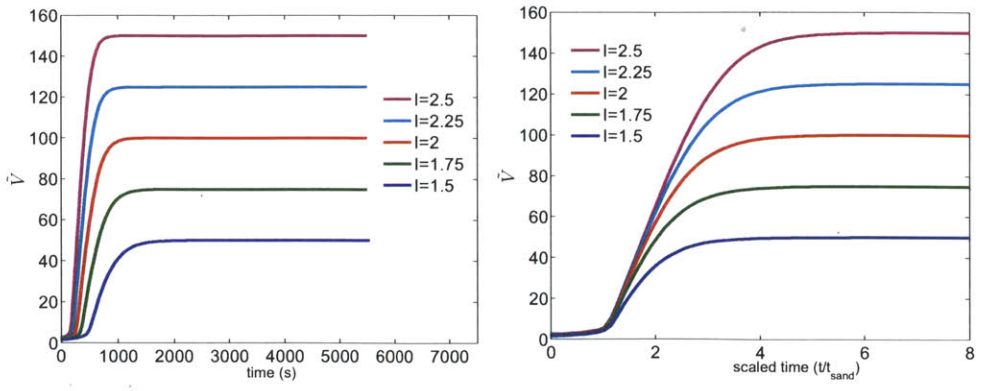

Figure 6-7: Transient Voltage Response

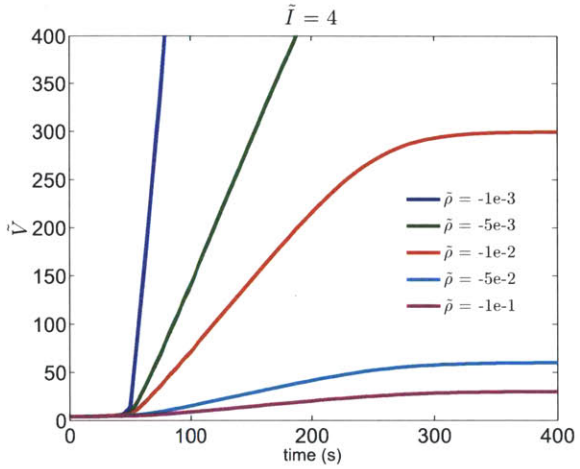

Figure 6-8: Transient Voltage Response for Varying Surface Charge

method to remove the de-ionized fluid. This section explores how convection may be used to extract the de-ionized fluid.

First, we consider a simple 1D model to examine convection parallel to the ionic current. Consider the scenario mentioned in Section 6.1. Instead of the right wall being solid, now it is a perfect porous electrode. This electrode allows fluid to pass through while maintaining the electronic characteristics of a solid electrode. Additionally, assume that the velocity of the fluid, u, is uniform throughout the channel and remains unidirectional. This assumption is especially valid for a channel consisting of a porous material. With these assumptions, the conservation and current

equations are as follows

$$u\frac{dc_+}{dx} = D\left[\frac{d^2c_+}{dx^2} + \frac{d}{dx}\left(c_+\frac{d\tilde{\phi}}{dx}\right)\right],\ u\frac{dc_-}{dx} = D\left[\frac{d^2c_-}{dx^2} - \frac{d}{dx}\left(c_-\frac{d\tilde{\phi}}{dx}\right)\right], \tag{6.19}$$

$$i_{\text{electrode}} = i_+ + i_-,\ \frac{i_+}{ze} = -D\left(\frac{dc_+}{dx} + c_+\frac{d\tilde{\phi}}{dx}\right),\ \frac{i_-}{ze} = D\left(\frac{dc_-}{dx} - c_-\frac{d\tilde{\phi}}{dx}\right) = 0. \tag{6.20}$$

It is important to note that due to the porous nature of the electrode, the current from the electrode, $i_{\text{electrode}}$, is not the same as the total current in the channel. The current in the channel will have an additional convection term, but since the fluid passes through the electrode, it does not appear in the electrode current.

Using the Peclet number ($Pe = \frac{uL}{D}$) as the dimensionless velocity, the dimensionless, potentiostatic equations are as follows

$$Pe\frac{d\tilde{c}}{d\tilde{x}} = \frac{d^2\tilde{c}}{d\tilde{x}^2} - \tilde{\rho}_s\frac{d^2\tilde{\phi}}{d\tilde{x}^2},\ \frac{d}{d\tilde{x}}\left[(\tilde{c} - \tilde{\rho}_s)\frac{d\tilde{\phi}}{d\tilde{x}}\right] = 0, \tag{6.21}$$

$$\tilde{i} = -(\tilde{c} - \tilde{\rho}_s)\frac{d\tilde{\phi}}{d\tilde{x}},\ \left.\frac{d\ln\tilde{c}}{d\tilde{x}}\right|_{\tilde{x}=1} = \left.\frac{d\tilde{\phi}}{d\tilde{x}}\right|_{\tilde{x}=1}. \tag{6.22}$$

Rearranging and using $\tilde{k}$, the total ion concentration, instead of $\tilde{c}$, the galvanostatic equations are

$$Pe\frac{d\tilde{k}}{d\tilde{x}} = \frac{d^2\tilde{k}}{d\tilde{x}^2} - \frac{\tilde{\rho}_s\tilde{i}}{\tilde{k}^2}\frac{d\tilde{k}}{d\tilde{x}},\ \frac{d}{d\tilde{x}}\left[\tilde{k}\frac{d\tilde{\phi}}{d\tilde{x}}\right] = 0, \tag{6.23}$$

$$\tilde{i} = -\tilde{k}\frac{d\tilde{\phi}}{d\tilde{x}},\ \left.\frac{d\tilde{k}}{d\tilde{x}}\right|_{\tilde{x}=1} + \frac{\tilde{\rho}_s\tilde{i}}{\tilde{k}(\tilde{x}=1)} = -\tilde{i}. \tag{6.24}$$

Using these equations, concentration profiles and current-voltage relationships can be found. In Figure 6-9 several concentration profiles are shown for varying voltage and Pe values. As before, increasing the applied voltage increases the amount of depletion. The addition of convection pushes ions to the right and the linear concentration profile is lost. As the flow rate increases the concentration profile appears more shock-like with a decreasing shock width. In this case the dimensionless concentration to the left of the depletion region approaches a constant value of 1.

Additionally, as the flow rate increases the depletion region shrinks, requiring a higher applied voltage to maintain its size. Figure 6-10 shows the current-voltage relationship for $Pe = 5$. Here the morphology of the curve is noticeable different from the case with no convection (Figure 6-2). However, at higher voltages the overlimiting current eventually becomes linear as seen in Section 6.1.

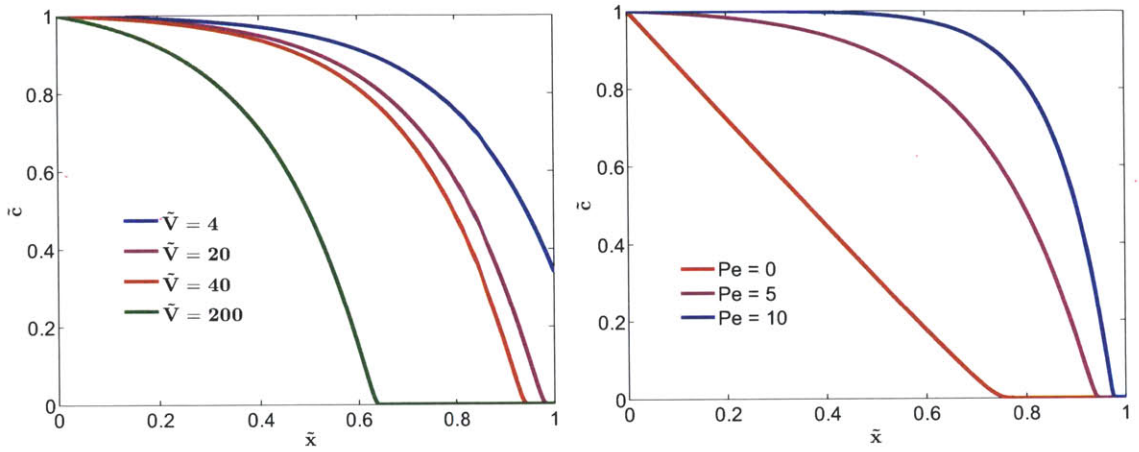

(a) (b)

Figure 6-9: Concentration Profiles for 1D Model with Convection. (a) $\tilde{\rho}_s = -0.01$, $Pe = 5$; (b) $\tilde{\rho}_s = -0.01$, $\tilde{V} = 40$

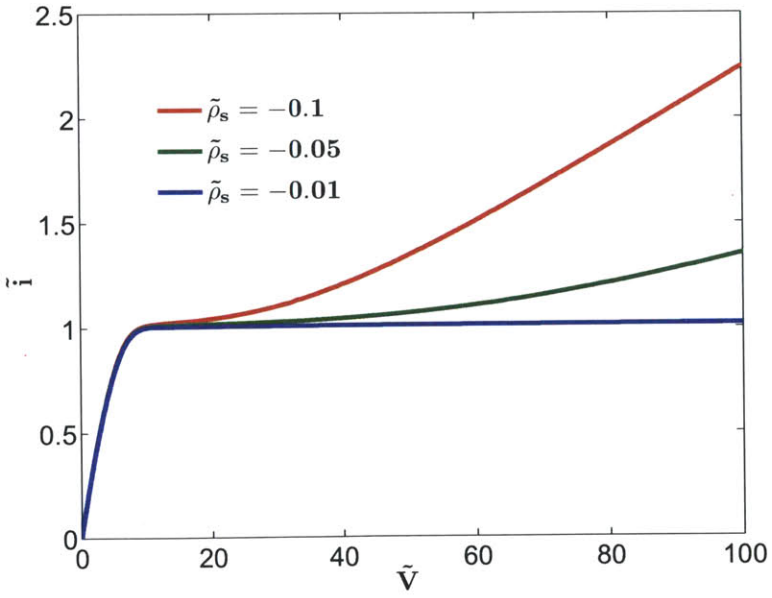

Figure 6-10: Current-Voltage Relationship for 1D Model with Convection. $Pe = 5$

In addition to concentration and current, the de-ionization energy can be esti-

mated. The energy per volume, A (with dimensionless $\tilde{A}$), is equal to the power required to de-ionize (IV) divided by the volumetric flow rate (Q)

$$A = \frac{IV}{Q} = 2kTc_0\frac{\tilde{i}\tilde{V}}{Pe},\ \tilde{A} = \frac{A}{2kTc_0} = \frac{\tilde{i}\tilde{V}}{Pe}. \tag{6.25}$$

$\tilde{A}$ will be a function of the surface charge density, $\tilde{\rho}_s$, the applied current, $\tilde{i}$, and the dimensionless velocity, Pe.

The dimensionless energy per volume of a fixed system is shown in Figure 6-11. In these plots $\tilde{A}$ is shown versus varying Pe and $\tilde{i}$ for two different values of $\tilde{\rho}_s$ (-0.01 and -0.0001). A black line indicating when the depletion region has formed ($\tilde{c} = 0.001$) is placed on top of these surface plots. Below this line $\tilde{c}$ is less than 0.001 and the energy per volume increases. The energy profile appears very similar in these two plots, with the values differing by a factor of 100. In the 1D case, surface conduction goes as $\tilde{\rho}_s\tilde{V}$. Therefore as $\tilde{\rho}_s$ decreases by a factor of 100, the voltage must increase by a factor of 100 to maintain the same level of conduction. This increase in necessary voltage is what leads to the 100-fold increase in energy.

In order to reduce the energy per volume required while maintaining depletion, the depletion region should be as small as possible. This is why increasing the flow rate (Pe) decreases $\tilde{A}$. Similarly, increasing the applied current past the point of early depletion wastes energy and increases $\tilde{A}$. Because this model is only 1D, all of the fluid recovered can be depleted, giving a recovery rate of 100%. While this model provides an estimate on the concentration profile, current-voltage relationship, and energy costs, it is not sufficient to define a realistic system. In the following section, a 2D model is suggested that provides more realistic results.

6.4 2D Steady State Model with Convection

So far only one-dimensional problems have been considered. In order to extract fluid from this type of system, perpendicular cross flow can be used. In this way, convection will run perpendicular to the applied potential/current, pushing fluid out

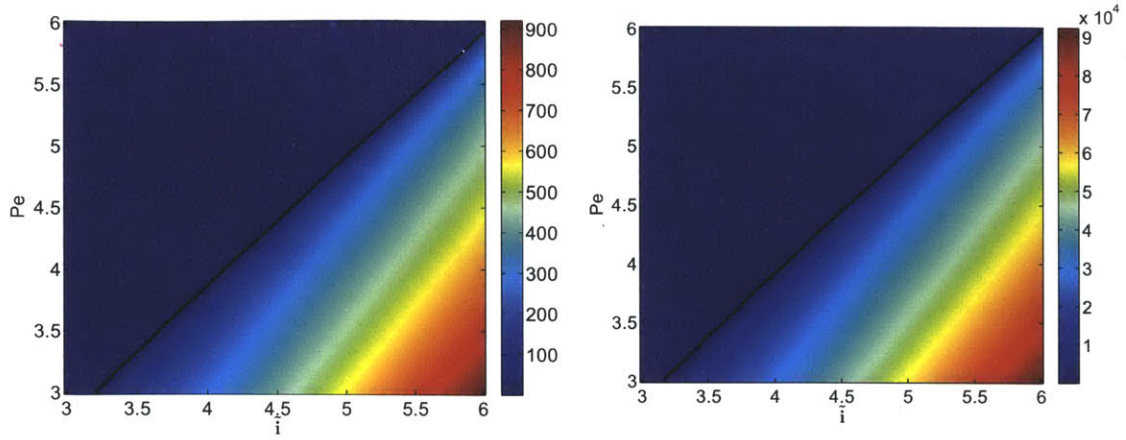

(a) (b)

Figure 6-11: Dimensionless Energy per Volume for 1D Model with Convection. The black line indicates where a depletion region has formed. Below this line the outlet concentration, $\tilde{c}$, is 0.001 or less. (a) $\tilde{\rho}_s = -0.01$; (b) $\tilde{\rho}_s = -0.0001$

of the system. Using flow fractionation, or splitting the outflow, de-ionized fluid can be collected. A schematic of this type of device is shown in Figure 6-12.

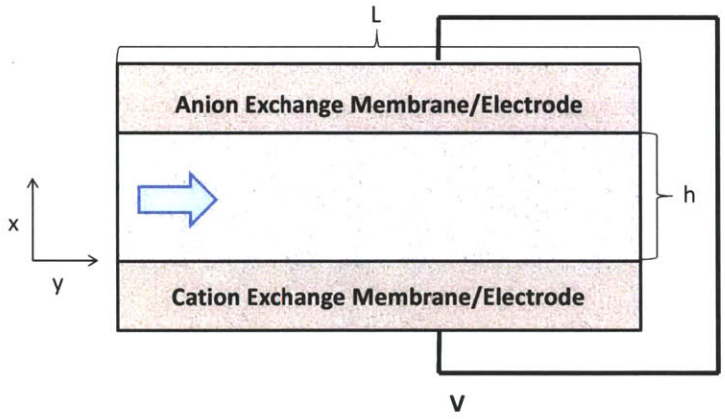

Figure 6-12: De-ionization Device Schematic

Several parameters will affect the efficacy and the efficiency of such a device, including the surface charge of the material, the geometry of the device, and the applied current/potential. In order to understand how these parameters relate to each other, a simplified 2D model was created. The purpose of this model is to help design a future de-ionization device and to give insight into de-ionization efficiency in a microfluidic device.

To begin, consider a porous structure of height, h, and length, L, where $x \in [0, h]$ and $y \in [0, L]$. Uniform, unidirectional flow with velocity, u, originates from $y = 0$. In this 2D model, assume that the flow velocity is large enough such that convection is dominant in the y-direction and that diffusion only occurs in the x-direction. As a result, potential is constant in the y-direction, and is only a function of x. The conservation equations are as follows

$$u\frac{dc_+}{dy} = D\left[\frac{d^2c_+}{dx^2} + \frac{d}{dx}\left(c_+\frac{d\tilde{\phi}}{dx}\right)\right],\ u\frac{dc_-}{dy} = D\left[\frac{d^2c_-}{dx^2} - \frac{d}{dx}\left(c_-\frac{d\tilde{\phi}}{dx}\right)\right]. \tag{6.26}$$

Nondimensionalizing as before, with $\tilde{x} = \frac{x}{h}$ and $\tilde{y} = \frac{y}{L}$, the dimensionless conservation equations are

$$\frac{uh^2}{LD}\frac{d\tilde{c}}{d\tilde{y}} = \frac{d^2\tilde{c}}{d\tilde{x}^2} - \tilde{\rho}_s\frac{d^2\tilde{\phi}}{d\tilde{x}^2},\ \frac{d}{d\tilde{x}}\left[(\tilde{c} - \tilde{\rho}_s)\frac{d\tilde{\phi}}{d\tilde{x}}\right] = 0. \tag{6.27}$$

In the previous sections the channel or porous structure was in contact with a reservoir of constant concentration. In this case, ions are being removed from both sides ($x = 0$ and $x = h$) therefore the boundary conditions are both Neumann type, that is

$$\tilde{x} = 0 : \tilde{\phi} = -\tilde{V},\ \frac{d\ln\tilde{c}}{d\tilde{x}} = \frac{d\tilde{\phi}}{d\tilde{x}}, \tag{6.28}$$

$$\tilde{x} = 1 : \tilde{\phi} = 0,\ \frac{d\ln\tilde{c}}{d\tilde{x}} = \frac{d\tilde{\phi}}{d\tilde{x}}, \tag{6.29}$$

$$\tilde{y} = 0 : \tilde{c} = 1. \tag{6.30}$$

Noticing that several parameters of interest are lumped together, the conservation equation can be rewritten with a new variable f, where

$$f = \frac{LD\tilde{y}}{uh^2} = \frac{L}{h}\frac{\tilde{y}}{Pe}. \tag{6.31}$$

The conservation equation is therefore

$$\frac{d\tilde{c}}{df} = \frac{d^2\tilde{c}}{d\tilde{x}^2} - \tilde{\rho}_s\frac{d^2\tilde{\phi}}{d\tilde{x}^2}. \tag{6.32}$$

With this change of variables, the conservation equation becomes the same as the 1D, transient equation, Equation 6.15. Therefore, the solutions from the previous section can be reworked and applied here. Example concentration profiles are shown in Figure 6-13 for $\tilde{\rho}_s = -0.01, -0.05$ and $\tilde{V} = 30$. As expected, increasing the surface charge increases the size of the depleted region, δ. Here δ was taken to be the point where $\tilde{c} = 0.001$. It is also important to note that at around $f = 0.1$ the concentration has reached its steady state value and no further de-ionization occurs. By setting $\tilde{y} = 1$ these plots can be used to examine the outlet concentration distribution. For example, in the case of $\tilde{\rho}_s = -0.05$ (Figure 6-13b) the outlet can be fractioned at $\tilde{x} = 0.25$ and if $f > 0.1$ only de-ionized fluid will be collected. This analysis can be used to determine the best geometry and flow rate. In order to maximize the flow rate, f should be minimized. In order to get full depletion, f should be set to its steady state value, which for these two cases is around 0.1. Additionally, scaling up the system will not be a linear process, since $f \propto \frac{L}{h^2}$.

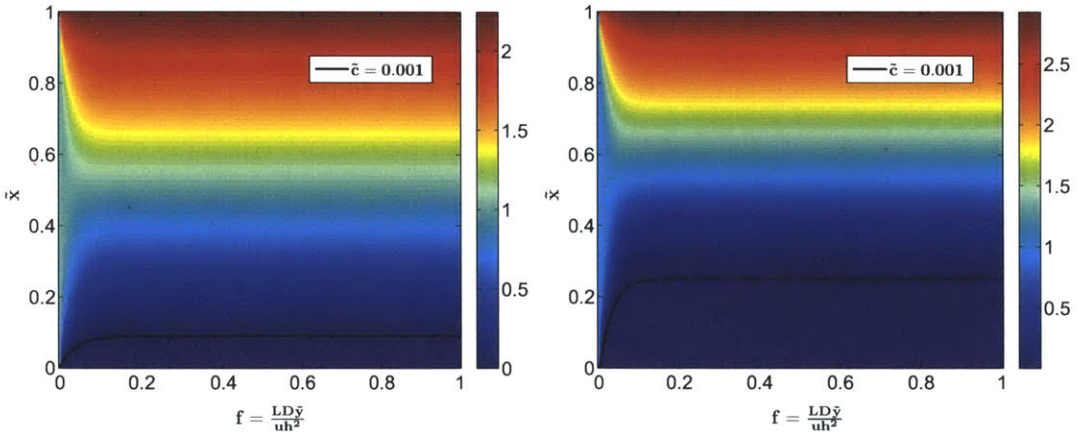

Figure 6-13: 2D Concentration Profile. a) $\tilde{\rho}_s = -0.01$ and $\tilde{V} = 30$, b) $\tilde{\rho}_s = -0.05$ and $\tilde{V} = 30$.

An important characteristic of any de-ionization technique is the energy required to de-ionize. For a volumetric flow rate of Q, with current, I, and voltage, V, the energy required per volume of de-ionized water is as follows:

$$A = \frac{IV}{\delta Q} = 2RTC_0 \frac{h}{L} \frac{f\tilde{i}\tilde{V}}{\delta} \tag{6.33}$$

The parameters $\tilde{i}$, $\tilde{V}$, and δ are related through the conservation and current equations. If f is at a steady state value, $\tilde{V}$ and δ can be found based solely on $\tilde{i}$ and $\tilde{\rho}_s$. As a result, it is advantageous to consider the dimensionless energy efficiency, $\tilde{A}$

$$\tilde{A} = \frac{AL}{2RTc_0hf} = \frac{\tilde{i}\tilde{V}}{\delta} \tag{6.34}$$

A plot of $\tilde{A}$ over a range of $\tilde{i}$ and $\tilde{\rho}_s$ values is shown in Figure 6-14. Due to the Neumann boundary conditions, depletion begins at $\tilde{i} = 2$ instead of at 1 as seen in the previous sections. For the most part, increasing the surface charge decreases the de-ionization energy. However, for lower currents the increase in surface charge actually prevents depletion. The increase in SC allows for a greater number of ions to be consumed at the reactive surface before depletion begins. Therefore an increase in surface charge at lower currents can shrink or even eliminate the depletion region, leading to a sharp increase in required energy. Additionally, increasing the applied current can lead to relatively sharp increases in $\tilde{A}$, this is particularly shown in the lower right hand corner of Figure 6-14. At this point the increase in power cost overwhelms the efficiency gained by creating a larger depletion region. Once $\tilde{i}$ and $\tilde{\rho}_s$ have been determined, the energy efficiency can be calculated. This efficiency can be enhanced by properly designing the system geometry. For example, the larger the aspect ratio, L/h, the lower the de-ionization energy, as seen in Equation 6.33.

In addition to energy requirements, in order to develop a practical device, water recovery must be considered. A very efficient device that only de-ionizes 1% of an incoming stream is not terribly useful. In this case many passes would be required to de-ionize a sufficient amount of water. Water recovery in this model corresponds to the size of the depletion region, δ. A plot of δ versus $\tilde{i}$ and $\tilde{\rho}_s$ is shown in Figure 6-15. The region of highest water recovery does not correspond to the region of lowest energy per volume (Figure 6-14). Therefore a balance must be struck between the two values, depending on the requirements of a desired system.

In order to complete a de-ionization device design, one other parameter needs to be addressed. Throughout this chapter the parameter $\tilde{\rho}_s$ has played an important

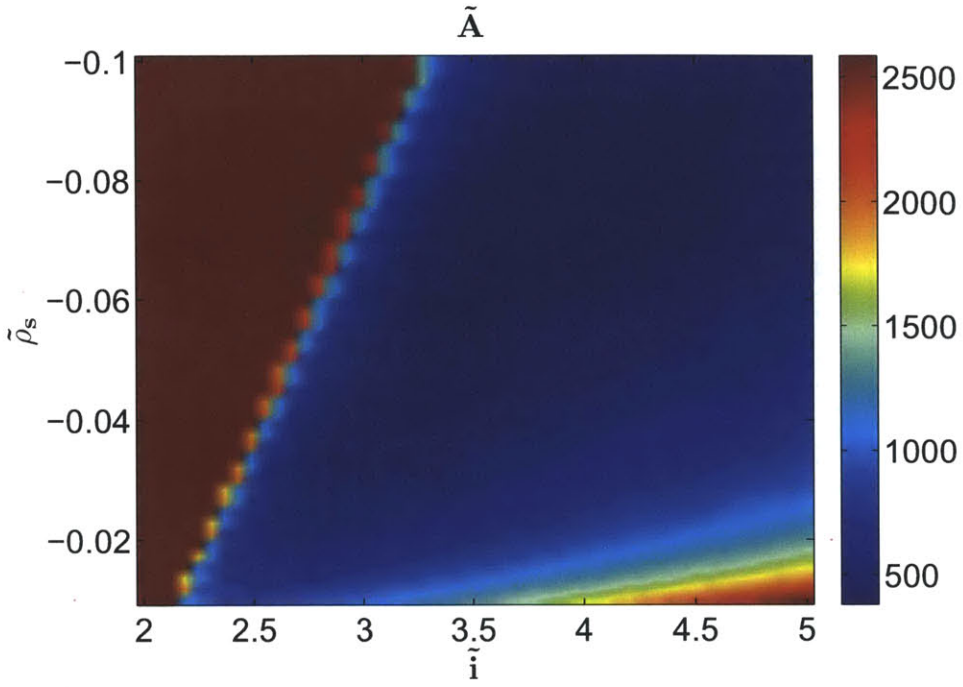

Figure 6-14: Energy per Volume of De-ionized Fluid

role. However, this parameter is a function of the initial anion concentration, c_0. The power of SC goes up as c_0 goes down. In order to have an effect on higher ion concentrations, the volume surface charge density, ρ_s of the material should be increased. This can be done by either altering the surface charge of the material, σ_s or decreasing the pore size. For instance, a typical silica bead in water has a surface charge density of about -0.001 coul/m^2 [61]. In a 1mM solution, a porous structure of these beads with a pore size of 10 μm will result in $\tilde{\rho}_s = -0.001$. However, if the pore size decreases to 100 nm, then $\tilde{\rho}_s = -0.1$ and SC plays are more dominant role. Based on this analysis, the smaller the pores, the better the de-ionization. However, the energy analysis conducted here did not take into consideration the force to pump the fluid through the porous material. As the pore size decreases the pump energy required increases. As a result, decreasing the pore size may not be the best solution. Alternatively, the surface of the porous material can be altered to create a more negative surface. With a judicious choice of porous material, a de-ionization device can be designed, taking into consideration the guidelines mentioned here. In order to maximize the energy efficiency, the device should be designed with a high aspect ratio.

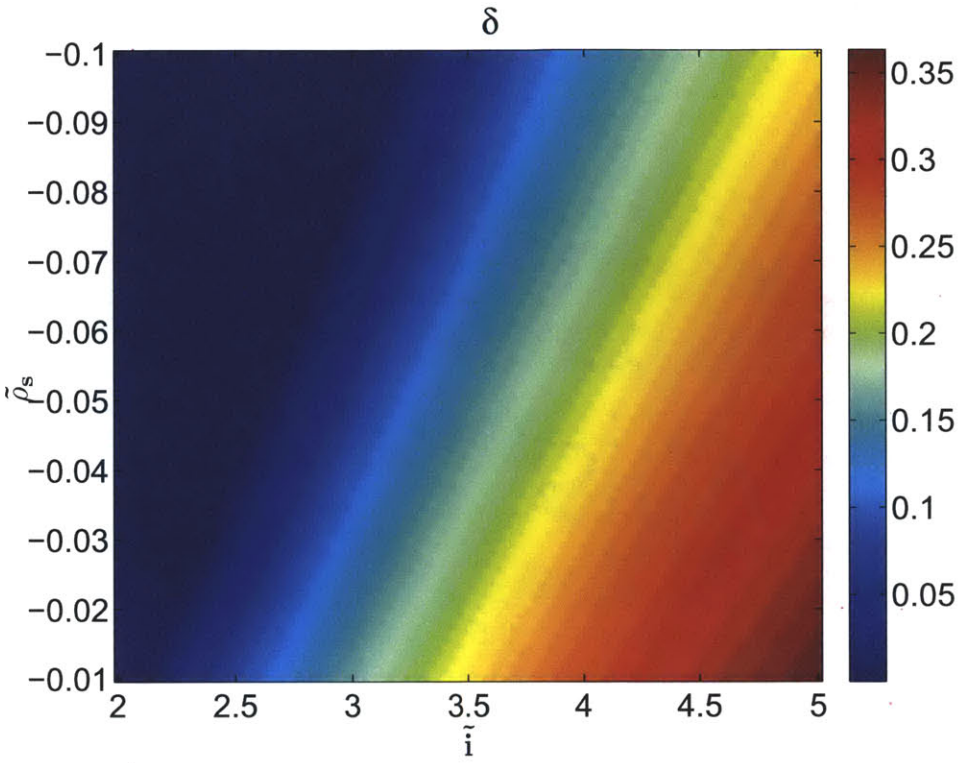

Figure 6-15: Water Recovery of De-ionized Fluid. Water recovery increases with increasing $\tilde{i}$ and decreasing $\tilde{\rho}_s$.

Additionally, the velocity should be maximized such that f defined in Equation 6.31 is kept low but at a steady state value. Based on Figures 6-14 and 6-15, the applied current should be above the limiting value but low enough such that the energy per volume and water recovery are at acceptable levels. In this manner SC can be used to de-ionize water in a novel way with simple materials.

Chapter 7

Summary

7.1 Continuous Electrochemistry

Continuous chemistry makes automation, rapid optimization, and chemical screening possible. Conducting continuous chemistry in a microchannel greatly reduces the amount of material required and leads to more uniform reaction conditions. Developing a microfluidic continuous electrochemical cell would bring these advantages to electrochemistry and open up new possibilities. In fact, a continuous electrochemical method has already been developed, the channel electrode. However, this method is limited and can only accurately measure current. Previously, there was no simple technique to accurately determine the voltage in a continuous, microfluidic system. If the voltage can not be determined, several areas of research can not be investigated, *e.g.* energy, thermodynamics, and screening techniques. This drastically limits the scope of the electrochemical experiments that can be performed with such a device.

Channel electrode devices consist of electrodes embedded in a wall of a fluidic channel. A potential or current is applied at these electrodes and the analyte in the fluid reacts at the electrode surface. The rate of reaction (current) is determined by the electric potential of the electrode. In order to accurately determine or impose this potential, a reference electrode is needed. In larger systems a macro reference electrode can be used. However, when considering micro systems this becomes more difficult. Placing a macro reference outside of the microchannel leads to a higher

cell resistance which can then lead to noise and electrical instability. The smaller the microchannel, the larger the cell resistance and the more important reference electrode placement becomes.

In order to place a reference electrode inside a microfluidic device, the electrode must be made smaller. However, not all of the components of a reference electrode are easily miniaturized. In order for a reference electrode to remain at a fixed potential it must not be contaminated by the analyte. However, this electrode must also remain in ionic contact with the working electrode. In a macro device this is solved by using a conductive physical barrier, such as a porous glass frit. The pores are kept small to prevent reference and analyte solutions from mixing while still allowing ions to conduct through the glass structure. While this is simple to fabricate and implement on a macro scale, it is non-trivial in a micro device. The existing methods for fabrication of microfluidic references either place the reference far away from the working electrode (leading to higher resistance) or are limited to special materials. This work investigated new methods for incorporating a true reference electrode into a microfluidic electrochemical device.

The first geometry investigated was the T-cell (Chapter 4). In this device two channels come together at a 90° angle in a T-junction. The analyte flows into one arm of the 'T' and reference solution flows over a reference electrode in the other arm. The position of the T-junction and the necessary electrodes can be varied depending on the experimental requirements. In this manner, a physical barrier is not needed to protect the reference electrode from contamination. The positive convection in the reference channel can prevent analyte from reaching the reference electrode, thereby preventing contamination. However, due to the small size of the microchannel, diffusion up the side channel (counter to convection) is possible (Equation 4.1). This back-diffusion may allow analyte contamination after all. Criteria for cell design and operation were developed to ensure that this form of contamination is eliminated. When these criteria are followed the reference electrode is protected and remains at a constant potential. This allows for an on-chip, microfluidic reference electrode placed closely to the working electrode. Unlike previous methods, this is done without having to

fabricate and align a physical barrier within the microchannel.

An improvement to the T-cell is the Y-cell. In the T-cell convection protected the reference electrode from contamination. However due to the small size of the microchannel several conditions need to be met to prevent unwanted mixing. In the Y-cell the small size of the channel is used as an advantage as it leads to laminar flow which allows for slower diffusive mixing times. In the Y-channel analyte and reference solutions are brought together in a Y-junction. These solutions flow next to one another and mix only by diffusion. The working and counter electrodes are placed on the analyte side and the reference electrode is placed on the reference side. If the geometry of the device is chosen properly, the reference electrode will never detect the presence of the analyte, due to the slow diffusion of analyte into the reference solution. In this manner the reference electrode can be placed quite close to the working electrode and yet remain uncontaminated. This process requires no specific materials and can be applied to any channel electrode system. Current methods that only allow for precise currents could be expanded to include accurate voltage measurements as well. This opens up continuous electrochemistry to investigate any homogeneous electrochemical systems that were previously done in batch experiments.

7.2 Surface Conduction

The previous section considered electrochemical systems where the important physics were occurring at or near electrodes. The other surfaces (the channel walls) were treated as inert boundaries, where their physical properties were ignored. However, the surface charge of a micro-structure plays an increasingly important role as the surface area to volume ratio increases. The typical surface charge on a glass surface is on the order of 1 $\mathrm{mC/m^2}$. This is equivalent to a charge concentration of 10^{-8} $\mathrm{mol/m^2}$. For a cylindrical micro-structure of radius, r, this would give a volume density of $2 \times 10^{-8}/r$ $\mathrm{mol/m^3}$. As r decreases this charge concentration increases and may become comparable to any electrolyte concentration inside the micro-structure. For instance at 1 μm, the wall charge concentration will be on the order of 0.01mM

for a glass substrate. Depending on the electrolyte concentration under consideration this can no longer be neglected.

The presence of this wall charge allows for an additional conduction pathway along the wall's surface. This surface conduction can then be used to support an overlimiting current and ion depletion region. Simple 1D models show how the ion depletion region grows with time with the onset of depletion corresponding to Sand time, the time at which a classic overlimiting system becomes unstable. Additionally, an explicit steady state current-voltage relationship can be determined with the overlimiting current varying linearly with potential.

This phenomenon's ability to create a depleted region may be applied to designing a de-ionization device. In order to successfully de-ionize, the material from the depleted region must removed. This can be done by flowing an electrolyte solution perpendicular to the applied electric field and using flow fractionation. Using a simplified 2D model, estimates can be made on potential device parameters in order to maximize water recovery and minimize the required energy. In this manner, surface conduction can be applied to create a novel de-ionization device.

7.3 Conclusions

Throughout this body of work, simple mathematical models were created and in some cases produced deep insight. Modeling the physical and chemical behavior of a system can save time and money over conducting physical experiments. In the case of continuous electrochemistry, fabricating and testing a new device will require about a week under the best circumstances. Alternatively, modeling the convection and diffusion in a 2D channel can be done in a day. Additionally, this model can be easily altered to investigate different channel geometries whereas a new physical system is required for experimental data.

While modeling can help clarify known issues, perhaps the largest benefit to modeling a new system is the possibility of identifying previously unknown issues. For instance, when creating models for the T-cell to investigate reference channel con-

tamination, a second form of contamination was found (Chapter 4). By looking at the modeling data, it was determined that re-circulation can occur over the working electrode, potentially altering the measured current. This was then validated experimentally. However, it would have been very difficult to determine the cause of this current change from experiments alone as re-circulation on this scale is difficult to visualize without special equipment. The insights gained from the model highlighted this issue and directed future experiments.

Changes in electrochemical systems can come from a variety of sources. The issues can be chemical, physical or electrical. Part of the challenge in working in electrochemical systems is determine which of these three areas is causing a change in the signal. In the end these devices are intended to measure chemical characteristics. Before doing so it must be certain that physical and electrical conditions are not masquerading as chemical reactions. For instance, the reduced current from re-circulation could be interpreted as reduced chemical activity. Potential shifts due to iR drop or an unstable reference electrode could be unknowingly mistaken for thermodynamic improvements in a new material. Therefore, whenever implementing a new system it is critical that the new system is validated with known materials (such as $IrCl_6^2$) to ensure that the electrochemical data obtained in such a system is correctly interpreted.

While mathematical models can give deep insights into physical problems, it is not always necessary for these models to be complicated. In the case of surface conduction a simple 1D model demonstrated the power of a new phenomenon and produced analytical expression for the steady state conditions. Expanding the model to include a simplified version of cross flow gave further insights into the potential application of this phenomenon. A more detailed model would have taken longer to produce and would be more numerically intensive, and would have produced similar results. By creating a simple model the basic underlying physics are highlighted and design guidelines can be extrapolated. If the goal of a project is to develop a real system, it is not always necessary to create the most detailed model possible. Often a model can be used to simply direct experimental research by pointing out

key components. In this case the precision of a model is less important compared to gaining a general idea of the forces involved.

Over the years, micro and nano scale research has been increasing. This trend is likely to continue. Typically micro systems are designed based on the previously used macro system. In some cases this shrinking is straightforward. Instead of using a large diameter tube, a micro capillary is used instead. However, not all components are easily miniaturized. Often complicated microfabrication techniques are developed to mimic components that are easily made on the macro scale. While this is often necessary, it would be advantageous in some cases to step back and consider the larger picture. In the case of reference electrodes a special physical barrier is used in macro devices. Instead of trying to duplicate this process on a smaller scale, the purpose of this barrier is replicated. Instead of trying to overcome the disadvantages of working on a micro scale, the advantages of such a system are exploited. In this manner a new type of functioning reference electrode is created, a system that works best at small length scales.

Going forward, this type of thinking could be applied to further expanding the possibilities for continuous electrochemistry. Even with a functioning reference electrode, a channel electrode can only handle homogeneous analyte. Heterogeneous materials that require being adhered to the working electrode surface can currently be investigated only in open systems. In these macro systems, typically a droplet of colloidal material is placed on a working electrode surface and the solvent is evaporated. Often a conducting polymer, such as Nafion, is placed over the sample to ensure good adhesion. It is possible to repeat such a procedure when assembling a channel electrode, but can only be done once. In order for a channel electrode to work with multiple heterogeneous samples, a method must be developed that not only adheres new samples to a working electrode surface, but also can remove them in a continuous fashion. In macro systems this is done by removing the solvent from a colloidal solution via evaporation. One way this may be done in a channel electrode is by electrolysis. By placing a large potential at the working electrode an aqueous solvent at its surface will be hydrolyzed. The remaining heterogeneous material will

remain and may in fact be pulled to the electrode surface due to electrophoresis. The smaller the channel, the easier this method is to implement as there is less solvent above the electrode to remove. After material has been adhered to the electrode surface it can then be removed by flowing a cleaning solution, such as an acid, over the electrode. Additionally, strong oxidizing or reducing potentials can be applied in an effort to clean the electrode surface. In this manner a new technique can be developed by considering the purpose of macro methods instead of mimicking the methods themselves.

This thesis laid the groundwork for two different systems involving electrochemistry and electrokinetics. Simple modeling and theoretical analysis demonstrated key points in these systems and gave insight into their operation. In the case of continuous electrochemistry, experimental results validated the mathematical model and established a new experimental technique. The next step is to apply this information and use it to either explore new chemistries (via continuous electrochemistry) or to design and implement a new electrokinetic device (via surface conduction).

Appendix A

Methods

A.1 Device Fabrication

The electrochemical cells described in this thesis are comprised of a polydimethylsiloxane (PDMS) channels and metal electrodes deposited on a glass substrate. Below are the fabrication details of these two parts and their assembly.

A.1.1 PDMS Channels

The PDMS channels are fabricated using standard soft-lithography techniques [62]. After dehydration at 200°C for at least 20 minutes, a 4 inch silicon wafer is spin coated with SU-8 2050 (MicroChem). The spin rate is chosen such that the SU-8 is of the desired thickness, where the thickness of the SU-8 corresponds to the eventual channel height. For guidelines on spin rate, see the manufacture's website. However, the numbers posted here are just guidelines. If precision of the channel height is important, several attempts should be made at different spin rates to determine the correct rate for the desired channel height. Several factors will contribute to the spin rate/thickness relationship. Older SU-8 may have a higher viscosity which will then require a faster spin rate to achieve the same resist thickness. Additionally, the spin coater is a shared machine and the settings may have been changed by another user, particularly the spin rate acceleration. Once the wafer has been spin coated with

SU-8 it is set on a hot plate to pre-bake. The pre-bake temperature and duration are suggested on the manufacture's website. However, once again these are guidelines that can be altered, particularly the pre-bake duration. Different users have found that too short or too long bake times prevent successful adhesion between the SU-8 resist and the silicon wafer. Trial and error may be needed to find the correct bake times. After the pre-bake, the wafer is exposed to UV light through a photomask. If the exposure time is not long enough the deeper levels of SU-8 will not be crosslinked and the features will lift off. If the exposure time is too long the features will spread out past the edges of the mask. Additionally, for thicker layers requiring longer exposure times, it is best to expose the wafer in intervals. This prevents the SU-8 from over heating, which could lead to reflow. For instance, if 85s of exposure is required an interval of 5s on and 4s off can be repeated 17 times. The total exposure time can be determined from guidelines set by the manufacturer. After exposure, the wafer is post-baked to harden the SU-8. The post-bake times suggested by the manufacturer are typically accurate. After the post-bake, the wafer is allowed to cool to room temperature and then is developed in PM Acetate. If the features do not survive development, several factors may be to blame. Thermal shock may lead to poor adhesion, if this is the case the wafer can be slowly heated to the required baking temperature and then slowly cooled when completed. High humidity can also lead to poor adhesion. In this case the dehydration step becomes particularly important. Alternatively, as mentioned above, the baking and exposure times may not be optimized correctly given the SU-8 thickness. Additionally, an unclean wafer surface may be to blame for poor resist adhesion. Once the SU-8 has been developed the features width and height can be determined via microscopy.

After the SU-8 has been made it can be used as a master for molding multiple PDMS devices. To prevent PDMS from sticking to the mold's surface a silane, (Tridecafluoro-1,1,2,2-Tetrahydrooctyl)-1-Trichlorosilane, is evaporated onto the mold's surface (this is done for every new PDMS device). This can be done by placing an open vial of the silane with the wafer in a vacuum chamber for 1-2 hours. The silane coats the master and will help cured PDMS release from the mold. In

order to prepare a PDMS solution, PDMS is mixed with a curing agent (Sylgard 184 by Dow Corning) in a 10:1 ratio. During the mixing of these two liquids, air gets stirred into the thick mixture and becomes trapped. Before proceeding, the air in the PDMS/curing agent mixture must be removed. This can be achieved by placing the mixture under vacuum until the solution is clear and the air has been removed. Once the mixture has been properly degassed, it can be poured over the SU-8 mold with care being taken to minimize the influence of ambient dust. If bubbles are introduced during this procedure, degassing can be repeated. The liquid PDMS is then placed into an oven 70°C for 1.5 hours. At this point the PDMS has formed a cured solid. After curing, the PDMS is gently peeled off of the SU-8 master. The PDMS is then cut into the desired pieces and cleaned repeatedly with Scotch tape (typical office variety is fine). Holes for the inlet and outlets are then punched and cleaned.

A.1.2 Electrodes

The electrodes are evaporated onto a Pyrex wafer and shaped using lithography and lift-off techniques. In addition to the electrodes, deposition included metal alignment marks. An image reversal photoresist, AZ 5214E, is spun onto a piranha cleaned 6-inch Pyrex wafer, achieving a thickness of about 1.5 μm. Image reversal photolithography (similar to that used for SU-8) and development in AZ 422 defined the electrode features. 200 nm of electrode metal (gold, silver, or platinum) is evaporated onto the wafer with a 20 nm titanium adhesion layer. After metal deposition, the wafers are submerged in acetone to remove the remaining resist, thereby lifting off the unwanted metal. The wafers are cleaned and cut into individual device pieces. Some reference electrodes are converted from gold or platinum to silver/silver chloride using a previously developed method [63]. Silver is electroplated onto the desired electrode and then chemically converted to silver chloride using aqueous $FeCl_3$.

A.1.3 Device Assembly

In order to bond the glass substrate to the PDMS channels, both pieces are placed in an oxygen plasma. After removing the glass and PDMS from the plasma they are immediately brought into contact with each other. When alignment is important (Y-cell and T-cell type 'a') an additional step is taken. To prevent irreversible bonding before proper alignment can take place, a few drops of ethanol are placed in between the glass and PDMS [64]. This allows the pieces to move around while preserving the effects of the plasma. Using a microscope, the PDMS channels are aligned using the metal alignment marks on the glass substrate. After alignment, the device is left in a 70°C oven overnight. This ensured that the ethanol is completely evaporated, leading to an irreversible bond between the PDMS and glass substrate. After bonding, fluidic and electronic leads are glued in place. Fluidic leads are made with PEEK tubing and glued with standard 5 minute epoxy. The electronic leads are first adhered using a conductive silver based epoxy to ensure good electronic contact. Then a layer of standard epoxy is added to ensure good physical stability.

A.2 Experimental Methods

Fluid is injected into electrochemical cells using Harvard Apparatus syringe pumps. Syringes from these pumps are connected to flexible fluoropolymer tubing which are then connected to the PEEK inlets and outlets of a device. Before experiments, in the case of Ag/AgCl reference electrodes, $FeCl_3$ is injected over the reference electrode. The oxygen plasma used to bond the device has the potential to chemically alter the surface of the Ag/AgCl electrode. By flowing $FeCl_3$ over the reference electrode, the electrode returns to its previous state. The working, counter, and reference electrodes are connected to a potentiostat (Uniscan Bistat 3200) and potentiometry is conducted via a computer. The software for this potentiostat controls the applied potential and measures the resulting current. In the case of cyclic voltammograms (CVs) it also controls the scan rate. In order to prevent noise from external electromagnetic sources, a Faraday cage is used. This cage is comprised of a copper mesh with 5 mm grid

spacing. The mesh is bent to form a rectangular prism. The electrochemical device sits inside the cage with the tubing and connecting wires fed through the copper mesh. During an experiment syringe pumps inject solutions at the chosen flow rates while the potentiostat applies the desired potential. In between chemical experiments the working electrode is cleaned with a 0.1M H_2So_4 or HNO_3 solution. As this acidic solution flows over the working electrode a CV is taken, extending to higher and lower voltages than those taken during an experiment. Typically the voltages are chosen such that water splitting clearly occurs at both ends of the scan. This scan is allowed to repeat until the resulting CV overlaps itself, indicating that the electrode has been cleaned. Once the electrode has been cleaned, it is rinsed with distilled, de-ionized water. At this point the system is ready to conduct another experiment.

Bibliography

[1] R.L. Hartman and K.F. Jensen. Microchemical systems for continuous-flow synthesis. *Lab on a Chip*, 9(17):2495–2507, 2009.

[2] K.F. Jensen. Microreaction engineering–is small better? *Chemical Engineering Science*, 56(2):293–303, 2001.

[3] A.J. Demello. Control and detection of chemical reactions in microfluidic systems. *Nature*, 442(7101):394, 2006.

[4] S. Krishnadasan and R.J.C. Brown. Intelligent routes to the controlled synthesis of nanoparticles. *Lab on a Chip*, 7(11):1434–1441, 2007.

[5] J.P. McMullen and K.F. Jensen. Integrated microreactors for reaction automation: New approaches to reaction development. *Annual Review of Analytical Chemistry*, 3:19–42, 2010.

[6] X. Zhang, C. Wiles, S.L. Painter, and S.J. Haswell. Microreactors as tools for chemical research. *Chimica Oggi/Chemistry Today*, 24:43–45, 2006.

[7] J.P. McMullen and K.F. Jensen. An automated microfluidic system for online optimization in chemical synthesis. *Organic process research & development*, 14(5):1169–1176, 2010.

[8] J.S. Swensen, Y. Xiao, B.S. Ferguson, A.A. Lubin, R.Y. Lai, A.J. Heeger, K.W. Plaxco, and H.T. Soh. Continuous, real-time monitoring of cocaine in undiluted blood serum via a microfluidic, electrochemical aptamer-based sensor. *Journal of the American Chemical Society*, 131(12):4262–4266, 2009.

[9] Y. Lin, C.A. Timchalk, D.W. Matson, H. Wu, and K.D. Thrall. Integrated microfluidics/electrochemical sensor system for monitoring of environmental exposures to lead and chlorophenols. *Biomedical Microdevices*, 3(4):331–338, 2001.

[10] E. Pavlovic, R.Y. Lai, T.T. Wu, B.S. Ferguson, R. Sun, K.W. Plaxco, and H.T. Soh. Microfluidic device architecture for electrochemical patterning and detection of multiple DNA sequences. *Langmuir*, 24(3):1102–1107, 2008.

[11] V.V. Nikonenko, N.D. Pismenskaya, E.I. Belova, P. Sistat, P. Huguet, G. Pourcelly, and C. Larchet. Intensive current transfer in membrane systems: Modeling,

mechanisms and application in electrodialysis. *Advances in colloid and interface science*, 160(1-2):101–123, 2010.

[12] B. Zaltzman and I. Rubinstein. Electro-osmotic slip and electroconvective instability. *Journal of Fluid Mechanics*, 579(1):173–226, 2007.

[13] S.M. Rubinstein, G. Manukyan, A. Staicu, I. Rubinstein, B. Zaltzman, R.G.H. Lammertink, F. Mugele, and M. Wessling. Direct observation of a nonequilibrium electro-osmotic instability. *Physical review letters*, 101(23):236101, 2008.

[14] W.J. Albery and M.L. Hitchman. *Ring-disc electrodes*. Oxford University Press, 1971.

[15] A.J. Bard and L.R. Faulkner. *Electrochemical methods: fundamentals and applications*. Wiley, 2001.

[16] J. Yamada and H. Matsuda. Limiting diffusion currents in hydrodynamic voltammetry: III. Wall jet electrodes. *Journal of Electroanalytical Chemistry*, 44(2):189–198, 1973.

[17] J.V. Macpherson, S. Marcar, and P.R. Unwin. Microjet electrode: A hydrodynamic ultramicroelectrode with high mass-transfer rates. *Analytical Chemistry*, 66(13):2175–2179, 1994.

[18] R.G. Compton and P.R. Unwin. Channel and tubular electrodes. *Journal of electroanalytical chemistry and interfacial electrochemistry*, 205(1-2):1–20, 1986.

[19] J.A. Cooper and R.G. Compton. Channel electrodes-A review. *Electroanalysis*, 10(3):141–155, 1998.

[20] V.G. Levich. *Physicochemical hydrodynamics*. Prentice-Hall Englewood Cliffs, NJ, 1962.

[21] T.E. Mallouk, V. Cammarata, J.A. Crayston, and M.S. Wrighton. Voltammetry at polymer-modified stationary and rotating microelectrodes. Application to determination of electron-transfer rates at polymer solution interfaces. *The Journal of Physical Chemistry*, 90(10):2150–2156, 1986.

[22] N.V. Rees, R.A.W. Dryfe, J.A. Cooper, B.A. Coles, R.G. Compton, S.G. Davies, and T.D. McCarthy. Voltammetry under high mass transport conditions. A high speed channel electrode for the study of ultrafast kinetics. *The Journal of Physical Chemistry*, 99(18):7096–7101, 1995.

[23] J.S. Newman and K.E. Thomas-Alyea. *Electrochemical systems*. Wiley-Interscience, 2004.

[24] R.G. Compton, A.C. Fisher, R.G. Wellington, P.J. Dobson, and P.A. Leigh. Hydrodynamic voltammetry with microelectrodes: Channel microband electrodes; theory and experiment. *The Journal of Physical Chemistry*, 97(40):10410–10415, 1993.

[25] N.P.C. Stevens, Q. Fulian, K.A. Gooch, and A.C. Fisher. Steady-state voltammetry using microwire electrodes under microfluidic control. *The Journal of Physical Chemistry B*, 104(30):7110–7114, 2000.

[26] S.M. Mitrovski and R.G. Nuzzo. An electrochemically driven poly (dimethylsiloxane) microfluidic actuator: Oxygen sensing and programmable flows and pH gradients. *Lab on a Chip*, 5(6):634–645, 2005.

[27] S.K. Yoon, G.W. Fichtl,.and P.J.A. Kenis. Active control of the depletion boundary layers in microfluidic electrochemical reactors. *Lab on a Chip*, 6(12):1516–1524, 2006.

[28] C. Amatore, N. Da Mota, C. Sella, and L. Thouin. Theory and experiments of transport at channel microband electrodes under laminar flows. 1. Steady-state regimes at a single electrode. *Analytical chemistry*, 79(22):8502–8510, 2007.

[29] O. Ordeig, N. Godino, J. del Campo, F.X. Muñoz, F. Nikolajeff, and L. Nyholm. On-chip electric field driven electrochemical detection using a poly (dimethylsiloxane) microchannel with gold microband electrodes. *Analytical chemistry*, 80(10):3622–3632, 2008.

[30] N. Triroj, M.A. Lapierre-Devlin, S.O. Kelley, and R. Beresford. Microfluidic three-electrode cell array for low-current electrochemical detection. *Sensors Journal, IEEE*, 6(6):1395–1402, 2006.

[31] R.L. Smith and D.C. Scott. An integrated sensor for electrochemical measurements. *Biomedical Engineering, IEEE Transactions on*, (2):83–90, 1986.

[32] S. Yee, H. Jin, and L.K.C. Lam. Miniature liquid junction reference electrode with micromachined silicon cavity. *Sensors and Actuators*, 15(4):337–345, 1988.

[33] H. Suzuki, T. Hirakawa, S. Sasaki, and I. Karube. Micromachined liquid-junction Ag/AgCl reference electrode. *Sensors and Actuators B: Chemical*, 46(2):146–154, 1998.

[34] H. Suzuki, H. Shiroishi, S. Sasaki, and I. Karube. Microfabricated liquid junction Ag/AgCl reference electrode and its application to a one-chip potentiometric sensor. *Analytical Chemistry*, 71(22):5069–5075, 1999.

[35] J. Strutwolf, G. Herzog, A. Homsy, A. Berduque, C.J. Collins, and D.W.M. Arrigan. Potentiometric characterization of a dual-stream electrochemical microfluidic device. *Microfluidics and nanofluidics*, 6(2):231–240, 2009.

[36] M.J. Willey and A.C. West. A microfluidic device to measure electrode response to changes in electrolyte composition. *Electrochemical and solid-state letters*, 9:E17, 2006.

[37] S.K. Kim, H. Lim, T.D. Chung, and H.C. Kim. A miniaturized electrochemical system with a novel polyelectrolyte reference electrode and its application to thin layer electroanalysis. *Sensors and Actuators B: Chemical*, 115(1):212–219, 2006.

[38] J. Zhou, K. Ren, Y. Zheng, J. Su, Y. Zhao, D. Ryan, and H. Wu. Fabrication of a microfluidic Ag/AgCl reference electrode and its application for portable and disposable electrochemical microchips. *Electrophoresis*, 2010.

[39] I.E. Henley, K. Yunus, and A.C. Fisher. Voltammetry under microfluidic control: Computer-aided design development and application of novel microelectrochemical reactors. *The Journal of Physical Chemistry B*, 107(16):3878–3884, 2003.

[40] S.M. Matthews, G.Q. Du, and A.C. Fisher. Microfluidic voltammetry: Simulation of the chronoamperometric response of microband electrodes sited within microreactors. *Journal of Solid State Electrochemistry*, 10(10):817–825, 2006.

[41] N. Zaborenko, E.R. Murphy, J.G. Kralj, and K.F. Jensen. Synthesis and kinetics of highly energetic intermediates by micromixers: Direct multistep synthesis of sodium nitrotetrazolate. *Industrial & Engineering Chemistry Research*, 49(9):4132–4139, 2010.

[42] K. Izutsu. *Electrochemistry in Nonaqueous Solutions.* Wiley - VCH, 2002.

[43] A.J. Bard. *Encyclopedia of the Electrochemistry of the Elements, Vol VI.* Marcel Dekker, New York, 1976.

[44] NV Rees and RG Compton. Hydrodynamic microelectrode voltammetry. *Russian Journal of Electrochemistry*, 44(4):368–389, 2008.

[45] R.G. Compton, M.B.G. Pilkington, and G.M. Stearn. Mass transport in channel electrodes. The application of the backwards implicit method to electrode reactions (ec, ece and disp) involving coupled homogeneous kinetics. *J. Chem. Soc., Faraday Trans. 1*, 84(6):2155–2171, 1988.

[46] J. Lyklema and M. Minor. On surface conduction and its role in electrokinetics. *Colloids and Surfaces A: Physicochemical and Engineering Aspects*, 140(1-3):33–41, 1998.

[47] J.J. Bikerman. Ionentheorie der elektrosmose, der strömungsströme und der oberflächenleitfähigkeit. *Z. Physikalische Chemie A*, 163:378–394, 1933.

[48] J.J. Bikerman. Wissenschaftliche und technische sammelreferate. *Colloid & Polymer Science*, 72(1):100–108, 1935.

[49] K.T. Chu and M.Z. Bazant. Surface conservation laws at microscopically diffuse interfaces. *Journal of colloid and interface science*, 315(1):319–329, 2007.

[50] M.Z. Bazant, K. Thornton, and A. Ajdari. Diffuse-charge dynamics in electrochemical systems. *Physical Review E*, 70(2):021506, 2004.

[51] S.J. Kim, S.H. Ko, K.H. Kang, and J. Han. Direct seawater desalination by ion concentration polarization. *Nature Nanotechnology*, 5(4):297–301, 2010.

[52] Y.C. Wang, A.L. Stevens, and J. Han. Million-fold preconcentration of proteins and peptides by nanofluidic filter. *Analytical chemistry*, 77(14):4293–4299, 2005.

[53] S.J. Kim, Y.C. Wang, J.H. Lee, H. Jang, and J. Han. Concentration polarization and nonlinear electrokinetic flow near a nanofluidic channel. *Physical review letters*, 99(4):44501, 2007.

[54] G. Yossifon, P. Mushenheim, and H.C. Chang. Controlling nanoslot overlimiting current with the depth of a connecting microchamber. *EPL (Europhysics Letters)*, 90:64004, 2010.

[55] A. Mani, T.A. Zangle, and J.G. Santiago. On the propagation of concentration polarization from microchannel-nanochannel interfaces part I: Analytical model and characteristic analysis. *Langmuir*, 25(6):3898–3908, 2009.

[56] T.A. Zangle, A. Mani, and J.G. Santiago. On the propagation of concentration polarization from microchannel-nanochannel interfaces part II: Numerical and experimental study. *Langmuir*, 25(6):3909–3916, 2009.

[57] A. Mani and M.Z. Bazant. Desalination shocks in microstructures. *Arxiv preprint arXiv:1108.0871*, 2011.

[58] W.M. Deen. *Analysis of transport phenomena*. Oxford University Press New York, 2012.

[59] H.J.S. Sand. Viscosity effects in thin-layer electrodeposition. *Philos. Mag*, 1:45, 1901.

[60] M. Van Soestbergen, P.M. Biesheuvel, and M.Z. Bazant. Diffuse-charge effects on the transient response of electrochemical cells. *Physical Review E*, 81(2):021503, 2010.

[61] S.H. Behrens and D.G. Grier. The charge of glass and silica surfaces. *The Journal of Chemical Physics*, 115:6716, 2001.

[62] Y. Xia and G.M. Whitesides. Soft lithography. *Annual review of materials science*, 28(1):153–184, 1998.

[63] B.J. Polk, A. Stelzenmuller, G. Mijares, W. MacCrehan, and M. Gaitan. Ag/AgCl microelectrodes with improved stability for microfluidics. *Sensors and Actuators B: Chemical*, 114(1):239–247, 2006.

[64] B.H. Jo, L.M. Van Lerberghe, K.M. Motsegood, and D.J. Beebe. Three-dimensional micro-channel fabrication in polydimethylsiloxane (PDMS) elastomer. *Microelectromechanical Systems, Journal of*, 9(1):76–81, 2000.